Universidade de Aveiro Departamento de Engenharia Mecânica
2016

Beatriz Condesso Macedo Lobo da Fonseca

Caracterização termomecânica de compósitos poliméricos com memória de forma

Thermomechanical characterization of shape-memory polymeric composites

Universidade de Aveiro Departamento de Engenharia Mecânica
2016

Beatriz Condesso Macedo Lobo da Fonseca

Caracterização termomecânica de compósitos poliméricos com memória de forma

Thermomechanical characterization of shape-memory polymeric composites

Dissertação apresentada à Universidade de Aveiro para cumprimento dos requisitos necessários à obtenção do grau de Mestre em Engenharia Mecânica, realizada sob orientação científica da Doutora Mónica Sandra Abrantes de Oliveira Correia, Professora Auxiliar do Departamento de Engenharia Mecânica da Universidade de Aveiro e da Doutora Maria Alexandra Lopes da Fonseca, Investigadora em Pós-Doutoramento do Departamento de Engenharia Mecânica da Universidade de Aveiro.

O júri / The jury

Presidente / President

Professor Doutor António Gil D'Orey de Andrade Campos
Professor Auxiliar da Universidade de Aveiro

Vogais / Committee

Doutor João André da Costa Tedim
Equiparado a Investigador Auxiliar, Universidade de Aveiro (Arguente)

Doutora Maria Alexandra Lopes da Fonseca
Bolseira de Pós Doutoramento, Universidade de Aveiro (Co-orientadora)

Agradecimentos / Acknowledgements

Aos meus pais, Carla e Carlos.
À minha irmã, Bárbara.
Obrigada por me apoiarem em tudo o que faço e por serem os melhores do mundo.

Aos meus amigos, que tornaram a minha passagem pela Universidade de Aveiro uma época inesquecível e muito feliz.

À minha família.

Palavras-chave

Efeito de memória de forma; Compósitos com memória de forma; Poliuretano (PU); Nanotubos de carbono; Grafeno; Microscopia eletrónica de varrimento (MEV); Calorimetria Diferencial de varrimento; Testes de tração; Propriedades termo-mecânicas.

Resumo

Os materiais com memória de forma são, atualmente, um tema em estudo pela comunidade científica devido ao seu grande potencial tecnológico. Estes materiais possuem a capacidade de reagir a um estímulo externo e, em consequência disso, alterar a sua forma. Tendo em conta a recente expansão na indústria biomédica, este trabalho de dissertação pretende dar resposta à aplicabilidade de materiais com memória de forma em dispositivos biomédicos, permitindo uma operabilidade mais eficiente dos mesmos. Para tal, foi considerado o uso do poliuretano com memória de forma, devido à sua elevada biocompatibilidade e à proximidade entre a temperatura de ativação térmica do material e da temperatura média do corpo humano. No entanto, o poliuretano termoplástico (TPU), e a generalidade dos polímeros com memória de forma, tem desvantagens relacionadas com o seu desempenho mecânico inferior comparativamente com as ligas metálicas com memória de forma e com o elevado tempo de recuperação de forma. Procurando o reforço mecânico e a melhoria das propriedades do poliuretano com memória de forma, foi realizado um trabalho experimental de processamento de nanocompósitos de poliuretano aditivados com nanopartículas de carbono. Para tal, foram usados nanotubos de carbono (CNTs), não tratados e sujeitos a funcionalização, e grafeno, uma vez que estes materiais possuem excelentes propriedades térmicas e mecânicas documentadas na literatura. Foram produzidos através do método de mistura mecânica por fusão e posterior injeção os nanocompósitos aditivados com 0.5 vol.%, 1.0 vol.% e 1.5 vol.% de nanotubos de carbono não tratados, nanotubos de carbono funcionalizados e grafeno não tratado. Foi realizada caracterização morfológica, térmica e mecânica dos nanocompósitos. Propriedades como a temperatura de transição vítrea (T_g), a temperatura de fusão (T_m), o calor específico (c_p), a difusividade térmica (α), o módulo de elasticidade (E), tensão de rotura (σ_b) e deformação de rotura (ε_b) foram avaliadas. Através desta dissertação foi possível avaliar a influência das diferentes nanopartículas e das diferentes concentrações usadas nas propriedades termo-mecânicas do material e posteriormente determinar uma relação entre os materiais e parâmetros usados. Foi possível ainda estabelecer algumas conclusões relativas à performance da memória de forma dos nanocompósitos.

Keywords

Shape-memory effect (SME); Shape-memory composites (SMCs); Polyurethane (PU); Carbon nanotubes (CNTs); Graphene; Scanning electron microscopy (SEM); Differential scanning calorimetry (DSC); Tensile tests; Thermo-mechanical properties.

Abstract

The shape-memory materials are nowadays an important subject in the scientific community due to their huge technological potential. These materials have the capability of being triggered by an external stimulus and, consequently, change their shape. Considering the recent development of the biomedical industry, this dissertation aims to develop the applicability of shape-memory materials into biomedical devices, enabling a more efficient operability. Therefore, the shape-memory polyurethane was chosen to this end due to their high biocompatibility and proximity between the thermal transition temperature of the material and the human body temperature. However, the thermoplastic polyurethane (TPU), and the shape-memory polymers in general, possesses major drawbacks related to the inferiority of its mechanical performance as compared with shape-memory alloys (SMAs) and its large shape recovery time. In order to pursue the mechanical reinforcement and improvement of the polyurethane properties, it was conducted an experimental study in which polyurethane nanocomposites containing carbon based nanoparticles were produced. It was used carbon nanotubes (CNTs), treated and non-treated, and graphene, as these materials exhibit excellent thermo-mechanical properties reported in the literature. The nanocomposites were produced through mechanical melt mixing and injection moulding and they were incorporated with 0.5 vol.%, 1.0 vol.% and 1.5 vol.% of non-treated CNTs, treated CNTs and non-treated graphene. It was performed the morphological, thermal and mechanical characterization of the nanocomposites. Thermo-mechanical properties, such as glass transition temperature (T_g), melting temperature (T_m), specific heat capacity (c_p), thermal diffusivity (α), elastic modulus (E), tensile strength at break (σ_b) and elongation at break (ε_b) were evaluated. In the present dissertation it could be analysed the influence of the different types of nanoparticles and different concentrations on the thermo-mechanical properties of the produced nanocomposites. Through this, the best relation regarding the materials and parameters used in this work was determined. It was also possible to draw some conclusions regarding the shape-memory performance of the nanocomposites.

Contents

List of Figures

List of Tables

Abbreviations

CNTs	Carbon nanotubes
c_p	Specific heat capacity
DSC	Differential scanning calorimetry
DW	Deionised water
E	Elastic modulus
E'	Storage modulus
EPT	Electrical percolation threshold
FE-SEM	Field emission scanning electron microscopy
FGO	Functionalized graphene oxide
FT-IR	Fourier Transform Infrared
Func.	Functionalization
GNPs	Graphene nanoplatelets
GNS	Graphene nanosheets
GO	Graphene oxide
Gra	Graphene
H	Hardness
k	Thermal conductivity
M50	Modulus at 50% elongation
M100	Modulus at 100% elongation
M300	Modulus at 300% elongation
MWNTs	Multi-walled carbon nanotubes
Ni-Ti	Nitinol
NT CNTs	Non-treated carbon nanotubes

PEEAMA	poly(ethylene-co-ethyl acrylate-co-maleic anhydride)
PP	Polypropylene
PS	Polystyrene
PVA	Polyvinyl alcohol
PTh	Polythiophene
PVDF	Poly(vinylidene difluoride)
RGO	Reduced graphene oxide
RSD	Relative standard of variation
SEM	Scanning electron microscopy
SiC	Silicon carbide
SMA	Shape-memory alloy
SME	Shape-memory effect
SMG	Surface-modified graphene
SMM	Shape-memory material
SMP	Shape-memory polymer
SMPC	Shape-memory polymer composite
SMPU	Shape-memory polyurethane
SPU	Segment polyurethane
SWNTs	Single-walled carbon nanotubes
$\mathbf{T_d}$	Degradation temperature
$\mathbf{T_g}$	Glass transition temperature
$\mathbf{T_m}$	Melting temperature
$\mathbf{T_{perm}}$	Transition temperature of the hard segments
$\mathbf{T_{trans}}$	Transition temperature of the soft segments
T CNTs	Treated carbon nanotubes
TEM	Transmission electron microscopy
TPU	Thermoplastic polyurethane
TRG	Thermally reduced graphene oxide
VGCF	Vapor grown carbon fiber

UHMWPE	Ultrahigh molecular weight polyethylene
ϕ_{i}	Volume fraction
σ	Stress
σ_{b}	Tensile strength at break
ε	Strain
ε_{b}	Elongation at break
γ	Electrical conductivity
α	Thermal diffusivity
β	Heating rate (in DSC)
ρ	Density

Chapter 1

Introduction

1.1 Background

Shape-memory materials have recently been an important research field in mechanical engineering. Due to their unique mechanical and thermal properties, these materials have been studied in order to be applied in a wide range of technological areas. Shape memory materials exhibit a special behaviour when exposed to certain temperature and tension or deformation conditions. These materials, after being loaded or deformed in specific thermo-mechanical conditions, can retrieve back to their initial pre-strain shape. The factors that influence the convenient work conditions are related to the morphology and constitution of the material used. The main groups of materials presenting shape-memory effect are shape-memory alloys (SMAs), shape-memory polymers (SMPs) and shape-memory ceramics. Although SMAs have been the most used shape-memory material for the last decades, mainly because of their excellent biocompatibility, high strength and modulus, larger attainable strain than shape-memory ceramics and glasses and lower recovery times, shape-memory polymers have been gaining ground due to their low cost and light weight [1–6]. These shape-changing materials have been used in several applications, such as: self-deployable structures, intelligent biomedical devices, smart textiles, releasable fasteners, heat shrinkable equipment, sensors and actuators [6].

Polyurethanes, specifically, are a class of engineering polymers that have been receiving attention from both industry and academia. These polymers detain two different repeating blocks: a soft, flexible one and a hard, stiff block. This molecular versatility enables the usage of polyurethanes in a broad field of applications, such as coatings, adhesives and injection moulded and elastomeric parts. Polyurethanes can be classified into thermosets and thermoplastics [7]. The primary physical difference between them is that thermoplastics can melt when heated, while thermosets cannot be remoulded or reshaped [8]. Consequently, since the thermal shape-memory effect involves the transformation from a shape A to a previously memorized shape upon heating up to a transition temperature, the polyurethane that must be used for this case is the thermoplastic polyurethane (TPU). Usually, the thermoplastic polyurethane synthesis occurs through reaction between diol and diisocyanate. The hard segments of this kind of polyurethane act as physical crosslinks and present a strong elastomeric behaviour below their melting temperature, while above this temperature they can be easily processed. The physical crosslinks result from the strong interactions between hard segments, that are formed through hydrogen bonding between urethane bonds. The

excellent polyurethane properties strongly depend on the hydrogen bonding interactions and, consequently, at high temperatures, when the hydrogen bonding interactions become weaker, the polymer may exhibit inferior mechanical properties. Besides, thermoplastic polyurethanes possess lower shape recovery stress and mechanical strength and higher shape-recovery time than those from SMAs. These drawbacks can be overcome by the addition of a nanofiller with the capability of improving and tailoring some characteristics of the polymer matrix at the expense of increased weight [5, 7, 9]. As an example, upon incorporation of carbon nanotubes (CNTs) within a TPU matrix were reported enhancements in fatigue life and creep resistance, increase of the modulus, strength, stiffness, acceleration of the crystallization and increase of thermal and electrical conductivity, which result in a faster shape recovery [7].

In order to disperse the nanofillers into the polyurethane matrix, several methods can be used, namely: mechanical melt mixing in blenders or twin screw extruders, dissolution of the polymer in a solvent followed by ultrasonication of the filler suspension and *in situ* polymerization of nanocomposites.

1.2 Motivation

Although there are already several researches focused on the SMPs performance and on the enhancement of their thermo-mechanical properties, there are also research gaps corresponding to issues that have not been fully investigated yet, regarding the optimal filler concentration to be incorporated in the polymeric matrix, which filler improves the thermo-mechanical properties the most, the influence of the chemical functionalization on the composite properties or even the the suitability of the composites preparation techniques itself, among others. This thesis aims to investigate some parameters that influence the shape-memory and thermo-mechanical properties of thermoplastic polyurethane, leading the way to further investigation of this subject. The motivation to study and characterize the thermo-mechanical properties of a shape-memory polyurethane filled with non-treated carbon nanotubes, treated carbon nanotubes and graphene nanosheets is the follow-up of the research that has been developed by GRIDS research group at University of Aveiro. These previous research developed by Fonseca et al. [10] compared the two main techniques to attain TPU nanocomposites filled with 0.1, 0.25 and 0.5 vol.% acid treated CNTs: *in situ* polymerization and mechanical melt mixing. An extensive characterization of the latter technique was accomplished. It was observed by scanning electron microscopy (SEM) a good dispersion of the CNTs in the polymeric matrix. Through thermal characterization it was determined an increase in the transition temperature (T_g), degradation temperature (T_d) and melting temperature (T_m) with increasing CNTs content, in relation to pristine TPU. It was also observed that both types of processed samples detained shape-memory effect and that the mechanical melt mixed nanocomposites presented lower recovery time than pristine TPU. Since better results were obtained for nanocomposites with higher carbon nanotube concentrations, in this investigation it will be tested nanocomposites containing filler concentration ranging from 0.5 to 1.5 vol.%, which is a range of values above the one studied in the previous GRIDS investigation. The reason why polyurethane was the chosen shape-memory polymer used in this investigation is related to its good biocompatibility and, therefore, its adequacy to biomedical applications, which is a field of engineering of growing importance. The usage of a shape-memory polymer capable of being actuated by internal human temperature in applications such as stents, implants and catheters, for example,

would be a very interesting medical solution.

1.3 Objectives

The main goal of this work is to develop a polyurethane based nanocomposite with improved thermo-mechanical and shape-memory properties by using a production method that could be easily implemented by industry. So, although *in situ* polymerization is an excellent technique to produce homogeneous nanocomposites with strong filler-matrix bonding, mechanical melt mixing would be a rather easier and less expensive technique for scaling up purposes. This being said, the main objectives of this thesis are to:

- carry out an analysis to establish the influence of different fillers on the overall shape-memory performance;
- assess means of easily produce shape-memory composites on an industrial scale;

To accomplish the above mentioned specific objectives three different fillers (treated carbon nanotubes, non treated carbon nanotubes and graphene) in three concentrations (0.5, 1.0 and 1.5 vol.%) are selected to be incorporated in the TPU matrix and a parametric analysis is intended to be carried in order to establish the suitability of each filler in terms of thermal and mechanical properties (i.e. relevant properties to attain the shape-memory enhancement). Moreover, the nanocomposites are intended to be processed by mechanical melt mixing. The morphology of the nanocomposites and the repeatability of the process will be assessed in order to verify the technique suitability for scaling up purposes.

1.4 Outline of the thesis

This thesis is divided into three parts: Part I: Concepts and State-of-the-art, Part II: Experimental procedure and Part III: Results and discussion.

Part I:

Chapter 2: Shape-Memory Effect - The underlying principle of shape-memory effect (SME) is explained. In this chapter are described the main groups of shape-memory materials: shape-memory alloys, shape-memory ceramics and shape-memory polymers. The advantages, drawbacks and applications of these materials are mentioned. This chapter also addresses the shape-memory composites and it is approached the particularities and special characteristics of the nanocomposite. It is referred and described some of the most relevant nanoparticles, including the ones used in this work.

Chapter 3: State of the art - Shape-memory polymer composites - This chapter presents a literature review of the recent developments and relevant experiments carried out by the research community.

Part II:

Chapter 4: Materials and Methods - In this chapter is described the experimental apparatus, materials and processing techniques used in this work.

Chapter 5: Characterization - The characterization methods and formulations to obtain the analysed properties are described.

Part III:

Chapter 6: Experimental results - The results regarding the morphological, thermal and mechanical characterization are presented. The thermo-mechanical behaviour of the nanocomposites is described according to the glass transition and melting temperatures, specific heat capacity, thermal diffusivity, elastic modulus, tensile strength at break and elongation at break results.

Chapter 7: Discussion - The obtained results are analysed in this chapter. The experimental values are compared with the expected behaviour provided by the bibliography and with other experiments aiming to investigate the same subject.

Chapter 8: Conclusions and Future works - In this chapter it is summarized the main conclusions drawn from this work and it is presented some suggestions of lines of investigation that would be interesting to be developed in the future.

Part I

Concepts and State-of-the-Art

Chapter 2

Shape-Memory Effect

The shape-memory effect can be described as the capability of stimuli-responsive materials to recover their original shape after being physically deformed to a temporary shape [11–13]. The shape-memory materials (SMMs) are characterized by their ability to "memorize" a macroscopic permanent shape and return to that same shape after being manipulated and "fixed" through specific thermal and stress conditions to a temporary latent shape. The recovery behaviour is related with the ability of a certain material to recover the inelastic strain energy, relaxing to the original stress-free condition [14–16]. Typically, SMMs are responsive to the presence of external stimulus, such as heat, stress, electric and magnetic fields, light or moisture [4, 12, 13]. The application of the stored strain energy resultant from the shape-memory effect into mechanical work, exerting force, is an interesting and promising usage of this mechanism [14]. Deformation and, consequently, strain energy is fixed by two means: (i) reversible morphology change caused by deformation (e.g. martensitic transformation for shape-memory alloys (SMAs); thermal or strain induced crystallization for shape-memory polymers (SMPs)) or (ii) elimination of molecular relaxation (e.g. quench through a glass transition or crystallization temperature for SMPs) [14].

The shape-memory effect has been classified into two main groups: one-way shape-memory effect and two-way shape-memory effect. One-way shape-memory effect is composed by two stages: (a) Programming and (b) Recovery. At stage (a), after the material is processed into its permanent shape, it is subsequently deformed until its temporary shape is reached and fixed. This process may consist in heating up, deforming and, then, cooling the sample. The sample exhibits its temporary shape while the permanent shape is stored. At stage (b) the shape-memory effect is triggered through exposing the sample to an external stimulus. The temperature raise above a suitable transition temperature is a very common mean of recovering the stored, permanent shape. Afterwards, to achieve solidification, it is required the sample cooling. The recovery of the transition shape is not possible. Only the permanent shape is "remembered". This complex process can be repeated in several cycles, exhibiting different temporary shapes [11, 16, 17]. Two-way shape-memory effect is defined by the capability of a material to recover the deformed shape [18]. Materials that perform two-way shape-memory effect exhibit in one cycle three different shapes, achieved by two subsequent shape changes. This effect is characterized for showing a reversible deformation behaviour in response to an on-off trigger [16, 18].

The shape-memory effect results from a combination of factors related to the structure and morphology of the material and also to the applied processing and the programming

technology [11]. Some metal alloys, ceramics and polymers have been proved to exhibit this effect [17]. Despite the macroscopic observable shape-memory response of these materials being similar, the magnitude of recoverability and performance varies greatly [13].

2.1 Shape-memory materials other than shape-memory polymers

2.1.1 Shape-memory alloys

The shape-memory effect (SME) has been studied since the 30's decade. From a chronological point of view, some of the main dates in the history of the shape memory alloys (SMAs) research will be referred. In 1932, Olander [19], a Swedish physicist, reported the solid phase transformation in SMAs and discovered the shape-memory effect in gold-cadmium (Au-Cd) alloys [1, 20]. Olander reported that Au-Cd alloys could be plastically deformed in their cold state and then recover to its original shape when exposed to high temperature [1]. This same effect was also observed by Chang and Read in 1951 [15]. In 1938, Greniger and Mooradian, achieved conclusions related to their experiments referring to SME in copper-zinc (Cu-Zn) alloys and copper-tin (Cu-Sn) alloys [1, 20]. However, only in the 60's decade, the shape-memory effect in the nickel-titanium alloys (Nitinol), the most common and important shape-memory alloy used nowadays, was discovered by Buehler et. al, at naval Ordnance Laboratory, USA [11, 20].

The shape-memory effect in alloys occurs due to the existence of two different stable crystalline structures: a high-temperature-favoured austenitic phase and a low-temperature-favoured martensitic phase [15]. In spite of being deformed in the low temperature phase, the material is capable of completely recovering its original, pre-deformed shape by the solid-solid transformation to the high temperature phase, i.e. reverse transformation, upon heating to a critical temperature (reverse transformation temperature) [1, 15, 17, 21]. The deformation may involve tension, compression, bending etc., as long as it does not exceed a critical value [17]. The deformation behaviour existing in SMAs is temperature dependent once it depends on the martensitic transformation of the material [22]. Thus, the "memory" effect results from a reversible, thermoelastic phase transformation, defined as a solid-solid transition between a crystallographically more ordered high temperature parent phase (austenite) and a crystallographically less ordered low temperature phase (martensite), which can be transformed into different "martensite variants" [1, 21, 23], as it can be seen in fig.2.1. However, the process of martensitic transformation involves not only the shape-memory effect of the material, but also the phenomena of superelasticity (SE), depending on the material's temperature.

There are three main families of SMAs, with a big commercial importance, which can incorporate two (binary system), three (ternary system) or even four components:

- Ni-Ti system alloys (NiTi, NiTiCu, NiTiFe, NiTiCo, etc.);
- Copper-based alloys (CuZn, CuSn, CuZnAl, CuAlNi, etc.);
- Iron-based alloys.

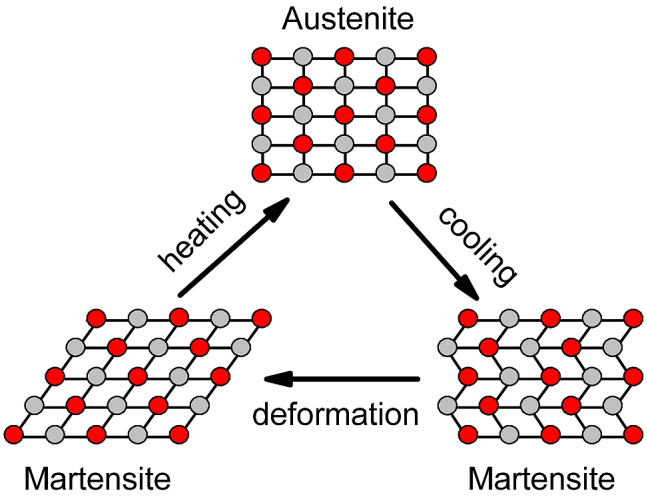

Figure 2.1: Shape-memory effect mechanism in a shape-memory alloy [24]

There are also shape-memory alloys formed by other intermetallic compounds (AuCd, TiPd, NiAl, InTi, etc.) [4, 20, 25].

The most preferable SMAs for the majority of the applications are the Ni-Ti system alloys, due to their large deformation and recovery force [1, 25, 26]. The NiTi SMA properties are summarised in table 2.1.

Although the copper-based and iron-based alloys are less expensive, easily workable in processing and commercially available, their instability, impracticability and low thermo-mechanic performance makes them rarely used. In fact, the iron-based SMAs have the weaker SME and, consequently, are mostly used as fastener/clamp for one-time actuation because of their low price [25].

Advantages and disadvantages of shape-memory alloys

SMAs are interesting materials with unique properties that allow their usage in different products and applications. The main advantages that shape-memory alloys offer are their good biocompatibility [1], high strength and modulus [4], larger attainable strain (up to 10% strain) than shape-memory ceramics and glasses (up to 1% and 0.1% strain, respectively) [2,3] and high recovery stress [5]. Although these characteristics are very appreciated in industry, there are also some drawbacks in comparison to other SME materials that disable the usage of SMAs in some areas, such as relatively small usable strain (up to 10% strain) compared to SMPs (up to 200% strain) [1, 2], low actuation frequency [1], low controllability [1], low accuracy [1], low energy efficiency [1] and higher cost, in relation to polymers or regular metals [25]. Also, SMAs can only be activated by magnetism and heat in a limited range of SMA transformation temperature [1, 3] and their processing is more difficult [3].

Table 2.1: Commercial NiTi SMA physical properties [1].

Property	Symbol	Units	Value	
			Martensite	**Austenite**
Corrosion Resistance	—	—	Similar to 300 series SS or Ti-alloy	—
Density	ρ_D	kg/m^3	6450 - 6500	
Eletrical Resistivity (aprox.)	ρ_R	$\mu\Omega$.cm	76 - 80	82 - 100
Specific heat capacity	c	J/kg.K	836.8	836.8
Thermal conductivity	k	W/m.K	8.6 - 10	18
Thermal expansion coefficient	α	m/m K^{-1}	6.6×10^{-6}	11×10^{-6}
Ultimate Tensile Strength	σ_{UTS}	MPa	895 (fully annealed) 1900 (hardened)	
Elastic modulus (aprox.)	E	GPa	28 - 41	75 - 83
Yield strength	σ_Y	MPa	70 - 140	195 - 690
Poisson's ratio	ν	—	0.33	
Magnetic susceptibility	χ	μEMU.g	2.5	3.8

Applications of shape-memory alloys

SMAs applications are frequently classified into four categories: free recovery, constrained recovery, work production (actuators) and superelasticity [2].

Free recovery: Existing in applications in which the only purpose of the memory effect is to origin motion or strain. For example, to cool a wire into the martensitic phase, then bend it to a new shape and, at last, heat it until it recovers its original permanent shape.

Constrained recovery: An application in which the memory element is hindered of changing its shape, and consequently, originates stress.

Actuator or work production applications: This is the class of applications that produce work through movement of the SMA against a stress. This situation is exemplified in a spring or wire that lifts a weight when heated and, possibly, drops the weight when cooled. The actuators can be classified as:

- Thermal: Actuators that operate through changes in room temperature;
- Electrical: Actuators that are actuated via direct current.

Superelastic or Pseudoelastic applications: These are isothermal applications that result in potential energy storage. The memory element is able to work as a "superspring". However, the temperature range in which SMAs exhibit this effect is small (usually only 80°C).

Practically, the real applications existing for a SMA are subdivided into the following groups:

- Automotive applications

  The mechanical simplicity, compactness (which leads to lighter, small scale, less expensive mechanical compounds) and higher performance makes the SMAs actuators

a good alternative to electromagnetic actuators. As an example there are in the automotive industry SMA activated automotive tumble flaps, automotive pedestrian protection system, cost effective side mirror actuators, micro-scanner system for optical sensing of the object's distance [1,23];

- Biomedical applications

  Ni-Ti alloys are widely used for biomedical purposes. Their biocompatibility, high corrosion resistance and non-magnetic unique physical properties, that allow this SMA to be used as a human tissue or bone, and superelasticity, which is suitable with the stress-strain behaviour of human bones and tendons, enables the response of this actuator at human body temperature. Although stainless steel is a less expensive material, NiTi alloys are frequently preferred.

  E.g.: endodontics, medical tweezers, stents, eyeglass frames, guide wires, sutures, implants and prostheses, anchors for attaching tendon to bone, etc. [1,23];

- Robotic applications

  This variety of applications involve micro-actuators, grippers, parallel manipulators and medical robotics, such as the creation of artificial muscles, artificial limbs, etc. [1];

- Industrial applications

  This area concerns products such as fasteners, seals, connectors, clamps, etc. [21];

- Aerospace applications

  Applications involving actuators, structural connectors, vibration dampers, deployment of antennas, release or deployment mechanisms, inflatable structures, manipulators, etc. [1,23];

- Consumer products

  SMAs used in goods such as rice cookers, coffee makers, air conditioners, watch-making, etc. [22,23];

- Aeronautics applications

  Technology used to filter out harmful frequencies, to reduce noise, etc. [23].

2.1.2 Shape-memory ceramics

Similarly SMAs, the shape-memory ceramics exhibit martensitic transformations which are responsible for the shape-memory effect and superelasticity exhibited by these ceramics [27].

Some of the most important shape-memory ceramics are: aluminium silicate (Al_2SiO_5), calcium silicate (Ca_2SiO_4), magnesium silicate (Mg_2SiO_4), zirconium dioxide (ZrO_2) and zinc sulfide (ZnS) [27].

Advantages and disadvantages of shape-memory ceramics

Shape-memory ceramics are a class of smart materials that present a range of properties different from shape-memory alloys. One of the most interesting advantages exhibited by shape-memory ceramics is their very high strength, which implies much higher stresses to

induce superelasticity. As it can be seen in fig.2.2, zirconia requires much higher stresses to induce the transformation, ≈ 1.7 GPa, than the SMAs, which only need several hundred MPa. These large stresses required to drive the shape-memory effect in shape-memory ceramics are expected to translate into large output stresses. Also, shape-memory ceramics detain an excellent combination of actuation stress and strain, generating an energy density of approximately 100 MJ/m^3. This energy density surpasses the ones from shape-memory alloys and even some of the multi-component actuator systems. Another advantage of shape-memory ceramics is related to the high operating temperatures of these materials, with ceramics being more refractory than metals. This way they can be used in high temperature applications. However, these materials present some drawbacks, such as their low attainable recovery stress, which is usually lower than 4% and their very high price. Also the non biodegradability of ceramics makes these materials non environmentally friendly [27].

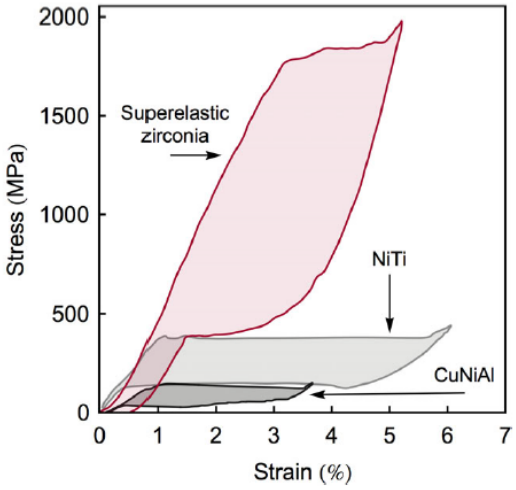

Figure 2.2: Stress-strain curves for zirconia micro-pillars and shape-memory metals, Ni-Ti and Cu-Ni-Al. [27]

Applications of shape-memory ceramics

Shape-memory ceramics are suitable for energy damping applications and actuators, due to their high output stresses. The aerospace and automotive field are also engineering areas where the shape-memory ceramics are able to be used due to their high operating temperature [27]. Nonetheless, this class of materials is not very used in industry.

2.2 Shape-Memory Polymers

Shape-memory polymers (SMPs) have been known since mid-1980s and studied by the scientific community due to their extraordinary behaviour when exposed to external stimulus such as temperature, light, electricity, magnetism, pH, etc [28–30]. Tailoring the properties of SMPs may be exploited by industry in order to develop interesting technological solutions to perform unique functions [28].

The return to the permanent, original shape of a SMP can be achieved through exposure to diverse external stimuli, such as heat, light, magnetic field, electricity, solution, etc. Depending

on which one of these triggers causes the shape-memory response, polymers can be classified, respectively, as thermo-responsive, photo-responsive, magneto-responsive, electro-responsive and chemo-responsive [28, 33]. The use of these triggers in SMPs causes a mechanical action that enables the recovery of large strains caused by deformation of the material [33, 35]. To enable the shape-memory effect, it is necessary a combination of a suitable polymer molecular architecture and polymer morphology together with a tailored processing and a particular programming procedure [3, 5, 11, 36].

2.2.1 Shape-Memory Polymer's molecular architecture

Shape-memory polymers are elastic materials which are chemically considered phase-segregated linear block copolymers composed by at least two separated phases: a hard one and a soft one [3, 9, 11, 25, 29, 31]. The mechanism which is responsible for the shape-memory effect in polymers lies in this dual-domain system composed by a hard (elastic) segment and a soft (transition) segment [25, 29]. In the polymer networks, the hard segments are strong chemical or physical crosslinks exhibiting the highest transition temperature (T_{perm}) and providing the mechanical strength of the material, especially at temperatures lower than T_{perm}. The hard segments behave as netpoints, responsible for the permanent shape of the SMP [3,5,9,11,29,31,36,37]. These netpoints are connected by chain segments, named soft segments, which possess the lower transition temperature (T_{trans}) in the polymer network and act as the reversible phase, determining the deformed shape. These soft segments may be ductile or stiff depending if an appropriate trigger is presented. They act as "molecular switches", fixing the temporary shape below transition temperature and losing rigidity when at or above transition temperature. Thus, they are also called switching domains. In order to obtain the necessary deformability, the switching domains must allow a certain orientation upon loading. Deformability is a factor that increases with the increasing length and flexibility of the chain segments [5, 9, 12, 25, 29, 31, 31, 36–38]. In fig.2.3 it is sketched the molecular mechanism of thermally induced shape-memory effect in SMPs.

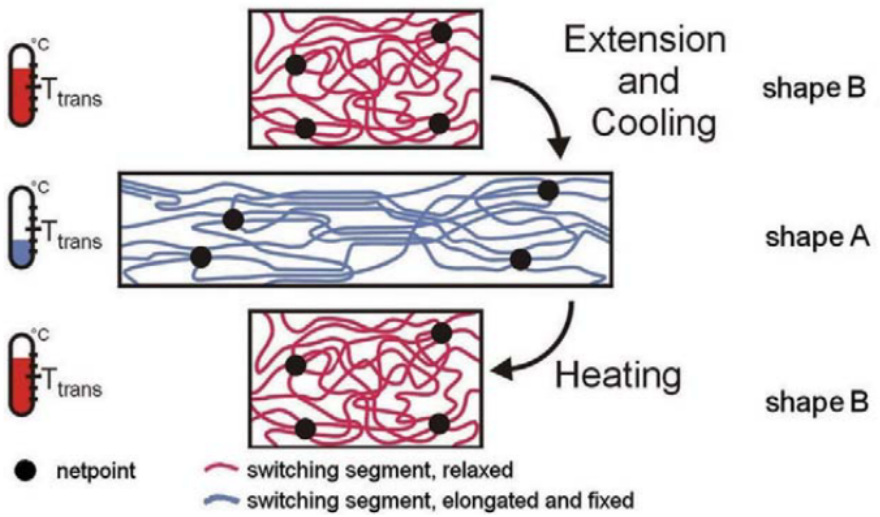

Figure 2.3: Molecular mechanism of the thermally induced shape-memory effect [31]

As already mentioned, the network architecture of SMPs is constituted by crosslinking netpoints connecting each other through polymer segments. SMPs structure, on the basis of the nature of the crosslinks, can be either classified as chemically (or covalently) crosslinked or as physically crosslinked [3,5,9,15,36,39,40].

Chemically crosslinked SMPs, known as shape-memory thermosets, are characterized by the strong covalent bonding between polymer chains, more stable than the connection existent in physical crosslinking, and their irreversible nature. Once cured, they can no longer be melted for recycling. The chemical bonding, which is created by reaction of two functional groups, makes these crosslinks very strong and, thus, difficult to break [3, 5, 9, 33, 36, 39, 41–43]. Physically crosslinked SMPs, called shape-memory thermoplastics, are a blend of linear polymer chains interconnected by physical crosslinks, behaving as hard segments [41]. In consequence of being physically formed, these hard segments are weaker than covalent crosslinks and therefore are reversible (which means that the polymers can be melted or dissolved in certain solutions) allowing the reconfiguration of the SMP permanent shape, contrarily to what occurs in thermosets. Both physically and covalently crosslinked SMPs can be either amorphous or semi-crystalline. [3,5,9,33,36,38,39,41,42].

In fig.2.4 it is represented the structural difference between physical and chemical crosslinking.

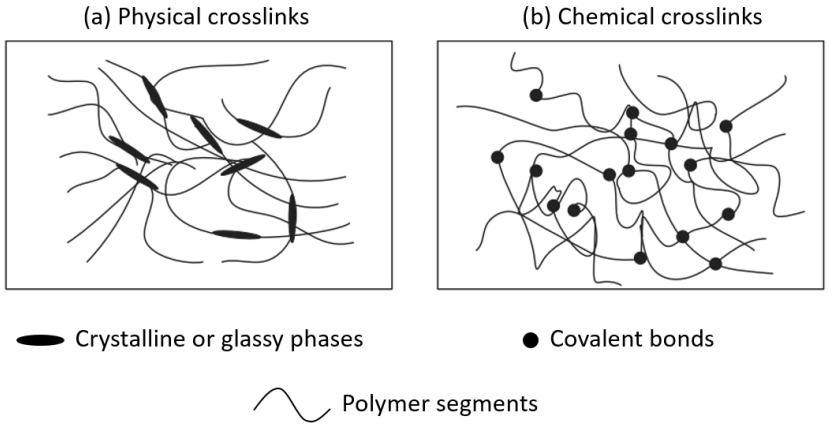

Figure 2.4: Illustration of the two shape-memory polymers crosslinking networks: (a)Physically crosslinked network and (b) Chemically crosslinked network [3]

On the basis of the nature of the switching segments, temporary networks are formed through vitrification, melting or other physical interaction that is reversible with temperature. Both melting temperature (T_m) of the crystalline segment and glass transition temperature (T_g) of the amorphous segment may be used as transition temperature (T_{trans}). However, melting temperature is usually preferred over glass transition temperature because of its sharpest transition, which provides a more determined polymer shape recovery temperature Therefore, SMPs network chains are typically divided into two classes: SMPs with crystalline switching segments ($T_{trans} = T_m$) and SMPs with amorphous switching segments ($T_{trans} = T_g$). [3,5,11,12,15,36,39,40,42,44,45].

Based in the SMPs classifications according to the nature of the permanent netpoints and the nature of the thermal transition related to the switching segments, SMPs can be designated by the following four classes [15]:

- Class I: Chemically crosslinked amorphous polymers ($T_{trans} = T_g$) [12, 15];
- Class II: Chemically crosslinked semi-crystalline polymer networks ($T_{trans} = T_m$) [12,15];
- Class III: Physically crosslinked thermoplastics ($T_{trans} = T_g$) [12, 15];
- Class IV: Physically crosslinked thermoplastics ($T_{trans} = T_m$) [12,15];

2.2.2 Shape-Memory effect mechanism in Shape-Memory Polymers

Macroscopic

The shape-memory behaviour in polymers is characterized by the fixation of a temporary programmed shape followed by the return to the original permanent shape by exposure to a specific environmental trigger [11, 46]. The temporary shape remains stable until an appropriate external stimuli is applied [5, 36]. From a simplistic point of view, this shape change is the result of the entropy-driven recovery of the imposed mechanical deformation, caused by the application of an external stress, temporarily fixed by formation of physical crosslinks and occurs around the material thermal transition [5, 36, 38, 47].

Contrarily to what happens in SMAs, which possess a highly predicable shape-memory mechanism related to reversible martensitic transformation, the SMPs exhibit a SME resulting from a dual-segment system composed by hard segments which determine the permanent shape and soft switching segments, with a certain transition temperature (T_{trans}), which determine the temporary transition shape [3,48]. Below T_{trans} polymers are stiff, while above T_{trans} they become relatively soft and, as consequence, they can be deformed [3, 11, 29, 49, 50].

A typical shape-memory thermo-mechanical cycle is composed by the following steps [31, 51, 52]:

1. Deformation of the polymer at a temperature (T_{high}) above transition temperature (T_{trans}), but below the highest transition temperature (T_{perm}), i.e. $T_{trans} < T_{high} < T_{perm}$;
2. Application of strain, constraining the sample shape, and coolling below transition temperature, $T_{low} < T_{trans}$;
3. After cooling, remove the strain;
4. Heating the sample above transition temperature, $T_{high} > T_{trans}$, to return to the original shape.

So, first of all, the material must be conventionally processed (compression, extrusion, injection molding, etc.) in order to obtain its permanent, desired shape. Afterwards occurs the programming process, which includes steps 1, 2 and 3 described previously. The latter, step 3, when the sample is unloaded after being cooled, is called Shape Fixity [11,12,20,28,33,35,37,49, 53]. Shape Fixity can also be obtained through cold drawing, i.e. drawing the sample at a low temperature. Now, the sample exhibits its temporary shape and keeps the permanent shape stored [11]. After programming is completed, shape recovery takes place. Upon reheating the sample to a temperature higher than T_{trans}, the stored mechanical strain is released and the material can return back to its original shape (step 4). The sample is able to keep its permanent shape until further programming occurs again [11, 12, 20, 28, 32, 33, 35, 37, 45, 49, 53].

The process explained above is called One-Way Shape-Memory Effect, in which recovery of the permanent shape can be observed but the return to the temporary shape does not occur [11]. The main steps of this process are represented in fig.2.5.

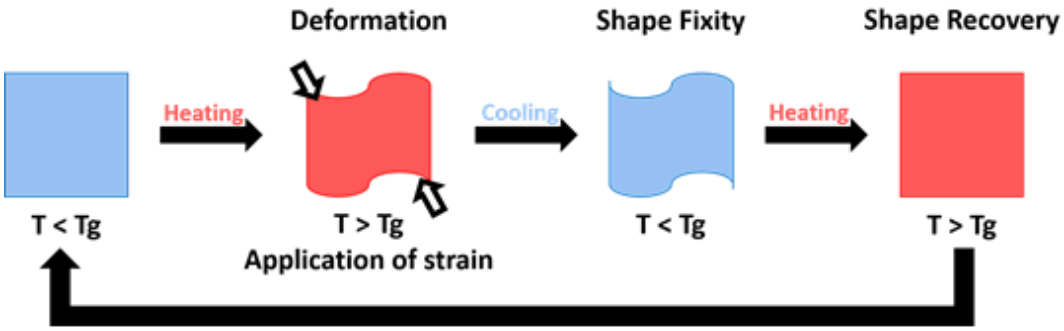

Figure 2.5: Schematic representation of shape-memory effect with four steps: (1) memorized shape after molding and cooling; (2) free deformation due to the rubber elasticity of the amorphous portion by heating over T_g and under an applied force; (3) shape fixity by cooling below T_g; and (4) shape recovery by heating over T_g under free load condition

Molecular

To a better understanding of what happens and can be observed at a macroscopic level it is important to explore the microscopic underlying mechanisms.

At low temperatures, both hard (elastic) and soft (transition) segments are rigid. When heated above the transition temperature of the switching domains (T_{trans}), that can be the glass transition temperature (T_g) or the melting temperature (T_m), but below the transition temperature of the hard segments (T_{perm}) the transition segment becomes soft, flexible and easy to deform, contrarily to the hard segments, which hold the polymer's permanent shape. The material enters a rubbery elastic state in which the polymer chains display a random coil arrangement, which corresponds to the state of highest entropy. At this point, the material is deformed to a certain strain and the polymer chains become oriented in a certain way due to the imposed stress and loose entropy. When cooled to a temperature below T_{trans}, the polymer adopts a rigid, glassy state. The flexibility of the constituent chain segments is limited or even non-existent. The hardening of the transition segment is triggered and, therefore, the temporary shape is fixed [9, 12, 31, 35, 36, 38, 54, 55]. The fixation of the deformed shape during cooling, which leads to the solidification of the switching domains, and the formation of additional reversible physical netpoints enable the maintenance of the temporary shape even after unloading. Upon unconstrained reheating above transition temperature, the transition segment becomes soft again, as consequence of cleavage of physical crosslinks in the switching phase. Consequently, they lose their ability to hold the elastic segment in place. At this stage, the chain segments regain their mobility and entropy and, therefore, the stored energy is released, resulting in recovery of the original, permanent shape [5, 9, 12, 31, 35, 36, 54, 55].

2.2.3 Advantages and disadvantages of Shape-Memory Polymers

Shape-memory polymers have been widely studied in the last decades and implemented in industry. Exhibiting shape-memory effect as well as SMAs, it is now considered strong competition to the latter class of materials.

The main advantages of SMPs compiled from various bibliography are the following: good biocompatibility [15, 20, 25, 55, 56]; potential biodegradability [15, 25, 56]; low density (0.9-1.3 g/cm^3) in comparison to SMAs (6 - 8 g/cm^3, 6.4-6.5 g/cm^3 for NiTi) and SM ceramics ($\sim$ 2 g/cm^3); light weight [5, 25, 37, 55]; operability over a broad range of temperature [10, 15]; easier processing than SMAs and PTZs (applicable to molding, extrusion and CNC) [3, 5, 10, 15, 30, 57, 58]; higher elastic deformations (up to 200%) than SMAs and PZTs [10, 15, 56]; lower processing/material cost than SMAs, shape-memory ceramics and piezoelectric materials [3,5,10,13,15,25,30,32,55,58]; their SME can be triggered not only by heat or magnetism (like SMAs) but also by light, electric fields, irradiation and pH changes [10, 25, 59]; substantially higher recoverable strains (up to 800%) than SMAs (less than 10%) and SM ceramics (less than 1%) [3,5,13,25,37,55]; large reversible changes of elastic modulus (as high as 500 times) are possible between the glassy and rubbery states [55]; excellent chemical resistance, since SMPs cannot be dissolved in any acid or base [60]; easier tailoring of the material properties (tune the switching temperature or stiffness through variation of structural parameters) than in SMAs [3, 5, 10, 15, 25, 32, 56].

On the other hand, it must be mentioned some known disadvantages of this type of shape-memory material (SMM), such as: low mechanical strength, ranging from 5 MPa to 100 MPa [4,9]; low elastic modulus [10,57]; low stiffness compared to metals and ceramics [13,53]; low recovery stress/force (1-3 MPa against 150-300 MPa for SMA) [4, 9, 10, 15, 53, 55, 57]; long response time, in the order of seconds, in comparison with the tens of ms for SMAs [10,57]; low achievable number of cycles [10]; harder to achieve large scale production of polymers without additives, which may compromise the biocompatibility in long term implantation [20];

2.2.4 Applications of Shape-Memory Polymers

Once SMPs have been discovered, their usage in industry has been broaden over the years. Their potential to surpass SMAs in shape-memory materials' applications is high and, due to their several advantages, SMPs have been applied in the following fields:

- Biomedical devices : Shape changing polymeric medical devices can be surgically placed in a temporary compact shape through a small incision and later triggered (heating to body temperature) to adopt a different permanent geometry relevant to their application [5,29,36,38]; Examples of biomedical applications for shape-memory polymers are: blood vessel stents [3,15,18,20,29,35,40,47,54,61,62], catheters (in the exterior of the body are stiff for an accurate manipulation by the physician, but when placed inside of the human body become softer and more comfortable) [15,55,61], implants [11,29,36,38,54], medical devices used in minimally invasive surgery [29,30,36,38,61], scaffolds for engineering new organs (tissue engineering) [20,61], intravenous needles that soften in the body [14,35,61], biodegradable sutures [15,40,54,63], biosensors [35], artificial muscles [40], orthopaedic braces and splints [55] and orthodontic wire [64].

  When medical devices, such as stents, are made of SMP material a second surgery to remove the SMP is avoided since the polymer can gradually dissolve in the body over

time [5, 11, 20, 36, 54]. In comparison with SMA, SMP exhibit properties closer to those of soft tissue [20];

- Textiles [5, 9, 14, 35, 36, 40, 54, 56, 65–68];
    1. Intelligent waterproof, breathable fabrics - Smart fabrics which are able to control the humidity between the body and the textile. At low temperatures, the fabrics are less permeable and retain body heat. At high temperatures, the fabrics moisture permeability increases and heat is released [5, 14].
    2. Room partition and wall hanging [35];
- Actuators [3, 15, 28, 33, 35, 40, 54];
- Temperature sensors [3, 15, 40] [30, 33, 35];
- Coatings, such as self-peeling reversible adhesive based on epoxy SMP that, when combined with a pressure-sensitive adhesive, reveals features similar to those of a gecko foot [28, 35];
- Cable applications (Heat shrinkable tubes) [5, 15, 28, 35];
- Micro-grippers - Use of SMP-based micro-grippers in industrial applications where objects must be manipulated in unreachable locations (e.g. complex machinery or microsystem assembly) [53];
- Packaging (such as packaging of thermal sensitive products) [3, 5, 35, 36];
- Aerospace applications - SMPs allow the self-deploying movement and avoid the use of any battery or source of energy for the deployment, representing a large reduction of weight [5, 35]; Examples of aerospace applications for SMPs are: self-deploying solar sails [5, 35, 54, 65], antenna for satellites [3, 5, 54], nano-rover wheels to dislocations in Mars [35, 54], spring-lock truss elements for large boom structures [3, 35], mirrors and reflectors [3] and morphing aircraft, which allow the internal structure to change shape and/or configuration [3, 35, 54, 65].
- Automobile engines, such as choke system [5, 11], self-disassembling fasteners [5, 9] and self-repairing auto bodies [35] [3].
- Smart toys [3, 5, 33, 66];
- Cutlery for handicapped people (e.g. specially designed spoon handle) [5, 35, 55];
- Rewritable digital storage media / Media recorders / Information storage that can allow thermally reversible recording [14, 15];
- Braille thin paper made of SMP (easy to erase errors through usage of a point heater) [54];
- Active assembly (e.g. SMP screws one-for-all solutions for a range of different sized holes) [54];
- Recreation/Sport products, such as tents, water and snow skis, surf and snow boards, life jacket [3];

- Food equipment, such as dishes and meal containers and hot/cold storage for food [3];

- Self-healing systems – Structures composed by piezo-electric monitoring system and SMPs activation systems. Upon damaging, the monitoring system identifies the location and magnitude of damage and SMPs are then resistively heated at the location of damage, repairing it [3].

2.2.5 Shape-memory polyurethanes

Shape-memory polyurethane (SMPU) is defined as a stimuli-sensitive multiblock copolymer composed by two alternating elements: hard segments (urethane), responsible for the physical crosslinking and fixing of the permanent shape, and soft segments (polyester or polyether diol), which enable the SME and the fixation of the temporary shape [4,5,12,20,30]. In fig.2.6 it is illustrated a schematic representation of the structure of the SMPU elastomer. Due to its SM properties, polyurethane has the ability to change its shape at a temperature above its transition temperature [12].

SMPUs have a wide field of applications due to their ample degree of freedom in property design, which allows SMPU to be crystalline or amorphous, depending on the molecular design, and providing a broad range of actuation temperatures between -20°C and 150°C. The design variables include different types and molecular weights of soft segments, different types of hard segments and different soft segment/hard segment composition [66].

The main characteristics of SMPUs are the ones mentioned below. SMPUs are thermoplastic materials and, although they exhibit excellent shape-memory properties, it can be noticed a reduction in the shape-memory performance over the repetition of the thermomechanical cycles [5, 35]. They present recovery strain up to 400% [20], actuation temperatures ranging from -20°C to 150°C [66], tailorable switching temperature through variation of soft segment content or molecular weight [12], high versatility [30], low thermal conductivity [35], high thermal-expansion coefficient [35] and excellent chemical properties, since SMPUs do not dissolve in any acid or base [4]. Also, SMPUs can be molded by injection, extrusion and blowing, similarly to conventional plastics [51] and can be coloured to any colour, since it is transparent [51]. The relative ease of preparation [30, 35] and low cost [35] of SMPUs are also major advantages for implementation in industry. Their high biocompatibility and ability to soften at body temperature make them very desirable as biomaterials [39, 69].

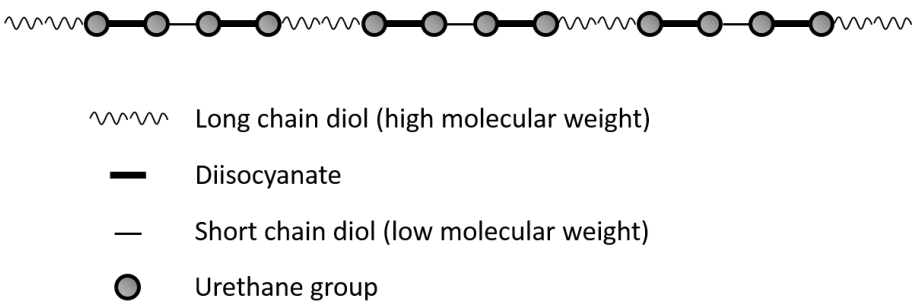

Figure 2.6: Illustration of the PU elastomer structure constituted by hard and soft domains. Adapted from [70]

2.2.6 Comparison between Shape-Memory Materials

In table 2.2 it is possible to compare the main properties of the more relevant shape-memory materials: shape-memory polymers, shape-memory alloys and shape-memory ceramics.

Table 2.2: Comparison of the main properties of shape-memory materials [3–5,15,20,51,58,71].

	SMPs	**SMAs**	**SMCs**
Density (g/cm^3)	0.9 - 1.3	6 - 8 (6.4 - 6.5 for NiTi)	2
State at low temperature	Hard	Soft	—
State at high temperature	Soft	Hard	—
Phase transformation	Glass transition or Melt	Martensitic	Ferroelastic
Shaping	Easy	Difficult	—
Critical temperatures (°C)	-10 - 100	-10 - 100	—
Transition temperatures (°C)	10 - 50	5 - 30	300
Processing conditions	$<$200 °C, low pressure	$>$1000 °C, high pressure	High temperature
E at T $<$Ttrans (GPa)	0.01 - 3	83 (NiTi)	—
E at T $>$Ttrans (GPa)	(0.1 - 10) $\times$ 10^{-3}	28 - 41	—
Stress required for deformation (MPa)	1 - 3	50 - 200	—
Recovery stress (MPa)	1 - 5	150 - 750	—
Recovery strain (%)	$>$400% (Typ. go up to 800%)	$<$10%	$<$4%
Recovery time	$<$1 s - several min	$<$1 s	—
Thermal conductivity (W/m.K)	0.15 - 0.30	18 (NiTi)	—
Biocompatibility and Biodegradability	Can be biocompatible and/or biodegradable	Can be biocompatible Not degradable	Can be biocompatible Not degradable
Corrosion performance	Excellent	Excellent	—
Cost (€/kg)	$<$20	$\sim$ 300	$>$500

* E - Elastic modulus

2.3 Shape-Memory Polymer Composites

Shape-memory polymer composites (SMPCs) have been studied as an alternative to neat SMPs, since they may exhibit large enhancements in thermo-mechanical properties in relation to the neat polymer matrix [5]. SMPCs are defined as a combination of two or more materials with different physical and chemical properties and a distinguishable interface. There are three main constituents in any composite: the continuous phase, called polymer matrix, the dispersed phase, formed by the micro/nano-sized reinforcement fillers (i.e. particles, fibers, platelets or tubes), and the interfacial region, responsible for the linkage between the matrix and the filler [5,72,73]. The polymer matrix may be an amorphous or crystalline thermoplastic material or a crosslinked polymer network. The function of the matrix is to hold and attach the fillers together and protect them from damage by distributing any stress through the whole body. The addition of small amounts of filler can cause an improvement in the material properties, such as modulus, strength, heat resistance, flame retardancy and lowered gas permeability [5]. Also, polymer composites can gain novel functions, such as electrical [14, 56, 74–78], magnetic [79–81] and optical [82–84] functions and biofunctionality [85,86]. The interfacial interaction between the polymer matrix and fillers, as well as the formation of a network of interconnected filler particles, causes the enhancement of material properties [5]. That happens because the addition of a filler into a polymeric matrix causes the modification of the SMP thermomechanical behavior [3].

SMPCs can widen the range of application of SMPs due to the variety of fillers that can be used (such as silica [30, 53, 87], carbon [75, 77, 78], iron [81, 88] , etc.) to reinforce the polymeric matrix, which can include conductive inclusions that enable thermo-response by Joule heating, electric and magnetic fillers that enable inductive heating by dissipation through hysteresis upon applying an alternating magnetic/electric field, and even fillers responsive to radiation [25].

Fillers can be classified either by their size or by their geometry. According to this two parameters, fillers can be divided into three categories: (i) particles (e.g. silica, metal, other organic and inorganic particles), (ii) layered materials (e.g. graphite and layered silicate) and (iii) fibers (e.g. nanofibers and single-walled and multi-walled nanotubes) [5], as represented in fig.2.7.

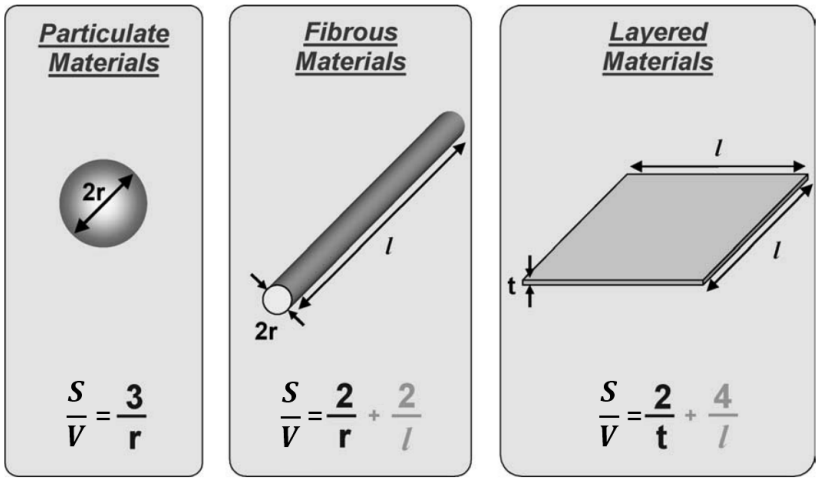

Figure 2.7: Surface area/Volume relations for different filler geometries [89]

The size of the filler influences the behavior and properties of the obtained composite and, therefore, SMPCs filled with nanometric, micrometric or macrometric fillers have different properties. It has been verified that the reduction of the size of the particle filler induces the enhancement of the thermomechanical properties of the composite through the increase of the matrix-filler contact area. This effect may be provided upon usage of nano-sized fillers [5].

Depending on the particle size, shape, specific area and chemical nature, nanoparticles can modify the following polymer matrix properties: electrical conductivity, thermal conductivity, mechanical properties, flame retardancy, density, physical properties (such as optic, magnetic or dielectric properties) [90].

2.3.1 Nanoparticles

Nanoparticles are defined as particles with diameter below micron dimension, generally below 100 nm. The decrease of the dimensions of the particle, increases the surface/volume ratio and become surface properties more important, influencing agglomeration behavior, i.e. clustering, and interfacial and physical properties [90].

Nanoparticles are classified according to their dimensional morphology as [72]:

1. Zero dimensional (e.g. nanoparticles, such as SiC, Fe_3O_4, Al_2O_3, ZnO, SiO_2)
2. One dimensional (e.g. nanotubes and nanowires, such as CNTs, Carbon fiber, NiTi fiber)
3. Two dimensional (e.g. silicate layers, graphene)
4. Three dimensional (e.g. zeolites)

In fig.2.8 is illustrated the several morphological classifications of nanoparticles referred above.

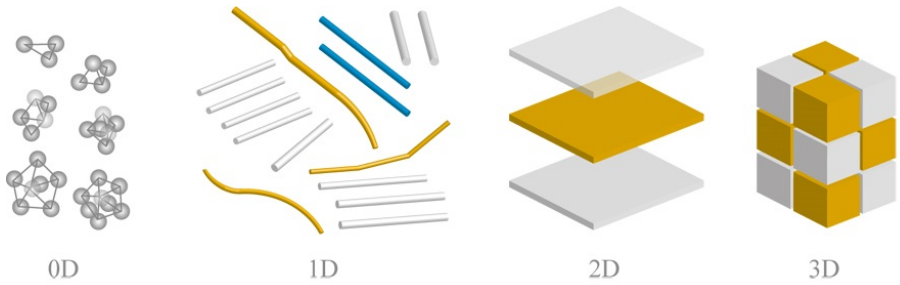

Figure 2.8: Morphological classification of the nanoparticles [91].

Nanofillers, such as tubes (e.g. single-walled carbon nanotubes and multi-walled carbon nanotubes) or plates (e.g. exfoliated graphite, layered silicates), possess a set of characteristics related to their nanometric properties and extreme aspect ratios which are distinguishable from the classic filled composites. The most relevant are: low percolation threshold (approximately 0.1- 2 vol.%); particle-particle correlation (orientation and position) arising at low volume fractions ($\phi_i < 0.001$); large number density of particles per particle volume (10^6 - 10^8 particles/μm^3); extensive interfacial area per volume of particles (10^3 - 10^4 m^2/mL); short distances between particles (10-50 nm at $\phi \sim 1-8$ vol. %); comparable size scales among the rigid nanoparticle inclusion, distance between particles, and the relaxation volume of polymer

chains [73]. These features make one and two dimensional nanomaterials extremely attractive, since their incorporation in a polymeric matrix improves SMPs mechanical properties, such as stiffness and shape-memory recovery stress [53, 92].

The main characteristics and particularities of two of the most used and promising nanofillers employed in nanocomposites are addressed in subsections 2.3.1 and 2.3.1.

Graphene

Graphene is defined as a single hexagonal atomic layer of sp^2 hybridized carbon exhibiting a two-dimensional sheet-like structure [54, 93–96]. It was first produced in 2004 by Novoselov and Geim [97] in the University of Manchester. In fig.2.9 it can be observed the structural model of graphene.

Graphene was considered one of the strongest and thinnest materials developed so far and is available as nanofiller in its original single-sheet structure and as a multi-sheet structure, known as graphene nanoplatelets (GNPs). The latter structure can be defined as a nanoscale platelet formed by two or more layers of graphene. The platelet thickness ranges from less than 0.34 to 100 nm [93, 98, 99]. Should also be noted the distinction between graphene and graphite, which is based on the number of layers in the structure. Basically, graphite is a structure made up of hundreds of graphene layers [100]. The cohesion between graphene sheets in graphite platelets and weak van der Waal binding between graphene and the polymer matrix greatly prohibit the load transfer, distribution and consequently, application of graphite in high-performance nanocomposites [95].

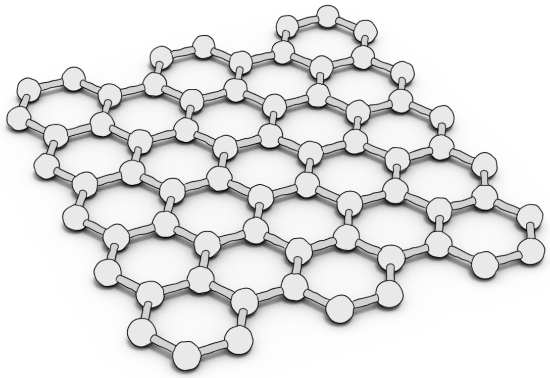

Figure 2.9: Structural model of graphene [101]

Graphene possesses outstanding properties which are dependent of its morphology and atomic structure [95], such as: exceptional electrical conductivity [54, 93, 94, 102] and thermal conductivity ($\sim$ 5000 W/m.s) [93–95, 102]; excellent thermal stability [93, 95]; excellent structural stability [95]; low density [95, 99]; high surface area (theoretically 2630 - 2695 m^2/g) [54, 93, 94, 99, 103]; high tensile strength [93, 94, 102]; high elastic modulus ($\sim$ 1.1 TPa) [95, 99]; high stiffness [95]; large elasticity [94]; high intrinsic mobility (estimated to be $\sim 2 \times 10^5$ cm^2/V.s; however in literature ranges from $\sim 10^2$ to 10^4 cm^2/V.s) [95]; transparency [94]; biocompatibility and non-toxicity [54, 95]; easy synthesis [95]. However, its easy re-agglomeration capability [95, 96, 104] is something to take into account when producing nanocomposites.

Graphene oxide (GO) consists of oxygenated functional groups, such as carboxyl, hydroxyl and epoxy, connected to the basal plane and edges of the graphene sheets and it is obtained from the exhaustive oxidation of graphite [93, 95, 105, 106]. GO is hydrophilic, i.e. can be easily dispersed in water, forming a stable colloidal suspension [93, 98, 106]. However, GO cannot be exfoliated in inorganic solvents [93]. GO has some advantages relatively to pristine graphene and graphite. The formation of GO expands the interlayer distances in graphite and provides effective interaction between the functional groups in GO and those in the polymer, preventing re-aggregation. On the other side, the formation of hydrogen bonds, metal-mediated bonds or polymerization between the graphene oxide sheets and the polymer improve the properties and cohesion of the composite and allows cheap fabrication [95]. However, GO is generally insulated due to its large quantity of functional groups. The lack not only of electrical conductivity but also of thermal conductivity determine GO as a non-multifunctional nanofiller [95, 96].

Carbon Nanotubes

Since their discovery by Ijima in 1991 [107], carbon nanotubes (CNTs) have been widely studied in the past decades as a promising engineering material. Their structure can be described as cylindrically rolled sheets of an hexagonal array of carbon atoms taking a cylindrical shape with a diameter that can range from a few Angstroms to several tens of nanometers [29, 100, 108]. These structures can be composed by a single carbon nanotube (SWNT) or by multiples carbon nanotubes (MWNT), as represented in fig.2.10 [109].

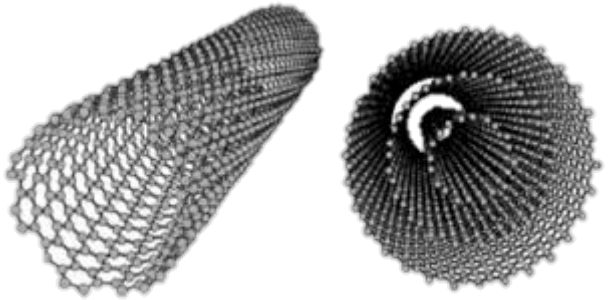

Figure 2.10: Structural model of carbon nanotubes (CNTs): in the left is represented a single-walled carbon nanotube (SWNT) and in the right is represented a multi-walled carbon nanotube (MWNT). (Adapted from [110])

Single-walled nanotubes (SWNTs) are carbon nanotubes constituted by a single rolled graphene sheet. The diameter of the individual tubes is small (typically $\sim$ 1nm) and their length can go up to 1 cm. The density of SWNTs goes from $\sim$ 1.33 to 1.40 g/cm^3. These structures are characterized for being curled and looped instead of straight [54, 100, 109, 111, 112]. Depending on their chirality (i.e. the way the single graphene layer is rolled-up), SWNTs may be insulating or metallic [113]. SWNT elastic modulus is comparable to that of diamond and its tensile strength is even higher than the one from high-strength steel [54]. The electric current density of SWNT is $\sim 1 \times 10^9$ Amp/cm^2, which is 1000 times bigger than that of copper ($\sim 1 \times 10^6$ Amp/cm^2). Thermal conductivity is predicted to be 6000 W/m.K at room temperature, which is almost the double of diamond's thermal conductivity ($\sim$ 3320

W/m.K). SWNTs are characterized for being stable up to 2800 °C in vacuum and up to 750 °C in air [54].

Multi-walled nanotubes (MWNTs) are defined as carbon nanotubes composed by at least two concentric graphene cylindrical layers separated by a distance of 0.35 nm. Basically, MWNTs are concentric single-walled nanotubes [100, 111, 112]. The connection between different nanotubes occurs due to the existence of weak van der Waals forces within these structures [100]. The MWNTs dimensions are variable. The length may range from few tens of nanometers to several microns, while the outer diameter can go from 2 to 100 nm. Virtually all the tubes are closed at both ends with caps containing pentagonal carbon rings [100, 109, 111, 112]. Besides, MWNTs are always conductive [113].

The increasing attention received by these structures is due to their outstanding characteristics, such as: excellent electrical conductivity [58, 114], which gives them the extraordinary ability to create electrically conductive networks (percolation paths) inside the SMPs (lower electric percolation threshold than that from other commonly used fillers; can range from 0.001 to more than 10 wt.%) [5, 54, 109, 113]; excellent thermal conductivity ($\sim$ 3000 W/m.K along the tube axis) [58, 114, 115]; thermal stability [58]; very low density [113, 114]; high aspect ratio (100 to 10000) [54, 100, 113–116]; wide contact surface with the matrix [113]; high tensile strength (10 GPa - 500 GPa) [58,108,113,114]; high elastic modulus (270 GPa - 1TPa) [58,108,114,116]; high hardness (nearly as hard as diamond) [114]; excellent flexibility [113]; chemical stability [100].

However, the use of particles with such incredibly small dimensions leads to some issues, such as clustering. The size, geometry, structural and physical properties of the carbon nanotubes as well as their concentration in the polymer are key factors that greatly influence the distribution and dispersion of the filler, the interaction with the polymer matrix and, consequently, its performance [100, 108, 113]. Clustering is in the nature of CNTs since they are strongly affected by extensive non-covalent attractive forces between nanotubes, known as van der Waals forces, which lead to the occurrence of aggregation and formation of bundles. Aggregation is undesirable since it may cause low dispersion within the polymeric matrix, resulting in the weakening of the overall properties of the nanocomposite. However, clustering can be controlled by the creation of specific reactions between the polymeric matrix and the fillers, providing new mechanical properties to the nanocomposite [76, 87, 100, 116, 117]. There are some methods that provide a high dispersion of CNTs and strong interfacial bonding between the filler and the polymer matrix, such as oxidation or chemical functionalization of CNTs, covalent bonding of polymer chains, etc. [54, 76, 93]. The chemical functionalization reactions include *in situ* radical polymerization, living anionic polymerization, polycondensation and direct attachment to the functional polymer [118]. The functionalization of the CNTs involves their surface modification and/or alteration of their morphology through dispersion. The cutting process in needed to disentangle the CNTs bundles and to provide active sites for chemical functionalization. Afterwards, may be attached to the CNTs' surface hydroxyl and carboxyl groups, promoting a more efficient linkage with the polymeric matrix [118, 119].

In order to achieve the highest property enhancement in a composite, it is required that the CNTs possess large aspect ratio, enough dispersion, good alignment and interfacial stress transfer [54]. The high aspect ratio of the particles and their wide contact surface with the matrix are two factors that largely contribute to the formation of more efficient percolation paths [113]. Alignment of CNTs according to the loading direction may improve the elastic modulus by 5 or more and a good interfacial strength between CNTs and the polymer matrix

is crucial to allow the force to be transferred to the CNTs [54]. The outstanding mechanical, electrical, thermal and magnetic properties of carbon nanotubes makes them excellent polymer nano-sized reinforcements. However, its high cost is an inconvenience [117].

As a result of the superior CNT properties summarized previously, high-performance light weight structural materials may be produced through incorporation of CNTs into polymers [5,54,76,100,109].

2.3.2 Comparison between nanofillers

In table 2.3 are compiled the main properties of some of the most used polymer reinforcements: carbon nanotubes (CNTs), graphene, graphite, carbon nanofibers and graphene nanoplatelets (GNPs).

Table 2.3: Theoretical and experimental properties of different fillers [98,119–122].

	CNT	**Graphene**	**Graphite**	**Carbon Nanofibers**	**GNPs**
Specific gravity (g/cm^3)	0.8 for SWNT 1.8 for MWNT (theoretical)	1.5 - 1.9	2.26	1.8-2.1	1.8-2.2
Specific surface area (m^2/g)	Typ. 10-200 (Can go up to 1300)	2630 - 2695	—	10 - 60	Typ. 10-1000 (Can go up to >2600)
Elastic modulus (TPa)	$\sim$ 1 for SWNT 0.3 - 1 for MWNT (axial direction)	$\sim$ 1.1	1 (in plane)	0.4-0.6	$\sim$ 1 (in plane)
Tensile strength (GPa)	50-500 for SWNT 10-60 for MWNT	120-140	0.013 - 0.060	2.7-7	$\sim$ 100-400
Electrical resistivity ($\mu\Omega$.cm)	5-50	$\sim$ 130	50 (in plane)	55-1000	50 (in plane)
Thermal conductivity (W/m.K)	3000 (theoretical)	$\sim$ 5000	3000 (plane) 6 (c-axis) (theoretical)	20 - 1950	5300 (plane) 6-30 (c-axis)
Magnetic susceptibility (EMU/g)	22×10^6 ($\perp$ with plane) 0.5×10^6 ($\parallel$ with plane)	N/A	N/A	N/A	22×10^6 ($\perp$ with plane) 0.5×10^6 ($\parallel$ with plane)
Thermal expansion ($\times 10^{-6}$ K^{-1})	Negligible	−4 - 3	1 (in plane) 29 (c-axis)	-1 (HT; axial)	-1 (in plane) 29 (c-axis)
Thermal stability (°C)	>700 (in air) 2800 (in vacuum)	N/A	450 - 650 (in air)	450 - 650 (in air)	450 - 650 (in air)

* $\perp$ = perpendicular, $\parallel$ = parallel.

Chapter 3

State of the art - Shape-memory polymer composites

The bibliography dedicated to the subject of combining fillers with a polymeric matrix and evaluate the characteristics of the composite *per se* and in comparison to the neat polymer is extensive. Enhancements in mechanical and thermal properties and in the electric and magnetic behavior of the polymer may be achieved with the addition of an optimal concentration of a suitable filler. Matrix - filler compatibility is also fundamental. Many kinds of composites were tested in the last decades and the research and analysis of the state of the art in this subject is a valuable tool to develop further studies in this area.

In 2002, Gall, Dunn, Liu et al. [53] fabricated and characterized a shape-memory composite of a resin reinforced with silicon carbide (SiC) nanoparticles. The composites were synthesized from a commercial shape-memory polymer resin system and were reinforced with SiC in the following weight fractions: 10%, 20%, 30% and 40%. The thermal analysis indicates that thermal transition is faster in the reinforced material, since the glass transition temperature (T_g) is lower than in the unreinforced material. So, the T_g of the material is sensitive to the presence and quantity of filler. This was explained by the modification of the kinetics of glass transition by the presence of a material different from the base polymer. The particle-matrix interface may have caused an increase in the nanoscale velocity or number of transition growth fonts, consequently resulting in a faster overall transition. The micro-indentation tests allowed the measurement of the elastic modulus. The unreinforced polymer possessed an elastic modulus of 1 GPa, while the polymer reinforced with 40 wt.% SiC exhibited a 3 GPa elastic modulus. These results show that the elastic modulus increases gradually with the increase of the content of the filler, SiC. This fact was explained by the relatively high SiC elastic modulus compared with the one of the polymer matrix. The same authors also made unconstrained strain recovery tests, which allowed to conclude that full shape recovery was attained for samples with SiC content from 0 wt.% to 30 wt.%. The samples with 40 wt.% SiC exhibited permanent deformation. According to their experiment, samples with higher SiC content generally recover faster, but to a lesser extent. The increase of the SiC fraction in the composite caused an increase of the attainable constrained recovery stress (force). The constrained bending recovery force in the nanocomposites increased by 50% when 20 wt.% SiC was added to the polymer. However, unconstrained recoverable strain (displacement) decreased and the authors explained that based on the lack of shape-memory characteristics exhibited by the SiC particles included in the nanocomposite.

In 2005, Cho, Kim, Jung et al. [75] tested mechanically and electrically nanocomposites of polyurethane reinforced with functionalized MWNTs. Samples with three different modified-MWNTs concentrations (3 wt.%, 5 wt.% and 7 wt.%) were produced by casting. The authors determined the modulus and stress at 100% elongation and found that they increased with increasing MWNTs content. Elongation at break decreased with increasing MWNTs content. According to the authors, severe surface modification diminishes mechanical properties. However, at optimal conditions, functionalization can increase the mechanical properties of shape-memory composites. The electrical conductivity for samples with 5 wt.% MWNT was in the order of 10^{-3} S.cm^{-1}, which was enough to heat the sample above 35°C (which is the transition temperature of the used polyurethane). The increase of MWNT content in the composite led to an increase of the electrical conductivity. In spite of that fact, the electrical conductivity of the modified-MWNT composite was lower than that of the unmodified-MWNT composite with the same nanotube content. Electro-active shape recovery was observed in the sample with 5 wt.% modified-MWCNT content.

In 2006, Goo, Paik, Jung, et al. [76] processed composites of MWCNTs/PU through in situ polymerization. An optimal filler concentration of 7 wt.% MWCNTs was used. The electrical resistance and specific resistance have proven to be almost constant until they reached the transition temperature. With the increase of the elongation up to 100%, the electrical resistance increased by 100%. Upon usage of an external force, they evaluated the actuation displacement that the composite could produce when the actuation force increased. It was observed that the actuation displacement decreased linearly as the actuation force increased.

In 2006, Schmidt [123] discussed the subject of electromagnetic activation of shape-memory nanocomposites filled with magnetic nanoparticles (Fe_3O_4). The produced samples possess 0, 1.9, 8.0 and 12.1 wt.% of Fe_3O_4. The thermal, mechanical and shape recovery properties were evaluated. Through transmission electron microscopy (TEM), they concluded that the Fe_3O_4 nanoparticles were homogeneously distributed in the polymeric matrix. Employing differential scanning calorimetry (DSC) tests they concluded that T_m, which in this case corresponds to the shape-memory composites' transition temperature, increased with the incorporation of Fe_3O_4 nanoparticles. The tensile tests enabled the evaluation of the samples' mechanical properties. The elastic modulus of the nanocomposites is higher than the one of the SMP without nanoparticles. The value of the tensile strength is similar in both neat and filled SMPs. Elongation at break decreased for the nanocomposites as compared with the neat SMP. Shape-memory effect was observed upon the execution of an electroactive shape-memory cycle. It was found that the response time of the nanocomposites decreased with increasing weight fraction of Fe_3O_4.

In 2006, Mondal, Hu, et al. [58] prepared and characterized MWNT/SPU (segment polyurethane) nanocomposites. Different weight fractions of functionalized MWNTs were added to SPU matrix: 0.25, 0.5, 1.0 and 2.5 wt.%. Through DSC and DMTA, it was concluded that the heat of fusion of the 0.25 wt.% MWNT/SPU nanocomposite was slightly higher than that of pure SPU, due to the existence of small MWNT content which enhanced the crystallization process. However, further increase in MWNT content led to a decrease in the nanocomposite's heat of fusion. Once the percentage of filler rose, the soft segments mobility is reduced, leading to a diminished crystallinity of these. Through the experiment

is shown that, with the increase of the MWNT weight fraction, the loss modulus peak is achieved at a slightly higher temperature. This implies that the T_g of the nanocomposite increases with the addition of MWNT and, consequently, it was observed an increase in the nanocomposite stiffness, due to the higher elastic modulus of the MWNTs compared to the one of neat SPU. To evaluate the shape-memory properties, cyclic tensile tests were performed. All samples obtained 100% shape fixity. Low contents of MWNT revealed to have small influence on shape recovery properties. At higher MWNT concentration, particularly 2.5 wt.%, shape recovery is higher due to strong interactions between the filler and the hard segments of the polymer.

Ni, Zhang, Fu et al. [108] in 2007 presented results of mechanical properties and shape recovery behavior of VGCFs (vapor grown carbon fibers)/SMP nanocomposites. Three types of nanocomposites with different weigh fractions of filler were produced through casting, corresponding to 1.7, 3.3 and 5.0 wt.% of VGCF. Scanning electron microscopy (SEM) analysis allowed to determine that nanocomposites with 5wt.% of VGCF exhibited a relatively good dispersion and random distribution of the nanofibers in the SMP. The results of the static tensile test revealed that, with the increase of the VGCF's weight fraction, the elastic modulus, yield stress and tensile stress values also increased. The shape fixity and shape recovery tests, allowed to conclude that the addition of VGCF up to 5 wt.% not only enhances the mechanical properties of the SMP, but also almost maintains the shape fixity level similar to the bulk SMP, since the results from the experiments revealed the strain fixity ratio for each specimen to be around 95%. In the first cycle, the nanocomposites showed a strain recovery ratio of less than 90%, in which nanocomposites with higher weight fraction had a lower ratio. However, after several cycles of training, the strain recovery ratio of the nanocomposites increased, tending to a constant value of 95%. Finally, concerning the recovery stress property, is became clear that it is larger for the nanocomposites than it is for the bulk SMP.

In 2014, Raja, Ryu and Shanmugharaj [56] produced two types of composites with the same polymer blend, 10 wt.% poly(vinylidene difluoride) (PVDF)/90 wt.% PU, but different fillers: pristine MWNT and functionalized MWNT. The fillers weight fractions employed to produce the composites were 1.0, 2.0, 3.0, 4.0, 5.0 and 10.0 wt.%. The method used to process the composites was melt processing. It was observed a good dispersion of the MWNTs in the polymer blend matrix, particularly in the functionalized MWNT nanocomposites. Clusters of carbon nanotubes were observed in pristine MWNT nanocomposites. The electrical properties revealed an increase of the electrical conductivity with the increase of MWNT content (both pristine and modified). Despite both types of nanocomposites had presented enhanced electrical conductivity in comparison with the base polymer blend matrix, modified MWNT nanocomposites showed higher electrical conductivity than pristine MWNT nanocomposites. The authors assumed that it was due to the enhanced dispersion of the functionalized MWNTs in the polymer blend matrix, resulting in a more effective conductive network. The study of the mechanical properties showed than the increase of the MWNT content (both modified and pristine) led to an increase of the elastic modulus and tensile strength of the nanocomposites and to a decrease of the elongation at break. However, the enhancement of the elastic modulus and tensile strength was higher for the nanocomposites filled with modified MWNTs. In this research, the results demonstrate that nanocomposites' thermal conductivity was higher than the one of the polymer blend matrix. As the MWNT content increased, thermal conductivity of the nanocomposite also

increased and was higher in nanocomposites filled with modified MWNT than it was with nanocomposites filled with pristine MWNTs. The electro-active shape-memory effect was evaluated. The measured shape recovery was about 95% in both types of nanocomposites. However, with the increasing number of shape-memory cycles the recovery ratio decreased in both types of nanocomposites. Shape recovery was faster in modified MWNT nanocomposites (15 s) than in pristine MWNT nanocomposites (30 s), in the first cycle.

The research article written in 2015 by Al Saleh [96] aimed to investigate the microstructure, processing behavior, electrical and mechanical properties of graphene nanoplatelets (GNP)/ polypropylene (PP) nanocomposites and GNP:CNT/PP hybrids. All the nanocomposites were produced through melt-mixing and further compression molding. The state of dispersion and adhesion of the nanofillers in the nanocomposites was observed resorting to SEM technology. The 2 wt.% GNP/PP nanocomposites presented large voids between the PP matrix and the GNP platelets, due to bad adhesion between these two elements. In the case of the 2:1 wt.% GNP:CNT/PP hybrid, it was reported the existence of small CNT aggregates and some thick graphene platelets. However, both single CNT particles and aggregates have shown a good state of adhesion to the PP matrix. The GNP/PP nanocomposites did not exhibit a sharp insulation-conductive transition. Although the sample did not have a typical percolation behavior, it was assumed by the authors that the electrical percolation threshold (EPT) was somewhere between 8.0 and 10 wt.% GNP. This high threshold concentration was explained by the GNP's platelet structure and aspect ratio and to an inadequate dispersion of the filler in the polymeric matrix. The addition of 1 wt.% CNT to the mixture revealed lower electrical resistivity for the GNP:CNT/PP hybrid system. The influence of GNP concentration on the electrical properties was also studied and their results has shown that the addition of up to 20 wt.% GNP has no significant effect on the tensile strength of the GNP/PP nanocomposites and GNP:CNT/PP hybrids. When considering toughness, it was found that an increase of GPN concentration from 2 wt.% to 10 wt.% caused a decrease and further addition of GNP produced no effect on toughness. On the contrary, the increase of CNT concentration led to an increase of toughness and also an increase of tensile strength.

Jomaa, Masenelli-Varlot, Seveyrat et al. [124] studied the elastic, electrical and electromechanical properties of grafted CNTs/PU nanocomposites. The volume fractions of grafted CNTs included in the samples were 0, 1.0, 2.0, 3.0, 4.0 and 5.0 vol.%. The results have shown well crystallized raw nanotubes and grafted CNTs in PU. The study of the mechanical properties of the nanocomposites revealed that addition of grafted CNTs into PU increases both tensile strength and elastic modulus, which was ascribed to the enhancement of the dispersion state and interfacial adhesion between functionalized CNTs and the PU matrix. About electrical conductivity, it was observed that at low frequencies the conductivity was almost independent of the frequency, while at higher frequencies occured a linear increase of the conductivity with the frequency. The electrical conductivity increased as the content of grafted CNTs increased. The electrical percolation threshold (EPT) was also studied and it was found to be approximately 5 vol.% grafted CNT. It was concluded that grafted CNTs/PU nanocomposites possess a higher percolation threshold than ungrafted CNTs/PU nanocomposites.

Chen, Pan, Li et al. [125] focused their investigation on the dielectric, mechanical and electro-stimulus response properties of hybrid GNS (Graphene nanosheets):MWNT/PU

nanocomposites. The results revealed densely and almost uniformly dispersed GNS, which consist of randomly aggregated crumpled sheets. MWNTs in the MWNT/ PU nanocomposites were heavily aggregated, forming clusters. GNS in the GNS/PU nanocomposites presented a better dispersion. In the hybrid GNS:MWNT/PU composites was possible to observe MWNTs and GNS combined together in some areas. It was claimed a homogeneous dispersion of nanofiller in the composite's polymer matrix. The dielectric properties were also analysed. As the applied frequency increased, the dielectric constant of the three types of composites decreased, denoting a typical behaviour of percolative conductor-insulator composites. It is clear that occured an enhancement of dielectric constant for the GNS:MWNT/PU composite, since the hybrid mixture of nanofillers results in a better dispersion of GNS and MWNT in the polymeric matrix. It was found that with the increase of filler content in the composites (MWNT, GNS and GNS:MWNT), both elastic modulus and tensile strength increased while elongation at break decreased, implying increase of stiffness and decrease of ductility of the composites. The highest values of elastic modulus and tensile strength were obtained in MWNT/PU composites. However, the highest electric induced strain values were attained in GRN:MWNT/PU composites.

In 2015, Jing, Liu, Pan et al. [93] prepared and studied nanocomposites of PU reinforced with functionalized graphene oxide (FGO). The synthesis of thermoplastic PU was performed using the prepolimerization method. The used weight fractions of FGO were: 0.1, 0.4, 0.7 and 1.0 wt.%. Mechanical properties were examined and a general enhancement of mechanical properties through the addition of FGO was claimed. The most efficient improvement was attained for the 0.4 wt.% FGO/PU nanocomposite, which was characterized by a tensile stress of 19.6 MPa, an elongation at break of 1035.3% and a toughness of 129.6 MPa. These values represent an increase of 34.2%, 27.6% and 64.5%, respectively, compared with those of pure PU. Through tensile tests it was demonstrated that tensile stress, elongation at break and toughness decreased with further addition of FGO. Comparing GO and FGO composites with the same loading content (0.4 wt.%), it was determined that FGO exhibited a larger effect of reinforcement than GO. In fact, toughness and elongation at break of 0.4 wt.% FGO/PU nanocomposite were 19.6% and 21.8% higher than those of 4 wt.% GO/PU nanocomposite. The elastic modulus was higher for the GO/PU nanocomposite than for the FGO/PU nanocomposite.

Also in 2015, Strankowski, Piszczyk, Kosmela et al. [94] studied the morphology and the physical and thermal properties of polyurethane filled with thermally reduced graphene oxide (TRG). The preparation of the nanocomposites was made through mixing PU granulate and TRG nanoparticles in four different weight fractions: 0.5, 1.0, 2.0 and 3.0 wt.%. The samples were then obtained by extrusion. Even though a high degree of nanofiller dispersion in polymer matrix was claimed, it was detected some filler agglomeration (10-100 nm) in the samples. The mechanical characterization revealed that an increase of weight percentage up to 1 wt.% caused a decrease of tensile strength. This effect was attributed to an irregular nanofiller dispersion within the polymer matrix, which resulted into the formation of carbon aggregates that worsen mechanical properties. However, the increase of the nanofiller content up to 2 wt.% led to an increase in tensile strength, reaching the highest value in comparison to all the other nanocomposites and neat PU. Further addition of TRG up to 3 wt.% led to a new decrease of tensile strength. The elongation at break was increased upon incorporation of TRG up to 1 wt.%. However, further addition of filler caused a decrease of the elongation at

break. About storage modulus (E'), the authors concluded that the addition of TRG caused an increase of E' in the viscoelastic region, which implies an improvement of the stiffness of the nanocomposite. Regarding to thermal characterization, the authors stated an increase of the glass transition temperature with TRG addition as a result of reduced chain mobility of soft segments. Degradation temperature of polyurethane was not significantly affected by incorporation of TRG.

A research on the properties of nanocomposites of reduced graphene oxide (RGO) incorporated into polyurethane was conducted in 2015 by Gupta, Singh, Tripathi et al. [117]. The nanocomposites were fabricated through the addition of five different RGO weight fractions: 0.1, 0.5, 1.0, 3.0 and 5.0 wt.%. The final samples were attained through solvent casting. Large quantities of entangled graphene sheets and some wrinkles at their surface were spotted through TEM. Some kind of crumpled silk curtain wave like structures were described by the authors as well as some transparent regions, indicating the presence of monolayer graphene. Regarding the mechanical properties, it was observed by the authors an increase of the hardness and elastic modulus with the increasing RGO content. An overall improvement of 139% in hardness and 129% in the elastic modulus was attained by RGO incorporation denoting a strong bonding between the polymer matrix and the functionalized filler.

In 2015, Ljubic, Srinivasan, Szoszkiewicz et al. [126] prepared and analysed the properties of polyurethane filled with surface modified graphene (SMG). The produced samples possessed weigh fractions of 0.2, 0.5, 1.0, 2.0, 3.0, 4.0 and 5.0 wt.% SMG. Rheology of SMG-polyol blend was studied and the data showed that an increase of SMG content led to an increase of viscosity at 25 °C. Physical and mechanical properties were evaluated. An increase in SMG content caused an increase in the nanocomposites' tensile strength. In fact, it rose from 0.9 MPa for 0.2 wt.% SMG to 2.3 MPa for 5.0 wt.% SMG. It was also observed an enhancement of the tensile strength for the nanocomposites as compared with the one of neat PU, since the value increased by three. Elongation at break was 43% and 34% higher in 2.0 wt.% and 5.0 wt.% SMG nanocomposites, respectively, in comparison with the neat polymer. Increasing content of SMG also led to an increase of the tensile stress at 50% and 100% elongation, also known as 50% Modulus and 100% Modulus. The recorded rise was about 150% in 50% Modulus and 167% in 100% Modulus for the 5 wt.% SMG/PU nanocomposite compared to the neat PU. The mechanical properties improvement denotes a strong reinforcing effect of SMG resulting from good linking in the filler-polymer interface. Storage modulus was investigated and it was observed an increase for the nanocomposites as compared with pure PU. A maximum storage modulus enhancement of 200% in comparison with pure PU was achieved by the 5 wt.% SMG/PU nanocomposite. Comparing functionalized and non-functionalized filled polymers with the same weigh fraction, it was possible to stablish a slighty higher storage modulus of the functionalized graphene nanocomposites. DSC was used in order to determine the glass transition temperature and it was observed a positive T_g shift of 2 °C in the nanocomposite with highest filler concentration (5 wt.% SMG). The electrical properties of SMG/PU nanocomposites were studied. Permittivity increased with the SMG content at the given temperatures of -50 °C, 25 °C and 90 °C. Actually, permittivity of the nanocomposite filled with 5 wt.% SMG was 38 in the glassy region (-50 °C) and 69 in the rubbery region (25 °C), while permittivity of the unfilled PU was 4 in the glassy region (-50 °C) and 12 in the rubbery region (25 °C). The authors concluded that dielectric permittivity

decreased with frequency.

The paper written by Gaidukovs, Kampars, Bitenieks et al. [127] was focused on the thermo-mechanical properties of a polyurethane filled with GO and CNT particles as a mixture of 1:1 by weight in following weight fractions: 0.05, 0.1 and 0.3 wt.%. In order to evaluate the influence of the content of filler in the nanocomposite's mechanical properties, the elastic modulus was determined. With the addition of the reinforcement, the elastic modulus increased till a concentration of 0.1 wt.%. However, for higher concentrations of filler, it decreased. The effect of filler addition on glass transition temperature was also studied and it was observed an increase of 5°C (from 85°C to 90°C) as the filler concentration increased from 0.05 to 0.1 wt.%. Further increase of CNT:GO weight fraction up to 0.3% caused decrease of the nanocomposite T_g down to 75°C.

This year, Kausar, Rahman [128] presented a work where it was produced polyurethane based nanocomposites in order to evaluate the mechanical, thermal and shape-memory properties. A polymer blend of PU and poly (ethylene-co-ethyl acrylate-co-maleic anhydride) (PEEAMA) was created with three fractions of PEEAMA: 50%, 70% and 90%, denominated PU/PEEAMA 50, PU/PEEAMA 70 and PU/PEEAMA 90, respectively. The PU/PEEAMA 50 was used to produce nanocomposites incorporating GNPs in three different weigh fractions (1.0, 3.0 and 5.0 wt.%). Mechanical properties of the produced nanocomposites were tested. An increase of GNP content led to an increase of tensile strength and to a considerable decrease of elongation at break. This was attributed to the restriction of the chain segments' motion through functional GNP addition that led to a decreased ductility. Both polymers blends and nanocomposites reached higher tensile strengths and lower elongations at break than neat PU. Increasing GNP content in the nanocomposites from 1.0 to 5.0 wt.% induced an increase on the elastic modulus from 30.5 to 36.9 GPa. Both polymer blends and nanocomposites presented a higher elastic modulus than neat PU. In fact, the elastic modulus of the PU/PEEAMA nanocomposite with 5 wt.% GNP is 57% higher than the one of the neat PU. At last, the heat-induced shape-memory test was performed. The shape-memory results show an 85% shape recovery for polymer blends. However, with the addition of GNP the shape recovery ratio increased to 95% for the nanocomposites with 1.0 wt.% and 3.0 wt.% GNPs and to 96% for the nanocomposite with 5.0 wt.% GNPs. The nanocomposites performed a recovery time which varied between 7 and 10 seconds. The recovery became faster with the increasing content of filler. Shape recovery was very low (less than 30%) when the used reheating temperatures were below or equal to 40 °C. The samples gained high recovery rate ($\sim$ 75%) using a reheating temperature of 50 °C.

In Table 6.1 are summarized the results obtained for the experiments described in this chapter.

Table 3.1: Summary of the state-of-the-art experiments.
SiC = Silicon carbide; NT = Non-Treated; T = Treated; CNTs= Carbon Nanotubes; E = Elastic modulus; M100 = Modulus at 100% elongation; σ_b = Tensile strength; ε_b = Elongation at break; γ = Electrical conductivity; T_g = Glass transition temperature; k = Thermal conductivity; H = Hardness; PEEMA= poly(ethylene-co-ethyl acrylate-co-maleic anhydride).

Matrix	**Filler**	**Mechanical properties**	**Electrical properties**	**Thermal properties**	**Ref.**
Epoxy	SiC 10.0 - 40.0 wt.%	↑ wt.% SiC ⇒ ↑E	—	↑ wt.% SiC ⇒ ↓ T_g	[53]
PU	NT CNTs T CNTs 3.0 - 7.0 wt.%	↑ wt.% CNTs ⇒ ↑ M100 ↑ wt.% CNTs ⇒ ↓ ε_b M100: NT CNTs < T CNTs	↑ wt.% CNTs ⇒ ↑ γ γ: NT CNTs > T CNTs	—	[75]
PVDF + PU	NT CNTs T CNTs 1.0 - 10.0 wt.%	↑ wt.% CNTs ⇒ ↑E ↑ wt.% CNTs ⇒ ↑ σ_b ↑ wt.% CNTs ⇒ ↓ ε_b E and σ_b: T CNTs > NT CNTs	↑ wt.% CNTs ⇒ ↑ γ γ: T CNTs > NT CNTs	↑ wt.% CNTs ⇒ ↑ k k: T CNTs > NT CNTs	[56]
PU	T CNTs 1.0 - 5.0 vol.%	↑ vol.% T CNTs ⇒ ↑E ↑ vol.% T CNTs ⇒ ↑ σ_b	↑ vol.% T CNTs ⇒ ↑ γ EPT: T CNTs > NT CNTs	—	[124]
PU	CNTs GNS GNS:CNT 0.5 - 2.5 wt.%	↑ wt.% filler ⇒ ↑E ↑ wt.% filler ⇒ ↑ σ_b ↑ wt.% filler ⇒ ↓ ε_b	↑ wt.% filler ⇒ ↑ ε_r	—	[125]
PU	FGO GO 0.1 -1.0 wt.%	↑ wt.% FGO ⇒ ↑ σ_b (until 0.4 wt.%) ↑ ε_b ↑ wt.% FGO ⇒ ↓ σ_b (0.4 - 1.0 wt.%) ↓ ε_b ↑ wt.% FGO ⇒ ↑E σ_b and ε_b: FGO ≈ GO E: GO > FGO	—	—	[93]
PU	TRG 0.5 - 3.0 wt.%	↑ wt.% TRG ⇒ ↓ σ_b (until 1.0 wt.%) ↑ ε_b ↑ wt.% TRG ⇒ ↑ σ_b (1.0 - 2.0 wt.%) ↓ ε_b ↑ wt.% TRG ⇒ ↓ σ_b (2.0 - 3.0 wt.%) ↓ ε_b	—	↑ wt.% TRG ⇒ ↑ T_g	[94]
PU	RGO 0.1 - 5.0 wt.%	↑ wt.% RGO ⇒ ↑E ↑ wt.% RGO ⇒ ↑ H	—	—	[117]

(Continue on next page)

Matrix	Filler	Mechanical properties	Electrical properties	Thermal properties	Ref.
PU	SMG 0.2 - 5.0 wt.%	↑ wt.% SMG ⇒ ↑ σ_b (except for 0.5 and 4.0 wt.%) ↑ wt.% SMG ⇒ ↑ ε_b (except for 0.5 - 2.0 wt.%) ↑ wt.% SMG ⇒ ↑ M50 ↑ wt.% SMG ⇒ ↑ M100 ↑ wt.% SMG ⇒ ↑ H	—	↑ wt.% SMG ⇒ ↑ T_g	[126]
PU	GO:CNT 0.05 - 0.3 wt.%	↑ wt.% GO:CNT ⇒ ↑E (until 0.1 wt.%) ↑ wt.% GO:CNT ⇒ ↓E (0.1 - 0.3 wt.%)	—	↑ wt.% GO:CNT ⇒ ↑ T_g (until 0.1 wt.%) ↑ wt.% GO:CNT ⇒ ↓ T_g (0.1 - 0.3 wt.%)	[127]
PU + PEEMA	GNPs 1.0 - 5.0 wt.%	↑ wt.% GNPs ⇒ ↑E ↑ wt.% GNPs ⇒ ↑ σ_b ↑ wt.% GNPs ⇒ ↓ ε_b	—	—	[128]

Part II

Experimental procedure

Chapter 4

Materials and Methods

In this chapter it will be described the experimental procedure, including the materials and processing methods used to obtain the shape-memory polyurethane nanocomposites as well as the characterization techniques applied to the specimens in order to determine their mechanical and thermal properties.

4.1 Materials

The thermoplastic polyurethane (TPU) that was used in this work was supplied by HUNTSMAN. The used TPU was ether-based and with the reference Irogran A 80 P 4699L. Its properties are compiled in table 4.1.

Table 4.1: TPU Irogran A 80 P 4699L properties [129]

Properties	Values
Specific gravity	1.10
100% Modulus	4.3
300% Modulus	8
Tensile strength at break	35 MPa
Strain at break	700%
Melting temperature	111 - 160 °C
Front barrel temperature for extrusion	180°C

In this work it was prepared polyurethane based nanocomposites with two types of nanoparticles, namely, carbon nanotubes (chemically treated and pristine ones) and graphene nanosheets.

The carbon nanotubes (CNTs) that were used in this work were multiwalled, with diameter between 20 and 40 nm and length ranging from 1 to 2 μm. They were purchased from Shenzhen Nanotech PortCo., Lda by the reference S-MWNT-2040. The main properties of such CNTs are presented in table 4.2.

Table 4.2: S-MWNT-2040 properties

Properties	Values
Outer diameter	20 - 40 nm
Length	1 - 2 μm
Purity	>97%
Density	2.16 g/cm^3
Specific surface area	70 - 150 m^2/g

Graphene was acquired from Graphene Laboratories Inc., with the designation of A-12 Graphene nanopowder and its main characteristics are summarized in table 4.3.

All the materials were dried in a TIRAclima TCC 4034 furnace chamber with set temperature of 100°C for 8 h, in order to achieve 0% humidity and were kept in a desiccator.

Table 4.3: A-12 Graphene nanopowder properties

Properties	Values
Thickness (average)	<3 nm (3 - 8 graphene monolayers)
Lateral dimensions	2 - 8 μm
Density	2.25 g/cm^3
Melting temperature	3652 - 3697 °C

4.2 Functionalization of CNTs

Due to the van der Waaals forces between the nanotubes, they tend to get together and create agglomerates. In order to prevent that and to avoid undesirable clustering effects in the TPU nanocomposites, chemical surface-modification can be made and it is capable to improve the composite's thermal and mechanical properties.

In this work it was used some CNTs that were subjected to a chemical treatment through the methodology proposed by Esumi in 1996 [130]. In such methodology it was applied a mixture of sulfuric acid (H_2SO_4) and nitric acid (HNO_3) in a proportion of 3:1 that was mixed with the CNTs. The mixture was then refluxed for 30 min at 140°C. Afterwards, the CNTs were washed with deionised water (DW) until pH $\sim$ 7 was achieved and then dried at 100°C until the DW was evaporated. Finally, the dried CNTs were powdered and stored in a desiccator.

The Fourier Transform Infrared (FT-IR) tests were performed to the pristine and functionalized CNTs and it was proved that the carboxylic group was created. The integrity of the CNTs was not affected by the chemical treatment, certifying the good quality of the functionalized CNTs.

4.3 Processing of the nanocomposites

The polyurethane nanocomposites were processed in an Internal Batch Mixer, Plastograph EC, from Brabender (fig.4.1) through mechanical melt mixing. The applied mixing conditions were: velocity of 100 rpm, mixing temperature of 140°C and time of mixture of 8 minutes. It was prepared polyurethane nanocomposites containing two types of nanoparticles: carbon nanotubes (treated and non-treated) and graphene (pristine), and with different volume fractions. The different nanocomposites, the corresponding compositions and designations can be observed in table 4.4.

After mixing, the produced nanocomposites were processed through injection molding in a HAAKE Minijet II, from ThermoFisher Scientific. The applied conditions to obtain the injected samples were injection temperature of 160°C, mould temperature of 80°C, injection pressure of 650 bar for 5s and a compaction pressure of 500 bar for 2s. It was prepared at least 8-10 samples for each polyurethane nanocomposite. The obtained samples presented a dumbbell geometry as it can be observed in fig.4.2. Their dimensions are in accordance with the test specimen type 5A, described in 527-2:1996 standard [131]. In fig.4.3 it can be observed some of the nanocomposites specimens produced and which were later submitted to characterization tests. The used injection mouling machine and mould can be seen in fig.4.4.

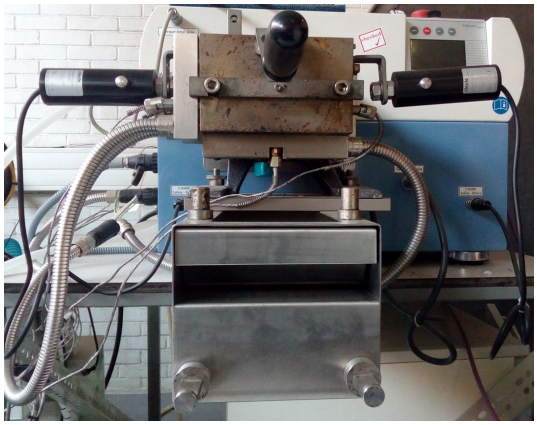

Figure 4.1: Melt mixing machine Plastograph EC, Brabender

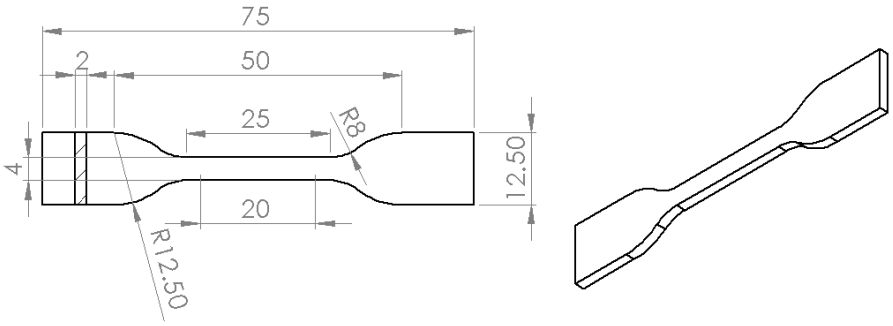

Figure 4.2: Test specimen type 5A (measurements in mm).

Table 4.4: Sample composition of TPU nanocomposites filled with MWNTs and graphene. Funct.=Functionalization; NT= Non-Treated (Non-Modified); T=Treated (Modified); Temp.=Temperature; CNT=Carbon Nanotubes; Gra=Graphene;

Designation	**Filler**	**Funct.**	**PU (vol.%)**	**Filler (vol.%)**	**Filler (wt.%)**	**Melt Mixing**
PU_ pure	—	—	100	0	0	—
PU_ 140	—	—	100	0	0	X
PU_ 05_ NT_ CNT	CNT	NT	99.5	0.5	0.98	X
PU_ 10_ NT_ CNT	CNT	NT	99.0	1.0	1.94	X
PU_ 15_ NT_ CNT	CNT	NT	98.5	1.5	2.90	X
PU_ 05_ T_ CNT	CNT	T	99.5	0.5	0.98	X
PU_ 10_ T_ CNT	CNT	T	99.0	1.0	1.94	X
PU_ 15_ T_ CNT	CNT	T	98.5	1.5	2.90	X
PU_ 05_ Gra	Gra	NT	99.5	0.5	1.02	X
PU_ 10_ Gra	Gra	NT	99.0	1.0	2.02	X
PU_ 15_ Gra	Gra	NT	98.5	1.5	3.02	X

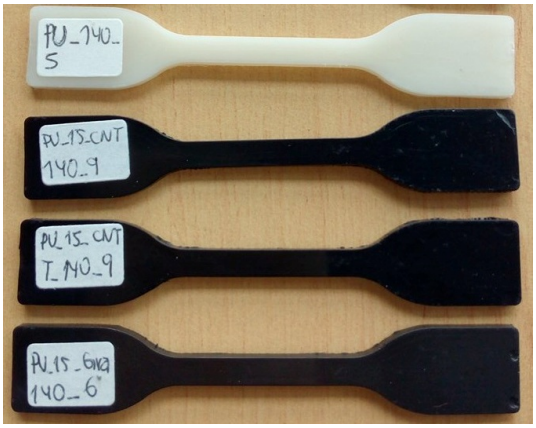

Figure 4.3: Mechanically melt mixed composite samples: PU_140, PU_15_NT_CNT, PU_15_T_CNT, PU_15_Gra (from top to bottom).

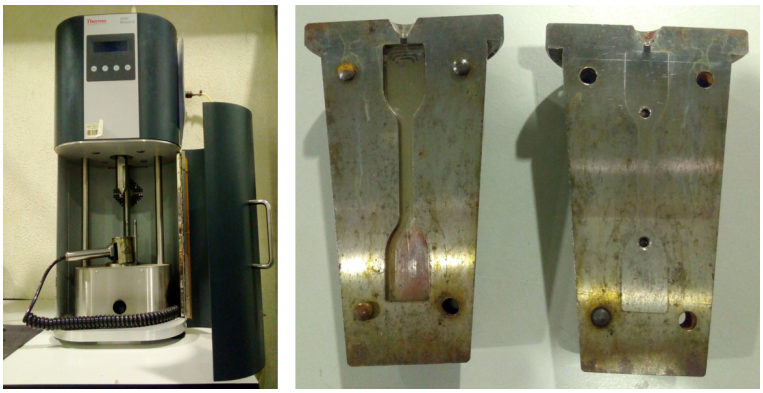

Figure 4.4: Injection moulding machine, HAAKE Minijet II, ThermoFisher Scientific, and mould.

Chapter 5

Characterization

5.1 Scanning electron microscopy (SEM)

In order to characterize the morphology of the different TPU nanocomposites and to evaluate the dispersion of the nanoparticles into the polymeric matrix it was used a Hitachi SU-70 Field Emission Scanning Electron Microscopy (FE-SEM) equipment (fig.5.1) with a resolution of 1 nm at 15 kV and a magnification that ranges from 30x to 800,000x. The samples were cryogenically fractured with liquid nitrogen and the deposition of a very thin layer of conducting carbon in their outer surfaces was applied in order to avoid some electrostatic charging of the material's surface when exposed to the electron probe [132]. The prepared specimen stub with the glued samples to be observed by SEM can be seen in fig.5.2.

Figure 5.1: SEM equipment, Hitachi SU-70

Figure 5.2: SEM samples in the specimen stub

5.2 Differential scanning calorimetry (DSC)

The thermal properties, such as glass transition temperature (T_g), melt temperature (T_m), specific heat capacity (c_p) and thermal Diffusivity (α) of the specimens were evaluated by using the DSC equipment Perkin Elmer DSC 4000 (fig.5.3), which was calibrated with an indium sample. The analysed samples possessed weight between 4.6 and 6 mg and were encapsulated in aluminium sample pans. The gas nitrogen used in the DSC process was at a pressure of 1.8 bar and provided with a flux of 20 mL/min. The implemented thermal cycle was composed by the following stages:

1. Hold for 10 min at 5°C;
2. Heat from 5°C to 200°C at a rate of 10°C/min;
3. Hold for 5 min at 200°C;
4. Cool from 200°C to 5°C at a rate of 10°C/min;
5. Hold for 10 min at 5°C;
6. Heat from 5°C to 200°C at a rate of 10°C/min;
7. Hold for 5 min at 200°C.

The capsules were always manipulated with tweezers in order to avoid contamination. The tweezers were also used to remove and replace the lid and cell cover from the heating chamber of the DSC equipment.

Aiming to obtain more reliable data, two DSC measurements were performed for each type of sample and, in each DSC output curve, T_g and T_m were measured twice in order to guarantee repeatability and, therefore, reduce the error.

This procedure followed the indications in the "Standard Test Method for Transition Temperatures and Enthalpies of Fusion and Crystallization of Polymers by Differential Scanning Calorimetry" [133] and was also supported by the bibliography [134, 135].

Figure 5.3: DSC equipment, Perkin Elmer DSC 4000

5.2.1 Calculations

Glass transition temperature (T_g)

The glass transition temperature is an important property in shape-memory polymers (SMP), since it may be used as shape-memory transition temperature. Therefore, its value decides the range of applications in which the SMP may be applied. T_g also can be tailored according to its molecular structure and, therefore, its final application.

At T_g the mechanical properties of a polymer switch between those of an elastic material, in its molten state, and those of a brittle one, in its rigid state, due to changes in chain mobility. The transition does not occur sharply at one unique temperature but rather over a range of temperatures. In fig.5.4 it is illustrated a typical example of a heat flow versus temperature graph at a T_g region. T_g is calculated as the temperature of the median point of the glass transition range in the heating ramp [54, 133, 135, 136]. The Perkin Elmer DSC 4000 software allows the interpolation calculus of T_g, given by the mid point between the two parallel lines before and after the glass transition slope. It is described in the bibliography that this technique is not very accurate and not very sensitive. A repeatability error of $\pm$ 1°C is acceptable in practice. To minimize errors in T_g, it is important to maintain the sample untouched in the apparatus during all the experimental process [134].

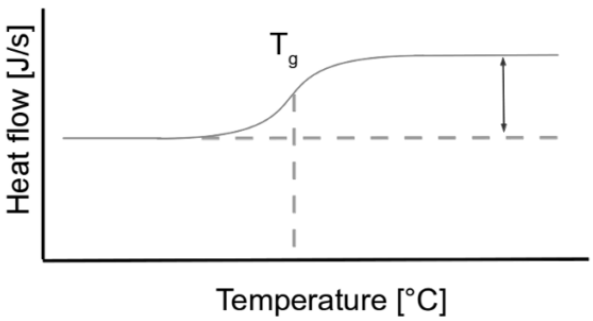

Figure 5.4: Heat flow - Temperature curve at a glass transition temperature region [135].

Melting temperature (T_m)

At melting temperature (T_m) the polymer chains can move freely without constrains or ordered arrangements. Melting is an endothermic process since it involves absorption of heat. Therefore, the heat flow to the sample increases in order to maintain the heating rate constant. Despite the continued heating, temperature remains constant during melting [135]. According to Höhne, Hemminger and Flammersheim [134], in DSC curves, a peak appears when the steady state is disturbed by thermally activated heat production or consumption in the sample. Peaks in heat flow rate curves, which are assigned to endothermic processes, are normally ploted "upwards" (positive direction) as heat added to a system is defined as positive in thermodynamics by international convention. Only processes associated with a heat (e.g. melting or crystallization) lead to peaks. Other transitions, such as glass transition, as seen previously, only lead to changes in the shape of the curve. T_m is, thus, defined as the temperature at the peak apex [54, 135], as it can be seen in fig.5.5.

In the Perkin Elmer software it is possible to establish the value of T_m using a software tool which enables the determination of the peak apex between two temperature points (at left and right of the peak).

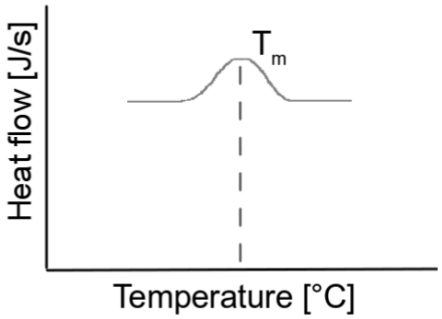

Figure 5.5: Heat flow - Temperature curve at a melting temperature region [135].

Specific heat capacity (c_p)

The heat capacity (C_p) of a system is defined as the amount of necessary heat to raise its temperature by 1°C. Therefore, the specific heat (c_p) is the heat capacity of a system per unit of mass. It is usually given in units $\frac{J}{kg.°C}$ [135].

The specific heat can be determined by DSC [135, 137]. The specific heat capacity is calculated through the equation 5.1 [134, 135, 137]:

$$c_p = \frac{\frac{dQ}{dt}}{m.\frac{dT}{dt}} \tag{5.1}$$

where:

c_p is the specific heat capacity, in $\frac{J}{kg.°C}$;

$\frac{dQ}{dt}$ is the heat flow given by the DSC curve, in W;

$\frac{dT}{dt}$ is the heating rate of the sample (β), in $\frac{°C}{s}$;

m is the sample mass, in kg.

In this work, the specific heat was calculated at different temperature ranges using equation 5.1.

Thermal Diffusivity (α)

The thermal diffusivity (α) is a thermophysical property that defines the speed of heat propagation by conduction when occurs a change of temperature [138]. Thermal diffusivity is calculated through the specific heat capacity, previously referred, the thermal conductivity (k) and the density of the material (ρ), and is given by the equation 5.2:

$$\alpha = \frac{k}{\rho \times c_p} \tag{5.2}$$

where:

α is the thermal diffusivity, in $\frac{m^2}{s}$;

k is the thermal conductivity, in $\frac{W}{m.°C}$;

ρ is the density, in $\frac{kg}{m^3}$;

c_p is the specific heat capacity, in $\frac{J}{kg.°C}$.

To calculate the thermal diffusivity it was used some values of thermal conductivity previously measured by researchers from GRIDS (the research group where the author is integrated), concerning pure polyurethane and nanocomposites incorporating 1.0 vol.% NT CNTs, 1.5 vol.% NT CNTs and 1.5 vol.% T CNTs. Although the previously referred specimens were submitted to the same processing methods, the mechanical melt mixing was performed at a temperature of 165°C, which differs from the mechanical melt mixing setup temperature used in this thesis (140°C). The results must be analysed taking into account this approximation.

5.3 Tensile tests

The tensile tests were performed using the tensile tester Shimadzu AGS-10kNX (fig.5.6), which possess a maximum load capacity of 10 kN. The tests were performed at room temperature and the conditions implemented in the tests were a cross-head speed of 20 mm/min, with a gauge length of 20 mm. The elongation of the specimens was measured through the use of a video extensometer which provide precise measurements of the dislocation of the gauge marks, positioned approximately equidistants from the midpoint of the test samples. For each type of material were tested between 3 to 5 specimens. The tests were made considering ES EN ISO-527-1:1996 [139] and BS EN ISO 527-2:1996 standards [131].

Figure 5.6: Tensile tester, Shimadzu AGS-10kNX

5.3.1 Calculations

Stress (σ)

The stress (σ) is calculated using the output values given by the tensile tester software, according to equation 5.3 [139]:

$$\sigma = \frac{\mathrm{F}}{\mathrm{A}} \tag{5.3}$$

where:

σ is the tensile stress, in MPa;

F is the measured force, in N;

A is the cross-sectional area of the specimen, in mm^2.

Elastic modulus (E)

The elastic modulus (E), or Young's modulus, is the mechanical property which measures the resistance of a solid material to being deformed elastically when a force is applied to it. It is defined on the basis of two specified strain values and its correspondent tensile stress values, as it can be seen in the formula 5.4 [139]:

$$\mathrm{E} = \frac{\sigma_2 - \sigma_1}{\varepsilon_2 - \varepsilon_1} \tag{5.4}$$

where

E is elastic modulus (MPa);

σ_1 is the stress (MPa) measured at the strain value ε_1=0.01;

σ_2 is the stress (MPa) measured at the strain value ε_2=0.05 .

Elongation at break (ε_b)

The elongation at break, or fracture strain, is defined as the ratio between the stretched gauge length after breakage of test specimen and its original, initial gauge length. This property determines the capability of a material to resist deformation without fracturing [139]. It can be determined as the maximum value of strain obtained in the tensile test values given by the software.

Elongation at break is given by eq. 5.5 [139]:

$$\varepsilon_b = \frac{\Delta L_f}{L_0} \tag{5.5}$$

where

ε_b is the strain;

L_0 is the gauge length of the test specimen, in mm;

ΔL_f is the maximum increase in the specimen length between the gauge marks, in mm.

Tensile strength at break (σ_b)

The tensile strength at break (σ_b) is defined as the stress at which the test specimen ruptures (in MPa) [139].

It can be determined as the maximum value of stress obtained in the tensile test values given by the software.

Part III

Results and Discussion

Chapter 6

Experimental results

6.1 Morphological characterization

Scanning electron microscopy is a technique which scans a focused beam of high-energy electrons over a surface in order to create an image. The signals created through the interaction between the sample and the electrons are then used to obtain information about the surface topography and composition.

It must be taken in consideration that the obtained images represent a specific limited area of the sample and the conclusions drawn from them may not be valid for the whole sample.

In fig.6.1 are represented images of the used nanoparticles: treated CNTs (a,b) and graphene (c,d).

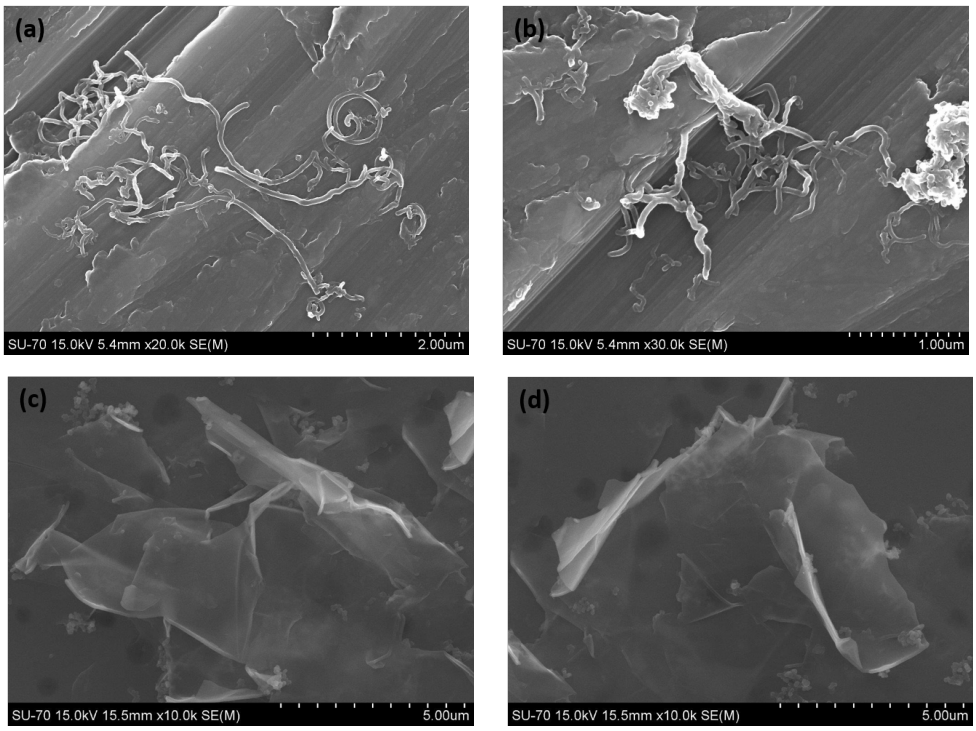

Figure 6.1: SEM images of the acid treated MWNTs (a,b) and of the graphene nanosheets (c,d).

In fig.6.1 it can be observed that the carbon nanotubes present a one dimensional morphology with tubular geometry without any agglomeration. Graphene nanosheets aspect is quite different. Graphene can be characterized as a two dimensional material with sheet like morphology. The shape of the nanosheets and the way they are folded, exhibiting wrinkles, presenting a wave like silhouette. The graphene sheets appears to present fine dispersion with no aggregated sheets.

The micrographs of the TPU based nanocomposites containing NT CNTs and T CNTs can be seen in fig.6.2 and fig.6.3, respectively. It can be claimed a relatively good dispersion of both types of filler in the polymer, since the carbon nanotubes appear to be individualised and cannot be seen agglomerates of such nanomaterial. The nanocomposite presents an overall visually uniform aspect. In fig.6.2(c) it can be observed an interesting detail, marked in the image revealing strong interfacial adhesion between the CNTs and the TPU polymer matrix.

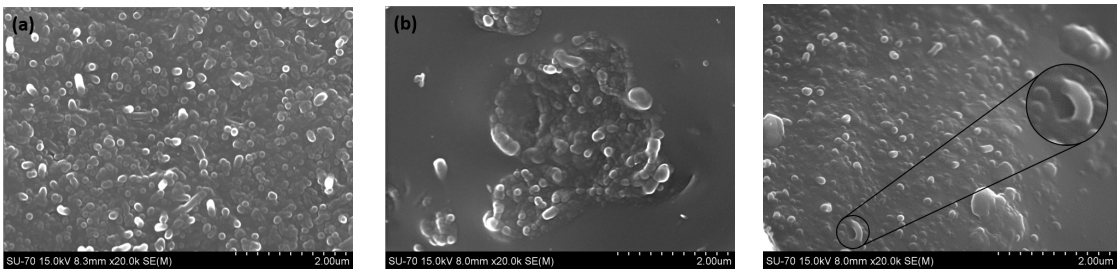

Figure 6.2: SEM micrograph from the non-treated carbon nanotubes/polyurethane nanocomposites: (a) PU_05_NT_CNT , (b) PU_10_NT_CNT and (c) PU_15_NT_CNT.

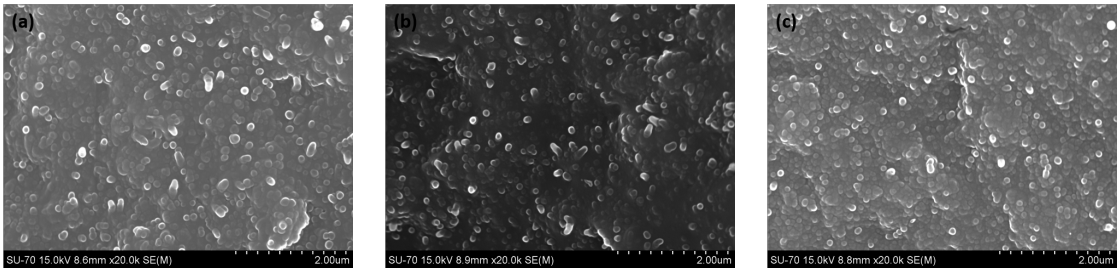

Figure 6.3: SEM micrograph from the acid treated carbon nanotubes/polyurethane nanocomposites: (a) PU_05_T_CNT , (b) PU_10_T_CNT and (c) PU_15_T_CNT.

In fig.6.4 are illustrated the SEM micrographs of the graphene/TPU nanocomposites. It can be clearly recognized the typical graphene nanosheet geometry referred previously, presenting a layered petal like morphology and wrinkles. The graphene nanosheets appear to be well incorporated in the polymeric matrix. Stacks of graphene nanosheets were not spotted in the SEM sample.

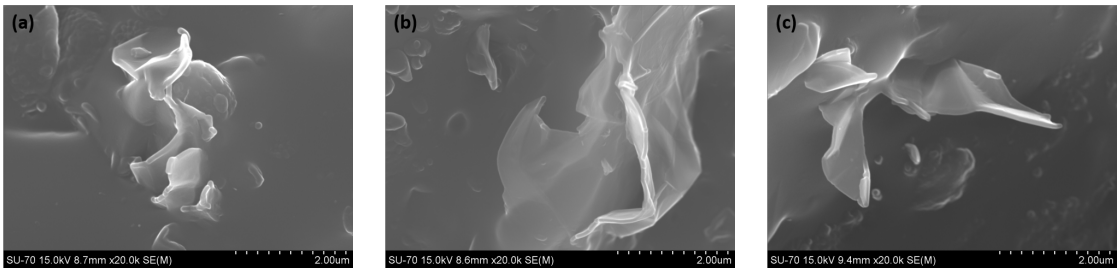

Figure 6.4: SEM micrograph from the graphene/polyurethane nanocomposites: (a) PU_05_Gra , (b) PU_10_Gra and (c) PU_15_Gra.

A general overview of the studied polyurethane nanocomposites can be seen in SEM images with less magnification shown in fig.6.5. In the subfigures (a) and (b), the white dots represent the top view of the carbon nanotubes, which look homogeneously dispersed in the sample. In the subfigure (c) it can be seen several bright white lines that are the graphene sheets side views, representing their silhouette. It can also be seen some folded graphene sheets embedded on the PU matrix. Graphene sheets appear to be randomly distributed in the sample and no evidence of stacking was found in these images.

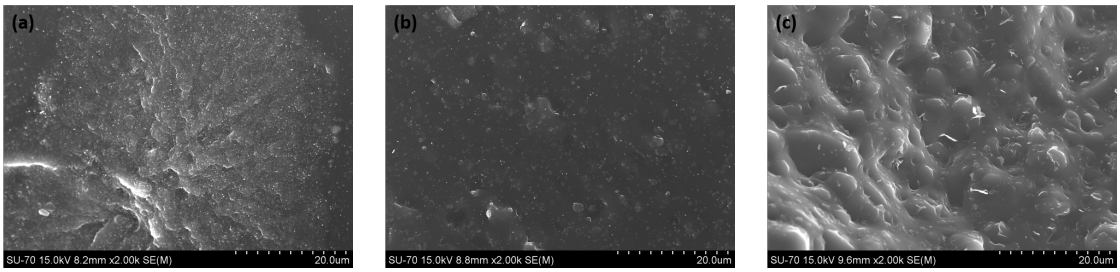

Figure 6.5: SEM images from the polyurethane based nanocomposites containing 1.5 vol.% of NT CNTs (a), 1.5 vol.% T CNTs (b) and 1.5 vol.% graphene (c).

6.2 Thermal properties

Differential Scanning Calorimetry (DSC) is a measuring method that allows the identification and quantification of thermal effects and its characteristics over a large range of temperature [134]. Through this technique, it was determined the glass transition temperature (T_g), melting temperature (T_m) and specific heat capacity (c_p) values for each specimen type. Additionally, it was made a comparative analysis of the thermal diffusivity (α) of the nanocomposites containing NT CNTs and T CNTs.

The Heat Flow - Temperature curves obtained through DSC can be seen in Appendix A.

6.2.1 Glass transition temperature (T_g) and Melting temperature (T_m)

In this section it will be described and analysed the differences in glass transition (T_g) and melting temperatures (T_m) for the different prepared nanocomposites. All the main results obtained through DSC are summarized in table 6.1. As it can be seen the obtained results are very similar and the standard deviation ranges of values cover each other, particularly in

the case of glass transition temperature. This situation occurs because the measuring method of this thermal transitions, specially the one for T_g, is quite manual and, therefore, incurs in errors caused by the human intervention.

Table 6.1: Experimental values of the thermal properties obtained by DSC

	$\mathbf{T_g}$ (°C)	$\mathbf{T_m}$ (°C)
PU_ pure	51.23 ± 0.76	153.52 ± 0.01
PU_ 140	50.61 ±0.57	146.51 ± 0.01
PU_ 05_ NT_ CNT	50.14 ± 0.16	146.03 ± 0.02
PU_ 10_ NT_ CNT	50.99 ± 0.22	150.02 ± 0.01
PU_ 15_ NT_ CNT	61.13 ± 0.01	150.19 ± 0.03
PU_ 05_ T_ CNT	51.09 ± 0.16	152.16 ± 0.07
PU_ 10_ T_ CNT	50.55 ± 0.01	150.13 ± 0.12
PU_ 15_ T_ CNT	51.72 ± 1.00	148.53 ± 0.04
PU_ 05_ Gra	51.46 ± 0.19	143.87 ± 0.01
PU_ 10_ Gra	50.62 ± 0.88	147.95 ± 0.12
PU_ 15_ Gra	50.26 ± 0.00	148.34 ± 0.02

Since glass transition temperature is the one used in the shape-memory effect activation of polyurethane, this is a very important parameter to be studied. Observing the values referring to the NT CNTs filled nanocomposites it can be noticed an increase of the glass transition temperature as the content of NT CNTs increases. However, comparing these with pure PU, it can be noticed that for the two lower NT CNTs concentrations the T_g values are quite similar to the T_g of pure PU. Only for higher volume concentrations of NT CNTs it can be observed an increase of up to 10°C, as compared with pure PU.

About the functionalized CNTs/PU nanocomposites, it cannot be determined a specific tendency. Observing the average values, it can be claimed that T_g is higher for the 1.5 vol.% T CNTs/PU nanocomposite as compared to other concentrations. In comparison with the unfilled PU specimen it was measured an enhancement of about 0.9%. However, the standard deviation values do not allow a clear conclusion.

Examining both nanocomposites filled with NT CNTs and T CNTs, it can be noticed that the values are quite similar, except for the nanocomposites incorporating 1.5 vol.% CNTs which present a T_g about 10°C higher for the nanocomposite filled with 1.5 vol.% NT CNTs.

When the filler mixed in the polymeric matrix is graphene, the tendency followed in this case is the reverse of the one exhibited by the NT CNTs/PU nanocomposites, since as the volume fraction of graphene increases, the average T_g value decreases. However, this tendency cannot be declared with certainty, since the standard deviation range of values makes it inconclusive.

Analysing the results obtained for the melting temperature T_m, it can be noticed that all the values attained for the nanocomposites are below the ones obtained for the pristine PU. Analysing the results corresponding to the nanocomposites loaded with NT CNTs, it can be

concluded that there is an upward trend in the obtained values of T_m as the volume fraction of NT CNTs increases. However, the T_m for all the nanocomposites filled with NT CNTs is lower than the one from pristine PU. The decrease is, however, not very significant, ranging from 3.33°C for the 1.5 vol.% NT CNTs/PU nanocomposite to 7.49°C for the 0.5 vol.% NT CNTs/PU nanocomposite, representing a maximum decrease of 4.9%.

For the T CNTs nanocomposites the tendency was reversed and it was observed a decrease of the T_m values with the increase of the T CNTs content. Comparing to the unfilled PU, it was observed a decrease in T_g ranging from 1.36°C for the nanocomposite filled with 0.5 vol.% T CNTs to 4.99°C for the nanocomposite containing 1.5 vol.% T CNTs, representing a maximum decrease of 3.3%.

Comparing the two kinds of filler referred before, NT CNTs and T CNTs, it can be observed that, in general, the T_m values for the nanocomposites with NT CNTs are lower than the ones with T CNTs, and both are lower than the T_m value for pure PU.

When the system is filled with graphene, the results follow the same order than the ones from the NT CNTs nanocomposites. So, there is an increase in the T_m values as the concentration of graphene is rising. In comparison with neat PU, it can be seen that the T_m values are lower than the one measured from the neat polymer. In fact 0.5 vol.% graphene, 1.0 vol.% graphene and 1.5 vol.% graphene nanocomposites exhibit values of T_m 6.3%, 3.6% and 3.4% lower than the one from neat PU.

Finally, when analysed all the nanocomposites loaded with different fillers with the same volume fraction, it can be stated that the graphene nanocomposites are the ones with the lowest values of T_m for each loading.

6.2.2 Specific heat capacity and Thermal diffusivity

Both specific heat capacity and thermal diffusivity define a material's ability to store and transfer heat. These properties allow a better comprehension of the genesis and behaviour of the materials.

In fig.6.6 it can be seen a graph exhibiting the computed c_p values for all the nanocomposites and for the pure PU. Below 30°C, the specific heat capacity increases slowly for all the samples tested. However, from 30°C to approximately 65°C occurs a sharp increase in the specific heat capacity. The inflexion point appears in all the samples at a similar temperature, around which is the glass transition temperature of the nanocomposites, calculated to be the average value of 51.73 ± 2.87 °C. Above the temperature of ≈65°C the specific heat capacity keeps raising, reaching a relative minimum at approximately 100°C and a new relative maximum between 142°C and 155°C. For the nanocomposites it was also attained a second relative maximum, revealing the existence of a second melting temperature. The decreasing of the specific heat capacity only occurs at 190°C. In fig.6.6, it can be observed that all the specimens present a similar behaviour, only changing the magnitude of the specific heat values, except for the PU_15_NT_CNT. This sample exhibits an abnormal curve shape, which is consistent with the disconnected glass transition temperature value obtained for this sample. This indicates that this nanocomposite does not display reliable results and should be further investigated in order to clarify these results. The specific heat capacity values of the neat PU are only surpassed by the ones from the nanocomposites containing 1.5 vol.% graphene and 1.0 vol.% NT CNTs.

It is also appropriate to analyse the behaviour of the specimens regarding the thermal diffusivity (α), which measures the propagation by conduction caused by a change of

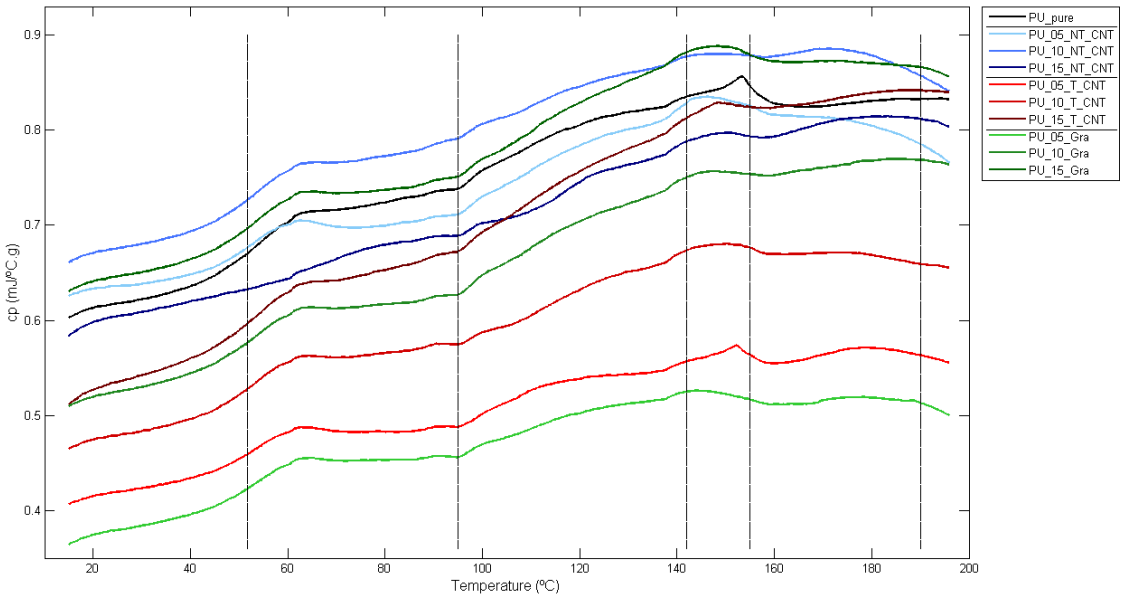

Figure 6.6: Specific heat capacity of the pure polyurethane and of the produced nanocomposites.

temperature.

In fig.6.7 it is presented the thermal diffusivity for two nanocomposites containing 1.5 vol.% NT CNTs and 1.5 vol.% T CNTs in comparison with the thermal diffusivity of the unfilled PU melt mixed at 140°C. As it can be noticed, thermal diffusivities of both NT CNTs and T CNTs filled nanocomposites are higher than the one from neat PU. In fact, the nanocomposite containing NT CNTs revealed to have higher thermal diffusivity than the nanocomposite incorporating T CNTs at the same concentration.

On the other side, in fig.6.8 it can be analysed the influence of the volumic fraction of filler in the thermal diffusivity results. It can be observed that the thermal diffusivity results from both nanocomposites containing 1.0 vol.% NT CNTs and 1.5 vol.% NT CNTs surpass the one from the sample composed by unfilled PU. Comparing the two filled nanomaterials, it is quite clear that the sample containing the highest quantity of NT CNTs, which is 1.5 vol.%, presents a higher thermal diffusivity than the one from the nanocomposite incorporating 1.0 vol.% NT CNTs.

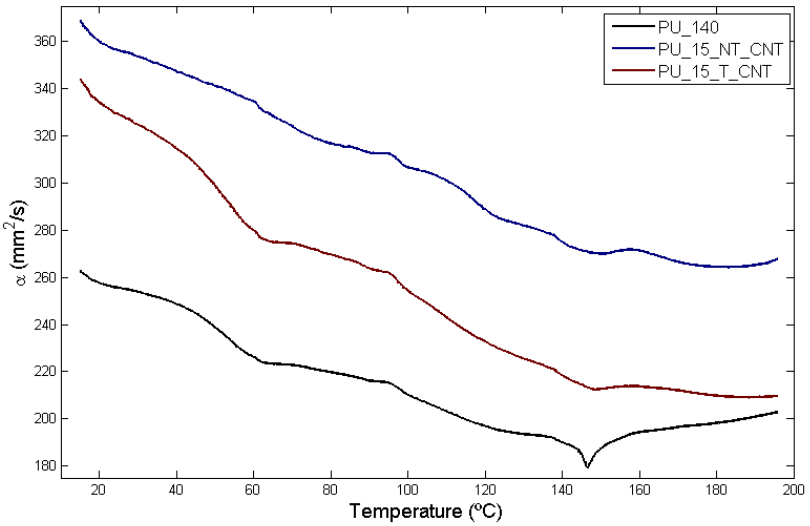

Figure 6.7: Thermal diffusivity of polyurethane melt mixed at 140°C and nanocomposites with 1.5 vol.% of non-treated carbon nanotubes and treated carbon nanotubes

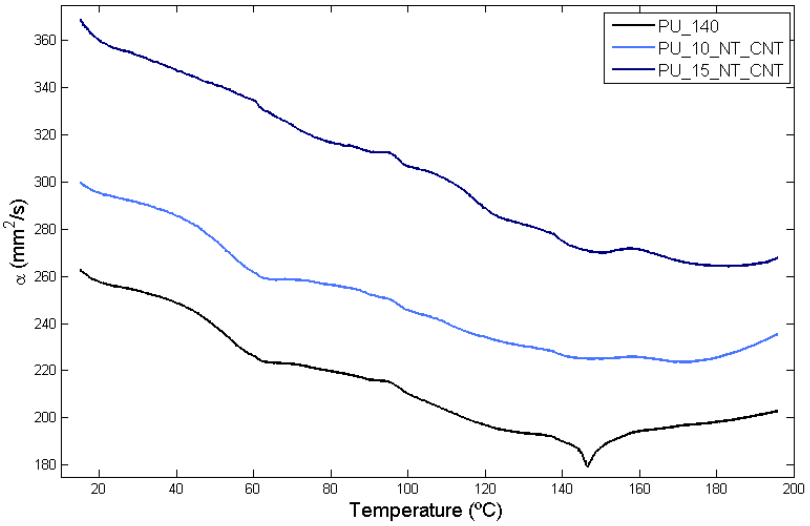

Figure 6.8: Thermal diffusivity of polyurethane melt mixed at 140°C and nanocomposites filled with 1.0 vol.% and 1.5 vol.% non-treated carbon nanotubes

6.3 Mechanical properties

In this section it will be presented and compared the differences between the mechanical properties of non-treated CNTs (NT CNTs), treated CNTs (T CNTs) and graphene (Gra) nanocomposites. The elastic modulus (E), tensile strength at break (σ_b) and elongation at break (ε_b) will be analysed.

The Stress - Strain average curves obtained through tensile tests can be seen in Appendix B.

An overview of the mechanical properties of the different nanocomposites can be observed in table 6.2. The results will be discussed and interpreted in the following sections.

Table 6.2: Mechanical properties provided by tensile tests

Designation	E **(MPa)**	σ_b **(MPa)**	ε_b **(%)**
PU_ pure	23.87 ± 0.49	18.94 ± 0.82	606.69 ± 14.07
PU_ 140	23.37 ± 0.86	18.89 ± 1.17	681.68 ± 63.90
PU_ 05_ NT_ CNT	25.47 ± 0.38	18.25 ± 0.93	670.72 ± 25.10
PU_ 10_ NT_ CNT	26.52 ± 0.43	17.81 ± 0.66	645.88 ± 16.18
PU_ 15_ NT_ CNT	29.19 ± 0.69	17.40 ± 0.82	618.58 ± 22.20
PU_ 05_ T_ CNT	23.59 ± 0.40	18.05 ± 0.30	672.05 ± 30.72
PU_ 10_ T_ CNT	25.81 ± 0.53	13.62 ± 1.41	538.88 ± 32.62
PU_ 15_ T_ CNT	26.24 ± 0.86	15.20 ± 1.12	548.59 ± 29.56
PU_ 05_ Gra	25.68 ± 1.00	20.23 ± 1.38	661.65 ± 27.98
PU_ 10_ Gra	29.45 ± 0.44	20.97 ± 0.13	644.97 ± 12.99
PU_ 15_ Gra	32.98 ± 0.16	20.43 ± 0.77	644.25 ± 9.41

6.3.1 Elastic modulus (E)

In this section it will be described and analysed the elastic modulus values obtained through tensile testing. In fig.6.9 it can be observed the elastic modulus for the produced nanocomposites. Observing the results for the NT CNTs nanocomposites it can be concluded that an increase of the NT CNT volume fraction leads to an increase of the elastic modulus. Also, the elastic modulus of the NT CNTs/TPU nanocomposites is higher than the one from the pure PU, attaining its maximum enhancement of 22.2% for the volume fraction of 1.5% as compared with the pure PU.

Regarding to the obtained results for the T CNTs nanocomposites, it was also observed an increase of the elastic modulus average value with the increase of the filler volume fraction. The highest elastic modulus average value acquired for the T CNTs nanocomposites was 26.24 MPa for the 1.5 vol.% T CNTs nanocomposite, corresponding to an enhancement of 9.8% as compared with pure PU.

Comparing both types of CNT/TPU nanocomposites, with treated and non treated CNTs, it can be observed that the T CNTs/TPU nanocomposites present smaller elastic modulus than the one for the NT CNTs/TPU nanocomposites for all the studied CNT concentrations.

For the graphene nanocomposites, it was determined a clear increase in elastic modulus as the graphene volume fraction rises. All the graphene filled nanocomposites increased the elastic modulus values as compared with pure PU. The highest E of 32.98 ± 0.16 MPa was

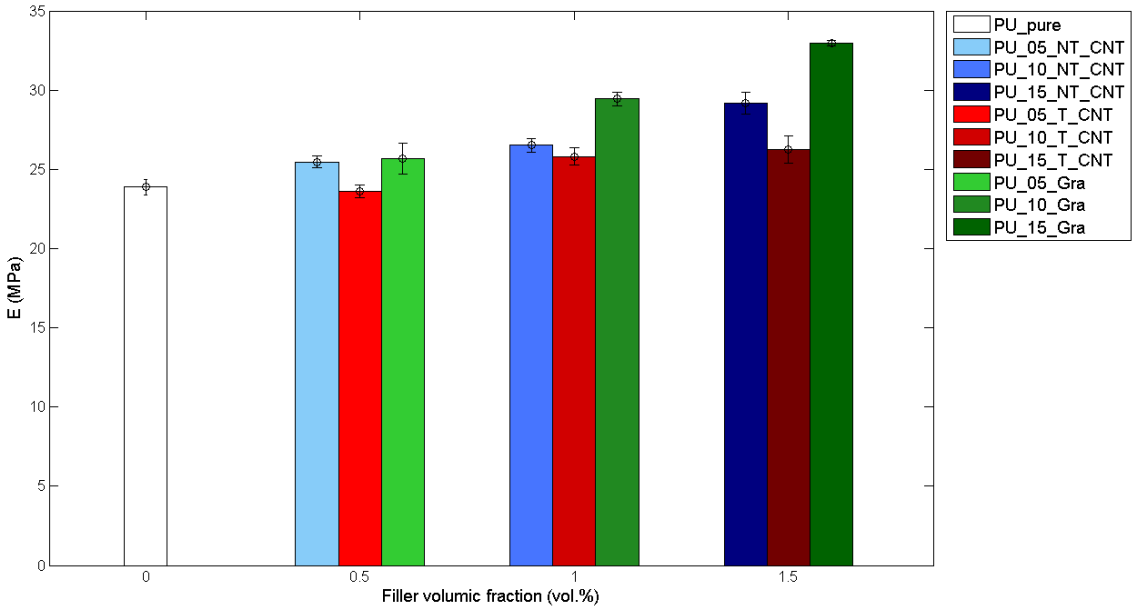

Figure 6.9: Elastic modulus for the produced TPU based nanocomposites in comparison with pure PU

obtained for the 1.5 vol.% graphene nanocomposite, corresponding to an enhancement of 38.1% as compared with the reference pure PU.

Finally, it can be observed that the TPU nanocomposites reinforced with graphene present the highest values of elastic modulus for all the used concentrations, as compared with the pure PU and even with the CNT/TPU nanocomposites.

6.3.2 Tensile strength at break (σ_b)

In fig.6.10 it can be observed the tensile strength of the processed nanocomposites. Analysing the tensile strength at break for the NT CNTs/TPU nanocomposites it is possible to conclude that there is a downward trend as the NT CNT volume fraction increases in the nanocomposites. It can be pointed out that the standard deviation values are quite high and for that reason the values of σ_b are not clearly distinguishable.

In the case of the T CNTs/TPU nanocomposites, the behaviour of the strength at break property is not as linear as it was observed for the NT CNTs/TPU nanocomposites, although it is clearly observed a decrease as compared with pure PU. As for the NT CNTs/TPU nanocomposites, the standard deviation does not enable to distinguish the values for the σ_b of the nanocomposites.

Comparing the behaviour for NT CNTs/TPU and T CNTs/TPU nanocomposites, it can be seen that in general the tensile strength at break values for both types of nanocomposites are very similar, with a tendency for a smaller value for the T CNTs/TPU nanocomposites. In all cases it is noticeable that the pure PU tensile strength at break average value is greater than the one presented by the nanocomposites. However, the standard deviation values do not allow to surely define if the tensile strength at break value corresponding to pure PU is

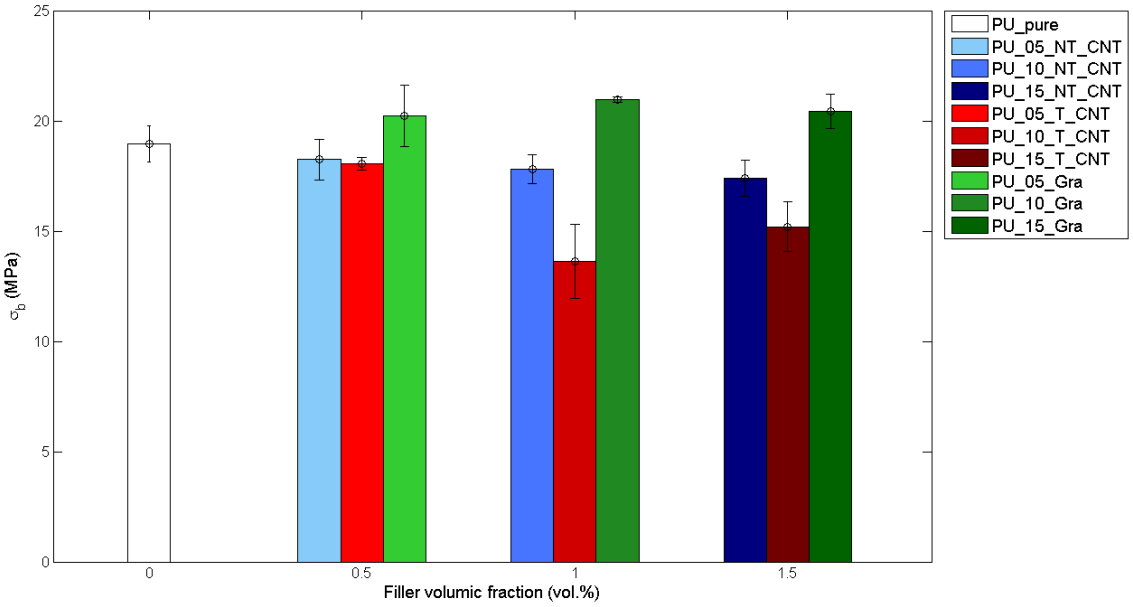

Figure 6.10: Tensile strength for the produced TPU based nanocomposites in comparison with pure PU

actually higher than the one from all NT CNTs nanocomposite.

Concerning to the graphene/TPU nanocomposites, it can be observed that the average tensile strength at break is very similar for the different filler loadings and higher than the one observed for pure PU. However, the standard deviation values do not allow a clear conclusion on this matter.

Comparing the tensile strength at break results for all the studied nanocomposites (containing NT CNTs, T CNTs and graphene), it can be clearly observed that the tensile strength at break for the CNTs/TPU nanocomposites presents the lower values compared to pure PU and even compared with graphene/TPU nanocomposites. The highest values are obtained for the graphene/TPU nanocomposites, which are higher than the value of σ_b for pure TPU.

6.3.3 Elongation at break (ε_b)

In fig.6.11 it is represented the elongation at break values for the processed nanocomposites. For the NT CNTs/TPU nanocomposites it is observed an enhancement of the elongation at break for the nanocomposites as compared with the one of pure PU, for all the NT CNTs concentrations. However, it can be observed a decrease of the elongation at break with the increase of the NT CNTs volume fraction. It may be pointed out that the standard deviation values are quite high and for that reason it is not possible to have a clear conclusion on that matter.

Analysing the elongation at break for the T CNTs/TPU nanocomposites, it can be seen that there is a maximum elongation at break value of 672.05% for the nanocomposite containing 0.5 vol.% T CNTs, followed by a decrease for higher T CNTs concentrations. In

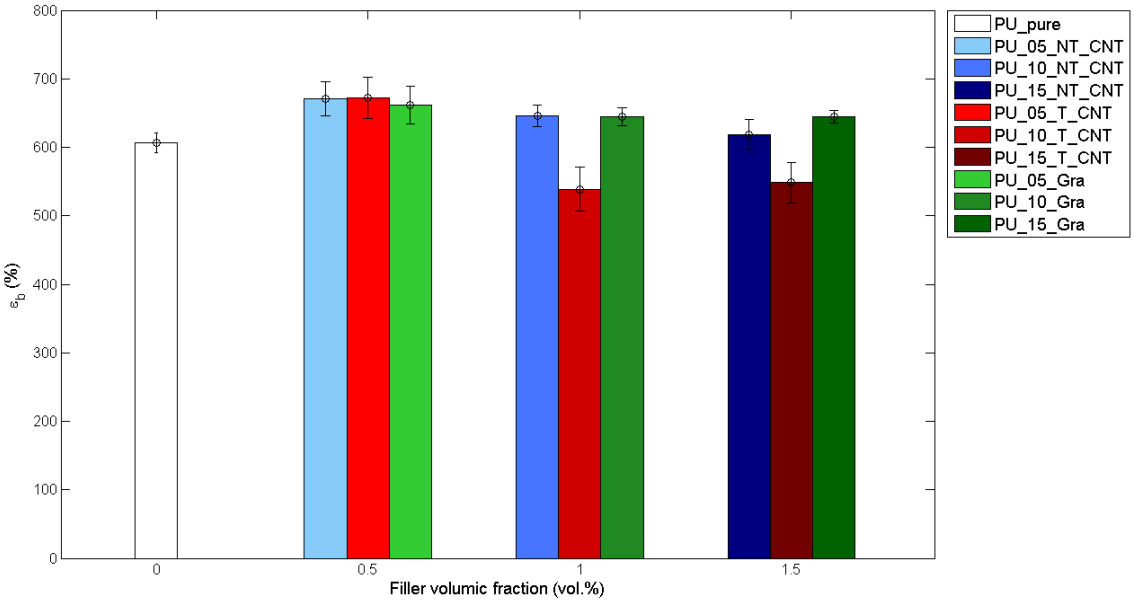

Figure 6.11: Elongation at break for the produced TPU based nanocomposites in comparison with pure PU

relation to pure PU, it can be clearly observed that the T CNTs/TPU nanocomposite with 0.5 vol.% T CNTs is the only one presenting higher ε_b. The nanocomposites containing 1.0 and 1.5 vol.% T CNTs detain smaller ε_b.

Comparing both types of CNTs, treated and non-treated, it can be seen that at the lower filler concentration of 0.5 vol.% the ε_b values are very similar. However, with increasing filler concentration it can be clearly observed a significant difference in ε_b, with the NT CNTs/TPU nanocomposites exhibiting higher ε_b than the one for T CNTs/TPU nanocomposites.

Observing the behaviour of the elongation at break of the graphene/TPU nanocomposites, it can be noticed a small increase of the ε_b for all the graphene/TPU nanocomposites as compared with pure PU. However, for different used concentrations the differences are not very significant.

Finally, the performance of all the prepared nanocomposites must be compared. For the TPU nanocomposites containing 0.5 vol.% of filler, it can be observed that the average values are quite alike for all types of nanoparticles, and such values are undoubtedly superior than the one obtained for pure PU. It was observed an enhancement of about 10% of the ε_b, compared with pure PU. For the nanocomposites with 1.0 vol.% of filler, the elongation at break for the NT CNTs and graphene nanocomposites are quite similar and superior to the pure TPU value. However, for the T CNTs/TPU nanocomposites it was observed a decrease of ε_b. The same was observed for the concentration of 1.5 vol.% of filler. It can be seen that the ε_b for both NT CNTs/TPU and graphene/TPU nanocomposites are similar and higher than the one observed for pure TPU and for the T CNTs/TPU nanocomposite.

Chapter 7

Discussion

7.1 Thermal properties

Through differential scanning calorimetry (DSC) it was obtained the glass transition temperature (T_g), melt transition temperature (T_m), specific heat capacity (c_p) and thermal diffusivity (α) of the nanocomposites.

The glass transition temperature is a macroscopic expression of the relaxation behaviour of nanocomposite systems. Its value is dependent of several structural parameters [140]. The expected change to occur in the glass transition temperature upon incorporation of a carbon based filler in a polymer matrix was an increase of its value in relation to the neat polymer. Further increase of the CNTs and graphene concentrations in the polymer matrix would, supposedly, gradually increase the value of T_g. The reason is the restricted mobility of the polymer molecules around the filler particles due to the interfacial interaction between the fillers and the polymeric matrix, resulting in an increasing of T_g [56, 66, 94, 141, 142]. Besides, due to the fact that the used fillers possess nanometric size, this amount of immobile material is even higher due to the high surface/volume ratio [141]. According to Ash et al. [143], the glass transition temperature of a filled composite should increase or at least be constant upon the addition of high modulus fillers, which is verified in the present experiments. T_g values remain quite similar to the one from unfilled PU with the addition of different concentrations of the different types of carbon based fillers. In fact, the maximum obtained decrease of T_g in comparison with the one from pristine PU was 1.09°C, which represents a decrease of 2.1%. Besides, it was registered a large increase of 9.90°C in the T_g from the 1.5 vol.% NT CNTs/TPU nanocomposite, which represents an increase of 19.3%. This result is inconsistent and quite variable in comparison with the rest of the results obtained for other nanocomposites, which may be an indication of an error. Further tests should be performed in order to stablish if the shift in T_g obtained for the 1.5 vol.% NT CNTs/PU nanocomposite is in fact representative of the material's behaviour or if it was in fact an error. Analysing the work of other investigators, Liu et al. [144] observed an increase of the T_g by approximately 10°C upon incorporation of 20 wt.% SiC. In the investigation of Fang et al. [140], it was measured an increase of 15°C in T_g for the 12 wt.% graphene nanosheets (GNS)/ polystyrene (PS) composite in comparison with the neat PS. Strankowski et al. [94] produced PU based composites reinforced with thermally reduced graphene (TRG). The results showed progressive increase of the T_g values from -27 °C for the pristine PU to -16°C for the nanocomposite possessing 3.0 wt.% TRG. Kim et al. [66] also registered an

increase of 4.71°C in the T_g for the PU based nanocomposite filled with 1.0 wt.% chemically modified TRG and an increase of 7.34°C in the T_g from the nanocomposite possessing 2.0 wt.% chemically modified TRG. However, when the filler concentration increased to 2.5 wt.% TRG, the value of T_g slightly decreased in comparison with the one from 2.0 wt.% TRG, reversing the growth trend, in spite of still being higher than the T_g from the neat PU. This decrease was assigned to particle aggregation and auto-inhibition processes. In the 2013's article from Fonseca et al. [10] it was also observed an increase of T_g with the addition of carbon nanotubes (CNTs), raising from -25°C for the neat shape-memory polyurethane (SMPU) to -16°C for the 0.5 vol.% CNTs/SMPU nanocomposite. This enhancement was ascribed to an homogeneous distribution of CNTs in the polymeric matrix. Although in the literature there are several reports of increasing of T_g upon incorporation of fillers, it can also be found other investigators that experienced a decrease in T_g with the addition of carbon based fillers. In 2003, Potschke et al. [141] obtained an increase of T_g, but only until 1 wt.% MWNTs (multi-walled carbon nanotubes) concentration. From that concentration to 15 wt.% MWNTs concentration, the correspondent nanocomposites exhibited a decrease in T_g, which was attributed to the processing step of filling the polymer with the MWNTs. Since the used method for the addition of the filler into the polymeric matrix was the same used in this thesis, i.e. mechanical melt mixing, this may be a reasonable explanation for the observed decreasing of T_g for the PU nanocomposites produced in this investigation.

In the case of the melting temperature, it is possible that the observed decrease in relation to the T_m of the neat PU may be explained by poor dispersion of the fillers within the polymer matrix, as sustained by Barkoula et al. [145].

In relation to specific heat capacity some observations must be pointed out. The fact that the inflection point occurs for all the samples at a similar temperature is mainly due to the polymeric matrix and not to the introduced filler, as stated by Weidenfeller [146]. Evaluating the general results, it can be claimed that, with the exception of the nanocomposites containing 1.5 vol.% graphene and 1.0 vol.% NT CNTs, the produced nanocomposites possess better thermal properties than those of neat PU. The fact that the nanocomposites possess lower specific heat capacity means that they need less heat to raise the temperature by 1°C per unit mass. Consequently, the transition temperature of the shape-memory material can be more easily tuneable and the shape-memory composite will require less energy to attain the same effect.

It is also appropriate to analyse the behaviour of the specimens regarding the thermal diffusivity. Thermal diffusivity measures the propagation by conduction caused by a change of temperature. This material-specific property measures how quickly a material reacts to a change of temperature [147]. Therefore, is desirable that the shape-memory material possesses high thermal diffusivity so that it can respond faster to a thermal stimulus and, consequently, present a lower recovery time [146]. As it could be seen in fig.6.7, both NT CNTs and T CNTs filled nanocomposites exhibit higher thermal diffusivity than the one from neat PU, resulting in an enhancement of the shape-memory properties of the material, since the thermal actuation response is expected to be faster for the produced nanocomposites than for the neat PU_ 140 specimen. Through the observation of fig.6.8 it can be seen that both nanocomposites possessing 1.0 and 1.5 vol.% NT CNTs present higher α than the neat PU, which is an important improvement from the shape-memory perspective, since both nanocomposites will be expected to perform thermal activation faster.

7.2 Mechanical properties

In this section it will be investigated the influence of different concentrations of filler in the mechanical properties of the nanocomposites. The mechanical properties evaluated on this thesis are: elastic modulus, tensile strength at break and elongation at break.

The elastic modulus is defined as a measure of stiffness of an elastic material. This property determines the body's resistance to be deformed elastically when it is submitted to a certain force. The tensile strength at break (σ_b) is defined as the tensile stress at the moment the material ruptures. While tested, the material reaches a point where the fully stretched molecules are no longer capable of sustaining the tensile stress, leading to the break of the material. The value of this property is given by the maximum stress attained by a material that is being stretched, before it breaks. At last, elongation at break is defined as the ratio between the changed length and the initial length of the specimen at rupture under tensile loading. It is a measure of the maximum strain attained by the material before breaking.

The results reveal that in all types of the studied nanocomposites, (filled with NT CNT, T CNT and graphene) it was observed an increase in the elastic modulus as the volume fraction of filler increases in the sample. This behaviour is in agreement with what is described in the literature. Ni et al. [108] support this fact in their article, in which elastic modulus of SMPU/CNTs nanocomposites became linearly higher with the increase of the filler weight fraction. Safadi et al. [148] also described an enhancement of 61.0% in elastic modulus with the increase of MWNTs content in PS matrix from 1.0 wt.% to 5.0 wt.%. The behaviour of the different nanocomposites regarding to the tensile strength at break property is not so easy to describe, since it does not follow a tendency. For the NT CNTs nanocomposites it can be observed a decrease of tensile strength at break with the increase of the concentration of NT CNTs into TPU, while for T CNTs nanocomposites the tensile strength at break value decreases till 1.0 vol.% T CNTs and then increases for 1.5 vol.% T CNTs. For the graphene filled nanocomposites, the relation between values is completely reversed, since the highest average value of tensile strength at break was achieved for the 1.0 vol.% graphene nanocomposite and then slightly decreases for 1.5 vol.% graphene. The literature validates the results obtained for the graphene nanocomposites, since tensile strength at break has been proved to usually be higher for nanocomposites with higher concentration of carbon based fillers. Both NT CNTs and graphene nanocomposites reveal a decrease of elongation at break average values with the increase of filler concentration. This behaviour can be explained since the incorporation of CNTs and graphene in the polymeric matrix causes an enhancement of the nanocomposite stiffness, and therefore the material loses ductility, tending to rupture earlier. Therefore, elongation at break tends to decrease slowly [125]. However, T CNTs nanocomposites do not exactly appear to follow this principle. The literature provides information about the mechanical behaviour of the nanocomposites that is consistent with the obtained results. Fang et al. [140] reported a linear increase of the elastic modulus and tensile strength at break upon rise of the GNS content for PS-based composites. Kim et al. [66] presented results sustaining that the increase of thermally reduced graphene (TRG) content in SMPU leads to a decrease in the elongation at break of the nanocomposites. Now, focusing on the CNTs filled nanocomposites results, according to relevant experiments reported in journal articles, the natural behaviour appears to be the increase of tensile strength at break with the increase of elastic modulus, as demonstrated by Safadi et al., [148], Coleman et al. [149], Raja et al. [56] and Fang et al. [140]. However, this relation is not always so predictable. Gagolkina

et al. [150] revealed some inconsistencies similar to the ones described in this thesis. The authors produced crosslinked polyurethane based nanocomposites containing CNTs and tested their mechanical properties. The results revealed that not always an increase of the elastic modulus corresponds to an increase of the tensile strength at break. A likely explanation for the higher elongation at break at the lowest content of CNTs (0.5 vol.%) exhibited in the present work is the fact that there might not be a completely homogeneous dispersion of NT and T CNTs in the polymer matrix, which at higher filler loading results in more fragility points, leading to an early breakage.

Compared with pure PU, the NT CNTs and the graphene nanocomposites present relevant enhancements of the elastic modulus average values. This behaviour was expected, since, according to Mallick [151] and Fang et al. [140], given the excellent mechanical properties of the carbon based nanofillers, their incorporation in a polymer matrix should result in composites with enhanced elastic modulus. This is a very much desirable improvement since it allows the creation of more stiff, resistant materials with enhanced mechanical properties. Qian et al. [152] report an enhancement of 35.0% in the elastic modulus of the 1.0 wt.% MWNTs/PS composite with filler average length of 15 μm. Zhang et al. [153] also report an enhancement of the elastic modulus by $\approx$ 115% for 1.0 wt.% MWNTs in polyamide 6 (PA6). This behaviour is also supported by Cadek et al. [154], when PVA (polyvinyl alcohol) was filled with 1.0 wt.% MWNTs and improved their elastic modulus by $\approx$ 77% in comparison with pristine PVA. In this work, it can be observed for both NT CNTs and T CNTs nanocomposites a decrease of the tensile strength at break as compared with the one of pure PU. However, when the filler is graphene, tensile strength at break average values are superior to the reference pure PU. The behaviour of the CNTs/TPU nanocomposites was not expected. It is described by the bibliography the enhancement of tensile strength at break upon incorporation of CNTs into SMP matrix, since the elastic modulus also increases. Analysing the elongation at break, NT CNTs/TPU and graphene/TPU nanocomposites exhibit similar behaviour, since in both cases the nanocomposites surpass the elongation at break value of the pristine PU. However, it was expected a decrease of the elongation at break upon incorporation of carbon fillers, since the increase in the stiffness of the nanocomposite also induces brittle behaviour. Ruan et al. [155] describe an enhancement of the elastic modulus and tensile strength at break of ultrahigh molecular weight polyethylene (UHMWPE) when containing 1.0 wt.% MWNTs. In fact, E and σ_{b} increased 25.0% and 38.4%, respectively, in comparison with the unfilled UHMWPE. In the article from 2004, Coleman et al. [149] also documented an increase in the elastic modulus from 1.92 $\pm$ 0.33 GPa for the pure polyvinyl alcohol (PVA) to 7.04 $\pm$ 1.5 GPa for the PVA nanocomposite containing 0.6 vol.% MWNTs, therefore representing a 266.7% increase. In Kim et al. [66] research it was observed an enhancement of 213.4% in the elastic modulus of the SMPU nanocomposite loaded with 2.5 wt.% MWNTs. Sahoo et al. [78] proved that for the PU based nanocomposites containing 2.5 wt.% and 5.0 wt.% MWNTs, the Young's modulus is nearly 200% higher than the one from pristine SMPU. The reason why 1.0 vol.% graphene nanocomposite exhibits larger σ_b than 1.5 vol.% graphene nanocomposite, in the present work, may be clarified by these authors. Sahoo et al. [78] witnessed this same effect in their experiments in 2007. In their case, the SMPU based nanocomposite containing 2.5 wt.% MWNTs obtained slightly higher σ_b than the nanocomposite filled with 5.0 wt.% MWNTs. This phenomenon was justified by the authors as a result of a decrease of nucleation due to excess of filler in the nanocomposite. Consequently, the higher degree of crystallinity in the nanocomposite with less filler concentration led to higher stiffness and, consequently, higher tensile strength at break. The same authors described an increase of the tensile strength at

break for both PU nanocomposites containing 2.5 wt.% and 5 wt.% MWNTs, compared to the unfilled PU. Dufresne et al. [156] experiments confirmed the elastic modulus increasing tendency upon incorporation of filler. E increased from 0.865 MPa to 3.54 MPa as the CNT loading in the poly(styrene-co-butyl acrylate) latex matrix increased from 1.0 wt.% to 15.0 wt.% . However, along with the increase of MWNTs content, it was verified some elastic modulus decrease, namely on 2.0 wt.% MWNTs and 7.0 wt.% MWNTs filled composites. It was observed by the authors an irregular elongation at break behaviour. As the CNTs concentration increased from 1 wt.% to 5 wt.% the ε_b values remained constant or slightly decreased. However, when the 7 wt.% CNTs loading was achieved, it occurred a slight increase of ε_b, beginning to decrease again until the CNTs concentration of 15 wt.%. The results revealed that poly(styrene-co-butyl acrylate) latex nanocomposites containing low content of CNTs (1.0 wt.% to 3.0 wt.%) presented ε_{b} equal to the one from the unfilled polymer, while at higher CNTs concentrations elongation at break revealed to be lower than the one from the reference unfilled polymer, ranging from values 27.0% to 29.2% lower, which is in agreement with the observed in the present work. Gupta et al. [117] observed an enhancement in elastic modulus for the reduced graphene oxide (RGO)/PU nanocomposite with 5.0 wt.% filler of approximately 129% in relation to pure PU. Using graphene nanosheets (GNS) as filler, Fang et al. [140] reported an increase of 57.2% of elastic modulus for the nanocomposite with 0.9 wt.% GNS. Ljubic et al. [126] produced PU based nanocomposites filled with surface modified graphene (SMG). It was observed that as the surface modified graphene (SMG) content increases in the PU based nanocomposite, the tensile strength at break increases. In the matter of elongation at break, it was not observed a clear tendency. In fact, in their experiments ε_{b} decreased from 186 $\pm$ 2 % to 144 $\pm$ 8 % as the SMG content increased from 0.2 wt.% to 2.0 wt.%. However, further increase in SMG weight fraction in the nanocomposites caused an enhancement of ε_b with the increase of SMG content from 2.0 wt.% to 5.0 wt.%. The described behaviour is actually quite similar to the one obtained experimentally in the present work. It can be claimed that, in general, the nanocomposites obtained higher elongation at break values than the one of unfilled PU. The results obtained in the present work are corroborated by Ren et al. [157], which prepared GNS/PU nanocomposites. The mechanical results obtained by the authors allow the conclusion that all the produced PU based nanocomposites filled with GNS present higher tensile strength at break and elongation at break than the one from the pristine PU. In fact, tensile strength at break increased from 15.7% to 236.1%, as the filler content increased from 0.1 wt.% GNS to 2.0 wt.% GNS, which is in accordance with the results obtained in this work. Both 1.0 vol.% and 1.5 vol.% T CNTs/TPU nanocomposites possess lower elongation at break values than the one obtained for the reference. As referred before, there is probably some heterogeneity in the CNTs filled nanocomposites, which may cause the decreasing of the elongation at break, in comparison with the one from the unfilled polymer.

Comparing NT CNTs and T CNTs nanocomposites, it can be concluded that for each filler concentration (0.5 vol.%, 1.0 vol.% and 1.5 vol.%) the elastic modulus and tensile strength at break average are higher for the NT CNTs nanocomposites. Regarding the elongation at break, it can be observed that for 1.0 and 1.5 vol.% concentration the NT CNTs/TPU nanocomposites possess higher elongation at break, while for the 0.5 vol.% concentration the NT CNTs/TPU nanocomposite exhibits higher elongation at break. Such observation was not expected since the chemical functionalization could improve the dispersion of the CNTs within the TPU matrix and prevent agglomeration of the CNTs, improving the overall mechanical properties of the nanocomposite material [56,156]. When submitted to an acid treatment with

H_2SO_4 and HNO_3, the carbon nanotubes tips open and carboxylic groups, such as -COOH and -OH groups, are introduced at the open ends, providing a better bonding between the CNTs and the polymeric matrix [158]. Most of the literature provides data that support the enhancement of the mechanical properties with the incorporation of surface modified CNTs rather than pristine ones. An example of that is the Raja et al. [56] investigation, where the authors used pristine and surface modified CNTs to reinforce blend of polyurethane and poly(vinylidene difluoride) (PVDF). They observed higher values of elastic modulus, tensile strength at break and elongation at break for the nanocomposites containing modified CNTs compared with the nanocomposites containing non-modified CNTs. Actually, the elastic modulus of the nanocomposite containing 3.0 wt.% functionalized CNTs is 13.2% higher than the one from the nanocomposite with 3.0 wt.% pristine CNTs. Also Cho et al. [75] studied PU based nanocomposites loaded with pristine and functionalized CNTs. For 3.0 wt.%, 5.0 wt.% and 7.0 wt.% filler concentrations, surface modified CNTs exhibit better elastic modulus than the one obtained for pristine CNTs. This investigation also sustains that severe surface modification lowers mechanical properties. However, a study leaded by Kim et al. [159] corroborates the data obtained in the present thesis. Concerning the direct comparison between pristine CNTs and CNTs submitted to different surface treatments, such as acid treatment with H_2SO_4 and HNO_3, amine treatment and plasma treatment, the authors produced epoxy nanocomposites filled with all the different kinds of processed and unprocessed CNTs referred above. In their study, the highest elastic modulus was obtained for the plasma treated CNTs/Epoxy composites, followed by the non-treated CNTs/Epoxy composites, amine treated/Epoxy composites, acid treated/Epoxy composites and, at last, pristine Epoxy. Non-treated CNTs/Epoxy composites exhibited an elastic modulus 13.1% higher than that from the acid treated CNTs/Epoxy nanocomposites. The acid treated CNTs/epoxy nanocomposite possesses higher tensile strength at break and elongation at break than the untreated CNTs/epoxy nanocomposite. Therefore, the inferiority of the tensile strength at break values for T CNTs/PU nanocomposites observed in the present work may be explained by the inadequacy of the used processing methods to fully take advantage of the chemical functionalization effects.

Comparing all the studied fillers (NT CNTs, T CNTs and graphene) it is possible to stablish that the graphene nanocomposites possess the higher elastic modulus and tensile strength at break values, followed by the value for the NT CNTs and T CNTs nanocomposites, respectively. Since pristine graphene typically possesses higher elastic modulus than CNTs (Table 2.3), it makes sense that graphene filled nanocomposites present higher E. However, in literature it is typically described the opposite, the superiority of the elastic modulus of nanocomposites filled with CNTs in comparison with the ones filled with graphene. The tensile strength at break results were also unexpected since, according to the bibliography, it is common to obtain higher tensile strength at break values for nanocomposites filled with CNTs than for the ones filled with graphene. At last, reviewing the elongation at break results obtained for all the different fillers, it becomes clear that there is not an unanimous performance. For the 0.5 vol.% concentration, the nanocomposite which attained the highest elongation at break was the one containing T CNTs. When the nanocomposites are loaded with 1.0 vol.% of filler, the one that obtained the greater value was NT CNTs/TPU nanocomposite. For the 1.5 vol.% loaded naocomposites, the one that achieved the highest value of average elongation at break was the 1.5 vol.% graphene/TPU nanocomposite. A study from Chen et al. [125], makes a comparison between PU nanocomposites loaded with MWNTs and with GNS. It was observed that, for every filler concentration, the elastic

modulus and tensile strength at break are higher for the nanocomposites filled with MWNTs. On the other side, the elongation at break presented higher values for the graphene/TPU nanocomposites. However, since in the present work the nanocomposites containing graphene were the ones exhibiting the highest elastic modulus, it makes sense that these nanocomposites are also the ones obtaining the highest tensile strength at break. When critically analysing the processing methods used and the overall experimental procedure, it actually makes sense that the nanocomposites containing treated CNTs were the ones obtaining the worst results of elastic modulus. The T CNTs used in this work were functionalized through a chemical oxidation treatment involving a mixture of concentrated sulfuric and nitric acid, which was later washed with distilled water in order to obtain an approximately neutral pH. This process not only introduces carboxyl and hydroxyl groups in the surface of the carbon nanotubes, but also disentangles and shortens them [119,160]. In fact, Liu et al. [161] reported a shortening rate of the nanotubes in a concentrated solution of sulfuric and nitric acid of 130 nm/h. In the present work, because the preparation of the nanocomposites was made through mechanical melt mixing, the compounds to be mixed were in their solid state. However, in literature, the most used methods to process the nanocomposite is *in situ* polymerization and solution cast. Mu et al. [162], for example, produced PU based nanocomposites incorporated with pristine and polydopamine treated carbon nanotubes, designated as NT CNTs and PDA-CNTs, through *in situ* polymerization and observed an enhancement of the elastic modulus for both nanomaterials. They also observed that the nanocomposites incorporated with and PDA-CNTs exhibited higher elastic modulus than the ones with NT CNTs. In 2016, Sattar et al. [163] prepared, through *in situ* polymerization, nanocomposites of polyurethane/polythiophene (PU/PTh) blend and amine functionalized MWNTs as filler. They observed that, in general, the nanocomposites containing the functionalized CNTs possessed better mechanical properties, including higher elastic modulus than the one from the unfilled polymer blend. It can be speculated that the reduction of the CNTs length induced by the chemical treatment and further mechanical mixing, results in a decreasing of the aspect ratio and probably in an increased agglomeration tendency. Such effects lead to weaker mechanical properties of the T CNTs/TPU nanocomposites as compared with the NT CNTs/TPU nanocomposites.

In table 7.1 it is summarized the variations of the values obtained for the mechanical properties of the nanocomposites in comparison with the ones for the neat TPU. It should be noted that the variation values are represented as a percentage and never as absolute values.

Table 7.1: Variation of the values obtained for the mechanical properties of the TPU nanocomposites as compared with the mechanical properties of the neat TPU.

Increase (↑) / Decrease (↓) of the mechanical properties (%)			
	E	σ_b	ε_b
PU_ 05_ NT_ CNT	↑ 6.6	↓ 3.7	↑ 10.6
PU_ 10_ NT_ CNT	↑ 11.0	↓ 6.0	↑ 6.5
PU_ 15_ NT_ CNT	↑ 22.2	↓ 8.2	↑ 2.0
PU_ 05_ T_ CNT	↓ 1.2	↓ 4.7	↑ 10.8
PU_ 10_ T_ CNT	↑ 8.1	↓ 28.1	↓ 11.2
PU_ 15_ T_ CNT	↑ 9.8	↓ 19.8	↓ 9.6
PU_ 05_ Gra	↑ 7.5	↑ 6.8	↑ 9.1
PU_ 10_ Gra	↑ 23.3	↑ 10.7	↑ 6.3
PU_ 15_ Gra	↑ 38.1	↑ 7.8	↑ 6.2

7.3 Repeatability analysis

The repeatability analysis was made by studying the relative standard of variation (RSD), also known as coefficient of variation, which is defined as a standardized measure of dispersion of a probability distribution that expresses the precision and repeatability of an assay. This statistical tool is especially useful when dealing with parameters which exhibit different units of measurement, which is the case here. It is given by the ratio of the standard deviation to the mean value. This is an important evaluation criterion of the quality of the produced samples since the implementation of this methodology of fabrication of nanocomposites in industry is a primary objective of this work, hence the lower the variability of the process, the more predictable and controllable it can be and, therefore, its adaptation to industry may be facilitated. The relative standard deviation values obtained for the different mechanical properties are represented in the figures 7.1,7.2, 7.3.

In fig.7.1 it is represented the relative standard deviation observed for the elastic modulus. It can be concluded that, for the unfilled PU, the most consistent results are the ones from the injected neat PU pellets. The samples in which the neat PU was melt mixed at 140°C or 185°C presented higher RSD, revealing that the mechanical melt mixing processing method adds variability to the results. For both NT CNTs and T CNTs nanocomposites, RSD increases with the increasing filler content, which implies that, as the concentration of filler increases, it occurs more variation in the results. This phenomenon was expected since with the increasing concentration of CNTs there is a higher probability of forming agglomerates in the polymer matrix, which adds variability to the results. Only the results concerning the graphene filled nanocomposites exhibit an opposite trend, since as the filler content increases the RSD of the elastic modulus decreases. Overall, it can be claimed that the results present good accuracy, since the RSD percentage is lower than 5% for all the nanocomposites produced. The most consistent and less variable nanocomposite specimens are the ones containing NT CNTs.

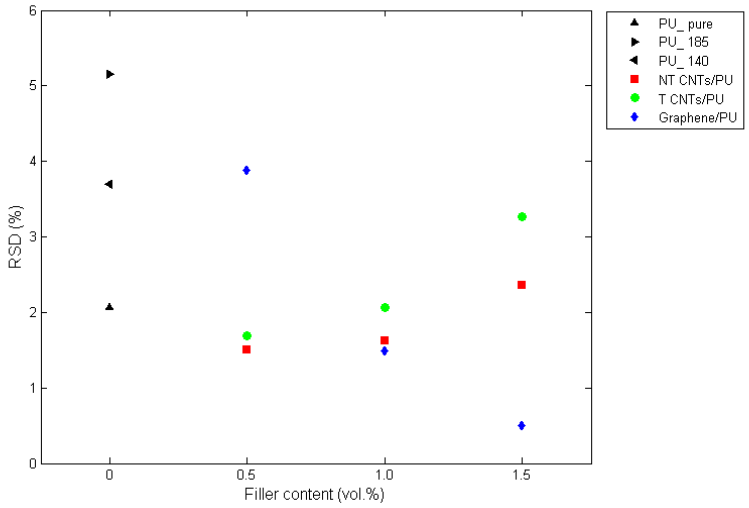

Figure 7.1: Relative standard deviation of the elastic modulus results obtained for the experimental tests of the different samples

In fig.7.2 it can be observed the relative standard deviation results concerning the tensile strength at break measurements. In this case, surprisingly, the sample of neat PU submitted to mechanical melt mixing at 185°C was the one exhibiting the lowest RSD between the unfilled materials. For both nanocomposites containing NT CNTs and graphene, it can be observed that the highest RSD are obtained for the filler concentration of 0.5 vol.%, while the filler loading at which these nanocomposites present the lowest RSD for tensile strength at break is 1.0 vol.%. The nanocomposites that incorporate graphene show a reverse behaviour. The filler content at which graphene nanocomposites exhibit the highest RSD is 1.0 vol.%, while the lowest RSD was measured for the 0.5 vol.% of filler content. It can be therefore claimed that the most consistent and less variable results belong to the nanocomposites that incorporate NT CNTs, regardless of the fact that the 1.0 vol.% graphene/PU nanocomposite presents the global minimum. However, NT CNTs filled nanocomposites are the only ones presenting an RSD lower than 6% for all the tested filler content. Overall, it can be stated that tensile strength at break presents good level of accuracy, with RSD values lower than 10%, except for the 1.0 vol.% T CNTs/PU sample.

At last, it can be seen in fig.7.3 the graph representing the relative standard deviation values for the elongation at break parameter. Examining the values provided for the unfilled PU materials, it can be observed that, similarly to what occurred for the tensile strength at break parameter, the sample showing the less dispersed values is the one which was submitted to mechanical melt mixing at 185°C, followed by the specimen which was not processed through melt mixing, with an RSD of 2.32%. Again, the NT CNTs and graphene nanocomposites reveal a more similar behaviour than that exhibited by the T CNTs filled nanocomposites. For the nanomaterials containing graphene, it can be stated that, as the filler content increases, RSD decreases, which was unexpected since the increase of nanomaterial in the polymer matrix could create an heterogeneous material than could lead to inconsistent results of elongation at break. In the case of the NT CNTs filled nanocomposites, the highest value of RSD was attained at the 0.5 vol.% of filler concentration. The value decreased when the filler content increase to 1.0 vol.% NT CNTs but, with further increase of the filler

content, RSD decreased increased to a value similar to the one obtained for the 0.5 vol.% T CNTs/PU nanocomposite. The nanocomposites incorporating T CNTs present again an abnormal behaviour, since the lowest value of RSD was obtained in the 0.5 vol.% T CNTs/PU nanocomposite, while the lowest value was measured at the nanocomposite containing 1.0 vol.% graphene. Globally, it can be concluded that all kinds of nanocomposites present satisfactory values of relative standard deviation, since the values do not surpass 7%. The most consistent and predictable nanocomposite is, again, the one filled with NT CNTs, which present RSD lower than 4%.

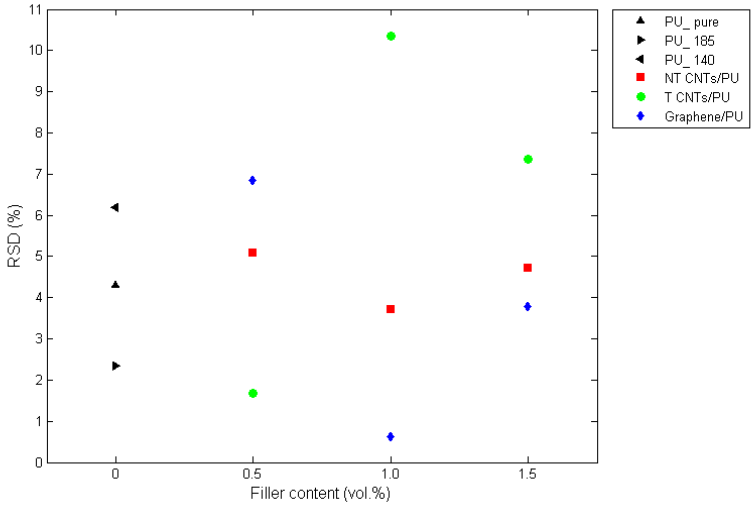

Figure 7.2: Relative standard deviation of the tensile strength at break results obtained for the experimental tests of the different samples

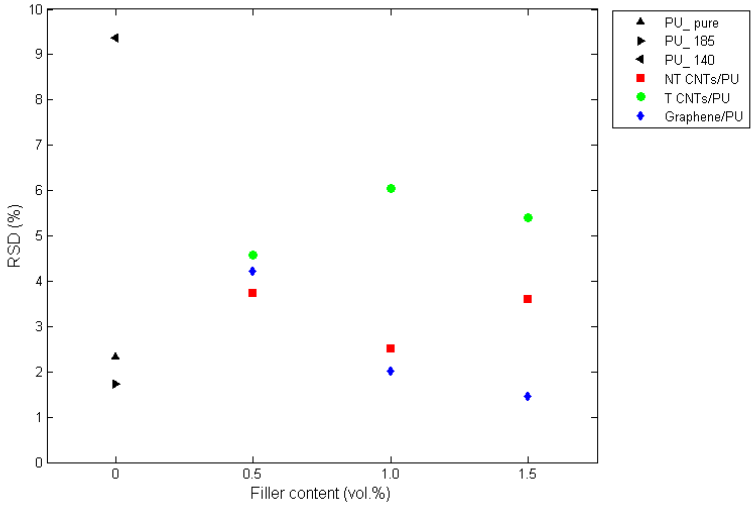

Figure 7.3: Relative standard deviation of the elongation at break results obtained for the experimental tests of the different samples

Chapter 8

Conclusions and Future works

8.1 Conclusions

Given the development of the medical industry, new solutions regarding biomedical devices have been demanded by the market. It is in this context that arises the shape-memory polymers applied to the medical industry. The good biocompatibility and tuneable thermo-mechanical properties of the shape-memory polyurethane (SMPU) makes it an attractive biomaterial. The shape-memory effect of SMPU allows it to be placed in a determined, compact shape and, through thermal activation at human temperature, deploy into its functional, permanent shape. Taking that into account, in this thesis were produced TPU nanocomposites containing two different types of carbon based fillers: carbon nanotubes and graphene. However, shape-memory polymers are not as stiff and mechanically resistant as the shape-memory alloys (SMAs) and their recovery time is much higher, which represent major drawbacks. Focused on the excellent thermo-mechanical properties of the carbon nanotubes and graphene, their incorporation within a polymeric matrix, aimed to enhance the overall properties of shape-memory polymer composites. The ease of the implementation of the processing method in the industry was also taken into account and it is the reason why the used processing method was mechanical melt mixing. This method allows large scale production and does not require major adjustments in a production line.

With the completion of this work, it can be claimed that all the objectives specified prior to the realization of the thesis were attained. It was successfully produced thermoplastic polyurethane (TPU) nanocomposites containing non-treated CNTs (NT CNTs), treated CNTs (T CNTs) and graphene in three different volume fractions: 0.5, 1.0 and 1.5 vol.%. Afterwards, the morphological, thermal and mechanical characterizations of the nanocomposites were performed and the results were analysed. The critical evaluation of the results allowed to draw conclusions about the potential of these nanocomposites and in which conditions the better thermo-mechanical properties were obtained.

Through scanning electron microscopy (SEM) it was possible to observe good dispersion of NT CNTs, T CNTs and graphene within the TPU matrix. However, it must be taken into account the limitations of this observation.

The differential scanning calorimetry (DSC) results show that the glass transition temperatures (T_g) of the nanocomposites are quite similar to each other and to the one from the neat PU. The average value exhibited by the nanocomposites, except PU_ 15_ NT_ CNT, was 50.90 $\pm$ 0.59°C. The TPU nanocomposite incorporating 1.5 vol.%

NT CNTs presents a large increase of 9.9°C, which is inconsistent with the rest of the results. The nanocomposites obtained values of T_m lower than the ones from neat PU. The T_m average of the nanocomposites was measured to be 148.58 ± 2.48°C.

It was concluded that the nanocomposites enhanced the thermal properties of the neat PU, since they obtained lower specific heat capacity (c_p) than the one from the neat PU, except for the PU_ 10_ NT_ CNT and PU_ 15_ Gra nanocomposites. These results reveal that, in general, the nanocomposites require less heat to rise their temperature by 1°C and their transition temperature can be more easily tuneable. The thermal diffusivity results enabled to draw some conclusions about the thermal response of the nanocomposite. Upon testing of nanocomposites containing NT CNTs and T CNTs in the same concentration (1.5 vol.%) it was possible to observe that both obtained higher thermal diffusivity than the unfilled melt mixed PU. However, the nanocomposite exhibiting higher α was the one containing NT CNTs. Likewise, the testing of different volume fractions of the same filler (NT CNTs) revealed that both PU_ 10_ NT_ CNT and PU_ 15_ NT_ CNT surpassed the thermal diffusivity of the pure melt mixed PU. The 1.5 vol.% NT CNTs/TPU nanocomposite attained higher thermal diffusivity than the TPU nanocomposite containing 1.0 vol.% NT CNTs.

The tensile tests provided information regarding the mechanical properties of the nanocomposites. It was observed an increase of the elastic modulus with the increasing volume fraction of NT CNTs, T CNTs and graphene. All the nanocomposites, except PU_ 05_ T_ CNT, improved the elastic modulus comparing with the unfilled PU. The filler which provided higher enhancement of the elastic modulus and tensile strength at break was graphene. Comparing with pure PU, the maximum enhancements achieved were 38.1% for the elastic modulus of the 1.5 vol.% graphene/TPU nanocomposite and 10.7% for the tensile strength at break of the 1.0 vol.% graphene/TPU nanocomposite. The graphene nanocomposites are the only ones possessing tensile strength at break higher than the neat PU. The nanocomposites with NT CNTs show higher elastic modulus and tensile strength at break than the nanocomposites incorporating T CNTs. The nanocomposites revealed an inconsistent behaviour regarding elongation at break. It was registered an increase of the elongation at break for the NT CNTs/TPU and graphene/TPU nanocomposites as compared with the pristine PU. The nanocomposites containing T CNTs only surpass the elongation at break value of pure PU with the concentration of 0.5 vol.% T CNTs. The maximum improvement of the elongation at break, as compared to pure PU, was 10.8% for the PU_ 05_ T_ CNT.

As final consideration, it can be claimed that the graphene/TPU nanocomposites were the ones revealing the best thermo-mechanical properties, exhibiting significant improvements. It should also be noted that NT CNTs/TPU nanocomposites showed better thermo-mechanical behaviour than the T CNTs/TPU nanocomposites. Therefore, the functionalization of the CNTs should be discharged, since the functionalization process involves costs that do not cause significant improvements.

It was proved that the processing method involving mechanical melt mixing followed by injection moulding allows the production of shape-memory polymer composite samples with good mechanical properties, enabling its easy implementation in industry with low costs.

8.2 Future works

With this work, several subjects regarding the behaviour of shape-memory polymer nanocomposites were clarified. However, as it is typical in a research work, several lines of investigation were opened. Therefore, it would be interesting to:

- **Test the shape-memory effect of the TPU nanocomposites incorporating carbon based fillers**
  In this work, it was evaluated the thermo-mechanical properties of the produced nanocomposites and it was made a morphological characterization of the samples. It was speculated the influence of those results in the shape-memory effect, however, it would be interesting to perform further analysis regarding the shape-memory effect of the nanocomposites in a proper climatic test chamber.

- **Produce and test TPU nanocomposites with carbon based fillers in higher concentrations**
  It was observed an enhancement of the elastic modulus with an increasing filler volume fraction. Therefore, the increase of the nanoparticles concentration within the shape-memory material to a value higher than 1.5 vol.% may further improve the mechanical properties of the material. The optimization of the filler concentration within the TPU matrix could be achieved through processing and testing of nanocomposites with filler concentrations differents from the ones used in this work.

- **Test other functionalization methods**
  The surface modification of the nanoparticles was expected to improve the filler dispersion and, therefore, the thermo-mechanical characteristics of the nanomaterial. However, it was observed in this work the opposite effect. Therefore, it is suggested the performance of other functionalizations rather than the acid treatment with H_2SO_4 and HNO_3 realized in the present work. The implementation of amine or plasma oxidation in the nanoparticles could be realized and the resultant nanocomposites should be tested.

- **Use other types of filler**
  There are several nanomaterials that upon incorporaton within the polymeric matrix could improve its properties. I think it would be valuable to test TPU based nanocomposites with new types of nanomaterials, such as: surface modified graphene (SMG), reduced graphene oxide (RGO), functionalized graphene oxide (FGO).

Bibliography

[1] J. Mohd Jani, M. Leary, A. Subic, and M. A. Gibson, "A review of shape memory alloy research, applications and opportunities," *Materials and Design*, vol. 56, pp. 1078–1113, 2014. [Online]. Available: http://dx.doi.org/10.1016/j.matdes.2013.11.084

[2] T. W. Duerig, K. N. Melton, D. Stöckel, and C. M. Wayman, *Engineering aspects of shape memory alloys*, 1st ed. Butterworth-Heinemann, 1990.

[3] J. Leng, X. Lan, Y. Liu, and S. Du, "Shape-memory polymers and their composites: Stimulus methods and applications," *Progress in Materials Science*, vol. 56, pp. 1077–1135, 2011. [Online]. Available: http://dx.doi.org/10.1016/j.pmatsci.2011.03.001

[4] Z. G. Wei, R. Sandström, and S. Miyazaki, "Shape-memory materials and hybrid composites for smart systems - Part I Shape-memory materials," *Journal of Materials Science*, vol. 33, no. 15, pp. 3743–3762, 1998. [Online]. Available: http://dx.doi.org/10.1023/a:1004692329247

[5] M. Behl, K. Gall, M. Heuchel, K. Kratz, A. Lendlein, S. Madbouly, A. Neffe, W. Wagermaier, C. Wischke, C. Yakacki, and J. Zotzmann, *Shape-Memory Polymers*, A. Lendlein, Ed. Springer, 2010.

[6] Q. Meng and J. Hu, "A review of shape memory polymer composites and blends," *Composites Part A: Applied Science and Manufacturing*, vol. 40, no. 11, pp. 1661–1672, 2009. [Online]. Available: http://dx.doi.org/10.1016/j.compositesa.2009.08.011

[7] V. Solouki Bonab and I. Manas-Zloczower, "Chemorheology of thermoplastic polyurethane and thermoplastic polyurethane/carbon nanotube composite systems," *Polymer*, vol. 99, pp. 513–520, 2016. [Online]. Available: http://dx.doi.org/10.1016/j.polymer.2016.07.043

[8] "Thermoset Vs. Thermoplastics," 2016. [Online]. Available: http://www.modorplastics.com/thermoset-vs-thermoplastics

[9] J. Carrell, "Multi-Trigger Mechanism with Shape Memory Polymer Nanocomposite," Dissertation, Texas Tech University, 2012.

[10] M. Fonseca, B. Abreu, F. Gonçalves, A. Ferreira, R. Moreira, and M. Oliveira, "Shape memory polyurethanes reinforced with carbon nanotubes," *Composite Structures*, vol. 99, pp. 105–111, 2013. [Online]. Available: http://dx.doi.org/10.1016/j.compstruct.2012.11.029

[11] A. Lendlein and S. Kelch, "Shape-Memory Polymers," *Angewandte Chemie - International Edition*, vol. 41, no. 12, pp. 2034–2057, 2002. [Online]. Available: http://dx.doi.org/10.1002/1521-3773(20020617)41:122034::AID-ANIE20343.0.CO;2-M

[12] J. Hu, *Advances in shape memory polymers*, 1st ed. Woodhead Publishing Limited, 2013.

[13] K. Gall, M. Mikulas, N. a. Munshi, F. Beavers, and M. Tupper, "Carbon Fiber Reinforced Shape Memory Polymer Composites," *Journal of Intelligent Material Systems and Structures*, vol. 11, pp. 877–886, 2000. [Online]. Available: http://dx.doi.org/10.1106/EJGR-EWNM-6CLX-3X2M

[14] H. Koerner, G. Price, N. A. Pearce, M. Alexander, and R. A. Vaia, "Remotely actuated polymer nanocomposites - stress-recovery of carbon-nanotube-filled thermoplastic elastomers," *Nature materials*, vol. 3, no. 2, pp. 115–120, 2004. [Online]. Available: http://dx.doi.org/10.1038/nmat1059

[15] C. Liu, H. Qin, and P. T. Mather, "Review of progress in shape-memory polymers," *Journal of Materials Chemistry*, vol. 17, no. 16, pp. 1543–1558, 2007. [Online]. Available: http://dx.doi.org/10.1039/b615954k

[16] A. Lendlein and M. Behl, "Shape-Memory Polymers for Biomedical Applications," *Advances in Science and Technology*, vol. 54, pp. 96–102, 2008. [Online]. Available: http://dx.doi.org/10.4028/www.scientific.net/AST.54.96

[17] K. Otsuka, C. M. Wayman, T. Saburi, T. Tadaki, T. Maki, Y. Suzuki, J. Van Humbeeck, R. Stalmans, K. Uchino, M. Irie, K. N. Melton, I. Ohkata, and S. Miyazaki, *Shape Memory Materials*, K. Otsuka and C. M. Wayman, Eds. Cambridge University Press, 1998.

[18] H. Park, P. Harrison, Z. Guo, M.-G. Lee, and W.-R. Yu, "Three-dimensional constitutive model for shape memory polymers using multiplicative decomposition of the deformation gradient and shape memory strains," *Mechanics of Materials*, vol. 93, pp. 43–62, 2016. [Online]. Available: http://dx.doi.org/10.1016/j.mechmat.2015.10.014

[19] A. Ölander, "An electrochemical investigation of solid cadmium-gold alloys," *Journal of the American Chemical Society*, vol. 54, no. 10, pp. 3819–3833, 1932. [Online]. Available: http://dx.doi.org/10.1021/ja01349a004

[20] F. El Feninat, G. Laroche, M. Fiset, and D. Mantovani, "Shape Memory Materials for Biomedical Applications," *Advanced Engineering Materials*, vol. 4, no. 3, pp. 91–104, 2002. [Online]. Available: http://dx.doi.org/10.1002/1527-2648(200203)4:391::AID-ADEM913.0.CO;2-B

[21] T. Videnic, M. Brojan, J. Kunavar, and F. Kosel, "A Simple One-Dimensional Model of Constrained Recovery in Shape Memory Alloys," *Mechanics of Advanced Materials and Structures*, vol. 21, no. 5, pp. 376–383, 2014. [Online]. Available: http://dx.doi.org/10.1080/15376494.2012.697599

[22] S. Miyazaki, R. Sachdeva, H. Hosoda, T. Inamura, Y. Liu, H. Kim, T. Habu, Y. Oshida, F. Farzin-Nia, K. Gall, M. Maitz, S. Shabalovskaya, J. Van Humbeeck, D. Stoeckel,

A. Pelton, T. W. Duerig, T. Yoneyama, C. Kobayashi, and L. Yahia, *Shape memory alloys for biomedical applications*, T. Yoneyama and S. Miyazaki, Eds. Cambridge: Woodhead Publishing Limited, 2009.

[23] C. Lexcellent, *Shape-memory Alloys Handbook*. John Wiley & Sons, Inc., 2013.

[24] Smart Wires, "Nitinol." [Online]. Available: http://smartwires.eu/index.php?id_cms=9&controller=cms&id_lang=1

[25] W. M. Huang, Z. Ding, C. C. Wang, J. Wei, Y. Zhao, and H. Purnawali, "Shape memory materials," *Materials Today*, vol. 13, no. 7-8, pp. 54–61, 2010. [Online]. Available: http://dx.doi.org/10.1016/S1369-7021(10)70128-0

[26] T. Uehara, J. Zurbitu, S. Kustov, A. Zabaleta, E. Cesari, J. Aurrekoetxea, H. Tobushi, K. Kitamura, Y. Yoshimi, K. Date, H. Luo, Y. Liao, E. Abel, Z. Wang, X. Liu, K. Andrianesis, Y. Koveos, G. Nikolakopoulos, A. Tzes, Y. Haga, T. Mineta, W. Makishi, T. Matsunaga, M. Esashi, C. Cismasiu, F. Amarante dos Santos, H. Li, H. Qian, and O. Akselsen, *Shape Memory Alloys*, C. Cismasiu, Ed. Sciyo, 2010.

[27] A. Lai, "Shape memory ceramics in small volumes," Dissertation, Massachusetts Institute of Technology, 2016.

[28] T. Chatterjee, P. Dey, G. B. Nando, and K. Naskar, "Thermo-responsive shape memory polymer blends based on alpha olefin and ethylene propylene diene rubber," *Polymer*, vol. 78, pp. 180–192, 2015. [Online]. Available: http://dx.doi.org/10.1016/j.polymer.2015.10.007

[29] A. Basfar and S. Lotfy, "Radiation-crosslinking of shape memory polymers based on poly(vinyl alcohol) in the presence of carbon nanotubes," *Radiation Physics and Chemistry*, vol. 106, pp. 376–384, 2015. [Online]. Available: http://dx.doi.org/10.1016/j.radphyschem.2014.08.024

[30] M. Huang, X. Dong, Y. Gao, Q. Xing, W. Li, and D. Wang, "Probing the structure evolution/orientation induced by interaction between polyurethane segments and SiO2 surface in shape memory process," *Polymer*, vol. 55, no. 16, pp. 4289–4298, 2014. [Online]. Available: http://dx.doi.org/10.1016/j.polymer.2014.06.060

[31] M. Behl and A. Lendlein, "Shape-memory polymers," *Materials Today*, vol. 10, no. 4, pp. 20–28, 2007. [Online]. Available: http://dx.doi.org/10.1016/S1369-7021(07)70047-0

[32] H. Lv, J. Leng, and S. Du, "A Survey of Adaptive Materials and Structures Research in China," pp. 1–8, 2009.

[33] J. Raasch, M. Ivey, D. Aldrich, D. S. Nobes, and C. Ayranci, "Characterization of Polyurethane Shape Memory Polymer Processed by Material Extrusion Additive Manufacturing," *Additive Manufacturing*, vol. 8, pp. 132–141, 2015. [Online]. Available: http://dx.doi.org/10.1016/j.addma.2015.09.004

[34] F. Li, X. Zhang, J. Hou, M. Xu, X. Luo, D. Ma, and B. K. Kim, "Studies on thermally stimulated shape memory effect of segmented polyurethanes," *Journal of Applied Polymer Science*, vol. 64, no. 8, pp. 1511–1516, 1997. [Online]. Available: http://dx.doi.org/10.1002/(sici)1097-4628(19970523)64:81511::aid-app83.0.co;2-k

[35] P. T. Mather, X. Luo, and I. A. Rousseau, "Shape Memory Polymer Research," *Annual Review of Materials Research*, vol. 39, pp. 445–471, 2009. [Online]. Available: http://dx.doi.org/10.1146/annurev-matsci-082908-145419

[36] M. Behl, M. Y. Razzaq, and A. Lendlein, "Multifunctional shape-memory polymers," *Advanced Materials*, vol. 22, no. 31, pp. 3388–3410, 2010. [Online]. Available: http://dx.doi.org/10.1002/adma.200904447

[37] T. Ohki, Q. Q. Ni, N. Ohsako, and M. Iwamoto, "Mechanical and shape memory behavior of composites with shape memory polymer," *Composites Part A: Applied Science and Manufacturing*, vol. 35, no. 9, pp. 1065–1073, 2004. [Online]. Available: http://dx.doi.org/10.1016/j.compositesa.2004.03.001

[38] A. Lendlein and S. Kelch, "Degradable , Multifunctional Polymeric Biomaterials with Shape-memory," *Materials Science Forum*, vol. 492-493, pp. 219–224, 2005. [Online]. Available: http://dx.doi.org/10.4028/www.scientific.net/MSF.492-493.219

[39] D. Ratna and J. Karger-Kocsis, "Recent advances in shape memory polymers and composites: A review," *Journal of Materials Science*, vol. 43, no. 1, pp. 254–269, 2008. [Online]. Available: http://dx.doi.org/10.1007/s10853-007-2176-7

[40] R. A. Weiss, E. Izzo, and S. Mandelbaum, "New Design of Shape Memory Polymers : Mixtures of an Elastomeric Ionomer and Low Molar Mass," *Macromolecules*, vol. 41, no. 9, pp. 2978–2980, 2008. [Online]. Available: http://dx.doi.org/10.1021/ma8001774

[41] M. Behl, A. Lendlein, H.-Y. Jiang, A. M. Schmidt, H. J. Qi, M. L. Dunn, K. Kratz, W. Wagermaier, M. Heuchel, W. M. Huang, B. Yang, J. Leng, H. Lu, S. Du, X. Lan, Y. Liu, W. Sokolowski, and J. Hu, *Shape-Memory Polymers and Multifunctional Composites*, J. Leng and S. Du, Eds. CRC Press, 2010.

[42] A. Alteheld, Y. Feng, S. Kelch, and A. Lendlein, "Biodegradable, amorphous copolyester-urethane networks having shape-memory properties," *Angewandte Chemie - International Edition*, vol. 44, no. 8, pp. 1188–1192, 2005. [Online]. Available: http://dx.doi.org/10.1002/anie.200461360

[43] A. Lendlein, A. M. Schmidt, M. Schroeter, and R. Langer, "Shape-memory polymer networks from oligo(ϵ-caprolactone)dimethacrylates," *Journal of Polymer Science: Part A: Polymer Chemistry*, vol. 43, no. 7, pp. 1369–1381, 2005. [Online]. Available: http://dx.doi.org/10.1002/pola.20598

[44] H. M. Jeong, S. Y. Lee, and B. K. Kim, "Shape memory polyurethane containing amorphous reversible phase," *Journal of Materials Science*, vol. 35, no. 7, pp. 1579–1583, 2000. [Online]. Available: http://dx.doi.org/10.1023/A:1004761206709

[45] B. K. Kim, Y. J. Shin, S. M. Cho, and H. M. Jeong, "Shape-memory behavior of segmented polyurethanes with an amorphous reversible phase: the effect of block length and content," *Journal of Polymer Science, Part B: Polymer Physics*, vol. 38, no. 20, pp. 2652–2657, 2000. [Online]. Available: http://dx.doi.org/10.1002/1099-0488(20001015)38:202652::AID-POLB503.0.CO;2-3

[46] J. Hu and S. Chen, "A review of actively moving polymers in textile applications," *Journal of Materials Chemistry*, vol. 20, no. 17, pp. 3346–3355, 2010. [Online]. Available: http://dx.doi.org/10.1039/B922872A

[47] C. M. Yakacki, "Shape-memory and shape-changing polymers," *Polymer Reviews*, vol. 53, no. 1, pp. 1–5, 2013. [Online]. Available: http://dx.doi.org/10.1080/15583724.2012.752745

[48] K. Bhattacharya, S. Conti, G. Zanzotto, and J. Zimmer, "Crystal symmetry and the reversibility of martensitic transformations." *Nature*, vol. 428, pp. 55–59, 2004. [Online]. Available: http://dx.doi.org/10.1038/nature02378

[49] B. K. Kim, S. Y. Lee, and M. Xu, "Polyurethanes having shape memory effects," *Polymer*, vol. 37, no. 26, pp. 5781–5793, 1996. [Online]. Available: http://dx.doi.org/10.1016/S0032-3861(96)00442-9

[50] T. Takahashi, N. Hayashi, and S. Hayashi, "Structure and properties of shape-memory polyurethane block copolymers," *Journal of Applied Polymer Science*, vol. 60, no. 7, pp. 1061–1069, 1996. [Online]. Available: http://dx.doi.org/10.1002/(SICI)1097-4628(19960516)60:71061::AID-APP183.0.CO;2-3

[51] H. Tobushi, S. Hayashi, A. Ikai, and H. Hara, "Thermomechanical Properties of Shape Memory Polymers of Polyurethane Series and their Applications," *Journal de Physique IV*, vol. 6, pp. C1–377–C1–384, 1996. [Online]. Available: http://dx.doi.org/10.1051/jp4:1996136

[52] H. Tobushi, T. Hashimoto, N. Ito, S. Hayashi, and E. Yamada, "Shape Fixity and Shape Recovery in a film of shape memory polymer of polyurethane series," *Journal of Intelligent Material Systems and Structures*, vol. 9, pp. 127–136, 1998. [Online]. Available: http://dx.doi.org/10.1177/1045389X9800900206

[53] K. Gall, M. L. Dunn, Y. Liu, D. Finch, M. Lake, and N. A. Munshi, "Shape memory polymer nanocomposites," *Acta Materialia*, vol. 50, no. 20, pp. 5115–5126, 2002. [Online]. Available: http://dx.doi.org/10.1016/S1359-6454(02)00368-3

[54] W. Huang, B. Yang, and Y. Q. Fu, *Polyurethane Shape Memory Polymers*. CRC Press, 2012.

[55] W. Sokolowski, A. Metcalfe, S. Hayashi, L. Yahia, and J. Raymond, "Medical applications of shape memory polymers," *Biomedical Materials*, vol. 2, no. 1, pp. S23–S27, 2007. [Online]. Available: http://dx.doi.org/10.1088/1748-6041/2/1/S04

[56] M. Raja, S. H. Ryu, and a. M. Shanmugharaj, "Influence of surface modified multiwalled carbon nanotubes on the mechanical and electroactive shape memory properties of polyurethane (PU)/poly(vinylidene diflouride) (PVDF) composites," *Colloids and Surfaces A: Physicochemical and Engineering Aspects*, vol. 450, no. 1, pp. 59–66, 2014. [Online]. Available: http://dx.doi.org/10.1016/j.colsurfa.2014.03.008

[57] I. A. Rousseau, "Challenges of Shape Memory Polymers: A Review of the Progress Toward Overcoming SMP's Limitations," *POLYMER ENGINEERING AND SCIENCE*, vol. 47, no. 11, pp. 2075–2089, 2008. [Online]. Available: http://doi.wiley.com/10.1002/pen.20921

[58] S. Mondal and J. Hu, "Shape Memory Studies of Functionalized MWNT-reinforced Polyurethane Copolymers," *Iranian Polymer Journal*, vol. 15, no. 2, pp. 135–142, 2006.

[59] J. Leng, H. Lu, Y. Liu, W. M. Huang, and S. Du, "Shape-Memory Polymers - A Class of Novel Smart Materials," *MRS Bulletin*, vol. 34, no. 11, pp. 848–855, 2009. [Online]. Available: http://dx.doi.org/10.1557/mrs2009.235

[60] C. Liang, C. Rogers, and E. Malafeew, "Investigation of Shape Memory Polymers and Their Hybrid Composites," *Journal of Intelligen Material Systems and Structures*, vol. 8, no. 2, pp. 380–386, 1997. [Online]. Available: http://dx.doi.org/10.1177/1045389X9700800411

[61] W. Small IV, P. Singhal, T. S. Wilson, and D. J. Maitland, "Biomedical applications of thermally activated shape memory polymers," *Journal of Materials Chemistry*, vol. 20, no. 18, pp. 3356–3366, 2011. [Online]. Available: http://dx.doi.org/10.1039/B923717H

[62] H. M. Wache, D. J. Tartakowska, A. Hentrich, and M. H. Wagner, "Development of a polymer stent with shape memory effect as a drug delivery system," *Journal of Materials Science: Materials in Medicine*, vol. 14, no. 2, pp. 109–112, 2003. [Online]. Available: http://dx.doi.org/10.1023/A:1022007510352

[63] A. Lendlein and R. Langer, "Biodegradable, Elastic Shape-Memory Polymers for Potential Biomedical Applications," *Science*, vol. 296, no. 5573, pp. 1673–1676, 2002. [Online]. Available: http://dx.doi.org/10.1126/science.1066102

[64] A. Nakasima, J. R. Hu, M. Ichinose, and H. Shimada, "Potential application of shape memory plastic as elastic material in clinical orthodontics," *European Journal of Orthodontics*, vol. 13, no. 3, pp. 179–186, 1991. [Online]. Available: http://dx.doi.org/10.1093/ejo/13.3.179

[65] Y. Liu, H. Lv, X. Lan, J. Leng, and S. Du, "Review of electro-active shape-memory polymer composite," *Composites Science and Technology*, vol. 69, no. 13, pp. 2064–2068, 2009. [Online]. Available: http://dx.doi.org/10.1016/j.compscitech.2008.08.016

[66] J. Kim, H. Jeong, H. Park, H. Jeong, S. Bae, and B. Kim, "Electroactive shape memory performance of polyurethane/graphene nanocomposites," *Reactive and Functional Polymers*, vol. 88, pp. 1–7, 2015. [Online]. Available: http://dx.doi.org/10.1016/j.reactfunctpolym.2015.01.004

[67] F. Ji, Y. Zhu, J. Hu, Y. Liu, L.-Y. Yeung, and G. Ye, "Smart Polymer Fibers with Shape Memory Effect," *Smart Materials and Structures*, vol. 15, no. 6, pp. 1547–1554, 2006. [Online]. Available: http://dx.doi.org/10.1088/0964-1726/15/6/006

[68] S. Mondal and J. L. Hu, "Temperature stimulating shape memory polyurethane for smart clothing," *Indian Journal of Fibre and Textile Research*, vol. 31, no. 1, pp. 66–71, 2006.

[69] A. Metcalfe, A. C. Desfaits, I. Salazkin, L. Yahia, W. M. Sokolowski, and J. Raymond, "Cold hibernated elastic memory foams for endovascular interventions," *Biomaterials*, vol. 24, no. 3, pp. 491–497, 2003. [Online]. Available: http://dx.doi.org/10.1016/S0142-9612(02)00362-9

[70] S. a. Madbouly, J. U. Otaigbe, A. K. Nanda, D. a. Wicks, S. Zhang, Q. Zou, L. Wu, H. Liu, and S. Zheng, "Rheological Behavior of POSS / Polyurethane - Urea Nanocomposite Films Prepared by Homogeneous Solution Polymerization in Aqueous Dispersions," *Macromolecules*, vol. 40, no. 3, pp. 4982–4991, 2007. [Online]. Available: http://dx.doi.org/10.1021/ma070186n

[71] L. Peponi, I. Navarro-Baena, and J. M. Kenny, "Shape memory polymers: properties, synthesis and applications," *Smart Polymers and their Applications*, pp. 204–236, 2014. [Online]. Available: http://dx.doi.org/10.1533/9780857097026.1.204

[72] M. Salavati-niasari and D. Ghanbari, "Polymeric Nanocomposite Materials," in *Advances in Diverse Industrial Applications of Nanocomposites*, B. Reddy, Ed. InTech, 2011, ch. 21, p. 588. [Online]. Available: http://dx.doi.org/10.5772/1931

[73] R. A. Vaia and H. D. Wagner, "Framework for nanocomposites," *Materials t*, vol. 7, no. 11, pp. 32–37, 2004. [Online]. Available: http://dx.doi.org/10.1016/S1369-7021(04)00506-1

[74] J. S. Leng, X. Lan, Y. J. Liu, S. Y. Du, W. M. Huang, N. Liu, S. J. Phee, and Q. Yuan, "Electrical conductivity of thermoresponsive shape-memory polymer with embedded micron sized Ni powder chains," *Applied Physics Letters*, vol. 92, no. 1, pp. 1–4, 2008. [Online]. Available: http://dx.doi.org/10.1063/1.2829388

[75] J. W. Cho, J. W. Kim, Y. C. Jung, and N. S. Goo, "Electroactive shape-memory polyurethane composites incorporating carbon nanotubes," *Macromolecular Rapid Communications*, vol. 26, no. 5, pp. 412–416, 2005. [Online]. Available: http://dx.doi.org/10.1002/marc.200400492

[76] N. S. Goo, I. H. Paik, Y. C. Jung, and J. W. Cho, "Development and application of conducting shape memory polyurethane actuators," *Smart Materials and Structures*, vol. 15, no. 5, pp. 1476–1482, 2006. [Online]. Available: http://dx.doi.org/10.1088/0964-1726/15/5/037

[77] J. Leng, H. Lv, Y. Liu, and S. Du, "Electroactivate shape-memory polymer filled with nanocarbon particles and short carbon fibers," *Applied Physics Letters*, vol. 91, no. 14, pp. 1–4, 2007. [Online]. Available: http://dx.doi.org/10.1063/1.2790497

[78] N. G. Sahoo, Y. C. Jung, H. J. Yoo, and J. W. Cho, "Influence of carbon nanotubes and polypyrrole on the thermal, mechanical and electroactive shape-memory properties of polyurethane nanocomposites," *Composites Science and Technology*, vol. 67, no. 9, pp. 1920–1929, 2007. [Online]. Available: http://dx.doi.org/10.1016/j.compscitech.2006.10.013

[79] A. Turabi, H. Karaca, H. Tobe, B. Basaran, Y. Aydogdu, and Y. Chumlyakov, "Shape memory effect and superelasticity of NiMnCoIn metamagnetic shape memory alloys under high magnetic field," *Scripta Materialia*, vol. 111, pp. 110–113, 2016. [Online]. Available: http://dx.doi.org/10.1016/j.scriptamat.2015.08.027

[80] P. R. Buckley, G. H. McKinley, T. S. Wilson, W. Small IV, W. J. Benett, J. P. Bearinger, M. W. McElfresh, and D. J. Maitland, "Inductively heated shape memory

polymer for the magnetic actuation of medical devices," *IEEE Transactions on Biomedical Engineering*, vol. 53, no. 10, pp. 2075–2083, 2006. [Online]. Available: http://dx.doi.org/10.1109/TBME.2006.877113

[81] R. Mohr, K. Kratz, T. Weigel, M. Lucka-Gabor, M. Moneke, and A. Lendlein, "Initiation of shape-memory effect by inductive heating of magnetic nanoparticles in thermoplastic polymers," *Proceedings of the National Academy of Sciences of the United States of America*, vol. 103, no. 10, pp. 3540–3545, 2006. [Online]. Available: http://dx.doi.org/10.1073/pnas.0600079103

[82] L. L. Beecroft and C. K. Ober, "Nanocomposite materials for optical applications," *Chemistry of Materials*, vol. 9, no. 6, pp. 1302–1317, 1997. [Online]. Available: http://dx.doi.org/10.1021/cm960441a

[83] R. Sainz, W. R. Small, N. a. Young, C. Valle, A. M. Benito, W. K. Maser, and M. in het Panhuis, "Synthesis and Properties of Optically Active Polyaniline Carbon Nanotube Composites," *Macromolecules*, vol. 39, pp. 7324–7332, 2006. [Online]. Available: http://dx.doi.org/10.1021/ma061587q

[84] R. Ravindranath, P. K. Ajikumar, N. B. M. Hanafiah, W. Knoll, and S. Valiyaveettil, "Synthesis and characterization of luminescent conjugated polymer-silica composite spheres," *Chemistry of Materials*, vol. 18, no. 5, pp. 1213–1218, 2006. [Online]. Available: http://dx.doi.org/10.1021/cm052121

[85] E. Chiellini, P. Cinelli, V. I. Ilieva, and M. Martera, "Biodegradable thermoplastic composites based on polyvinyl alcohol and algae," *Biomacromolecules*, vol. 9, no. 3, pp. 1007–1013, 2008. [Online]. Available: http://dx.doi.org/10.1021/bm701041e

[86] D. Zhang, M. A. Kandadai, J. Cech, S. Roth, and S. A. Curran, "Poly(L-lactide) (PLLA)/multiwalled carbon nanotube (MWCNT) composite: Characterization and biocompatibility evaluation," *Journal of Physical Chemistry B*, vol. 110, no. 26, pp. 12 910–12 915, 2006. [Online]. Available: http://dx.doi.org/10.1021/jp061628k

[87] C. Chevigny, F. Dalmas, F. Boué, and J. Jestin, "Tuning the Mechanical Properties in Model Nanocomposites : Influence of the Polymer-Filler Interfacial Interactions," *Journal of Polymer Science, Part B: Polymer Physics*, vol. 49, no. 11, pp. 781–791, 2011. [Online]. Available: http://dx.doi.org/10.1002/polb.22246

[88] C. Yakacki, N. Satarkar, K. Gall, R. Likos, and J. Hilt, "Shape-Memory Polymer Networks with Fe_3O_4 Nanoparticles for Remote Activation," *Journal of Applied Polymer Science*, vol. 112, no. 7, pp. 3166–3176, 2009. [Online]. Available: http://dx.doi.org/10.1002/app.29845

[89] E. T. Thostenson, C. Li, and T. W. Chou, "Nanocomposites in context," *Composites Science and Technology*, vol. 65, no. 3-4, pp. 491–516, 2005. [Online]. Available: http://dx.doi.org/10.1016/j.compscitech.2004.11.003

[90] T. Hanemann and D. V. Szabó, "Polymer-Nanoparticle Composites: From Synthesis to Modern Applications," *Materials*, vol. 3, pp. 3468–3517, 2010. [Online]. Available: http://dx.doi.org/10.3390/ma3063468

[91] A. I. Gusev, "Glossary of Nanotechnology and related terms." [Online]. Available: http://eng.thesaurus.rusnano.com/wiki/article1371

[92] Z. G. Wei, R. Sandstrom, and S. Miyazaki, "Shape memory materials and hybrid composites for smart systems - Part II Shape-memory hybrid composites," *Journal of Materials Science*, vol. 33, no. 15, pp. 3763–3783, 1998. [Online]. Available: http://dx.doi.org/10.1023/a:1004674630156

[93] Q. Jing, W. Liu, Y. Pan, V. V. Silberschmidt, L. Li, and Z. Dong, "Chemical functionalization of graphene oxide for improving mechanical and thermal properties of polyurethane composites," *Materials and Design*, vol. 85, pp. 808–814, 2015. [Online]. Available: http://dx.doi.org/10.1016/j.matdes.2015.07.101

[94] M. Strankowski, L. Piszczyk, P. Kosmela, and P. Korzeniewski, "Morphology and the physical and thermal properties of thermoplastic polyurethane reinforced with thermally reduced graphene oxide," *Polish Journal of Chemical Technology*, vol. 17, no. 4, pp. 88–94, 2015. [Online]. Available: http://dx.doi.org/10.1515/pjct-2015-0073

[95] Z. Xu, N. Li, Z. Wang, Z. Shi, C. Miao, C. Zheng, O. Liang, Y.-H. Xie, L. Li, S. H. Huh, T. Ogino, T. Tsukamoto, S. Eigler, X. Wang, S. Chen, H. Salavagione, G. Martínez, G. Ellis, H.-i. Lee, H. M. Jeong, E. Rut'kov, N. Gall, E. Voloshina, Y. Dedkov, F. Giannazzo, S. Sonde, V. Raineri, U. Bangert, M. Gass, R. Zan, C. T. Pan, H. Zhang, S. He, C. Chen, W. Zheng, Q. Yan, F. Zhuge, R.-W. Li, C. He, Z. Liu, X. Zhou, A. Jorio, E. Martins Ferreira, L. Cançado, C. Achete, R. Apaz, T. Valla, Z. Pan, K. Tahy, T. Fang, P. Zhao, A. Konar, C. Lian, H. Xing, M. Kelly, D. Jena, J.-S. Moon, K. Gaskill, P. Campbell, Y. Ohno, K. Maehashi, K. Matsumoto, L. Dong, Q. Liu, L. Wang, and K. Chen, *Physics and applications of graphene -Experiments*, S. Mikhailov, Ed. InTech, 2011.

[96] M. H. Al-Saleh, "Electrical and mechanical properties of graphene/carbon nanotube hybrid nanocomposites," *Synthetic Metals*, vol. 209, pp. 41–46, 2015. [Online]. Available: http://dx.doi.org/10.1016/j.synthmet.2015.06.023

[97] K. S. Novoselov, A. K. Geim, S. V. Morozov, D. Jiang, Y. Zhang, S. V. Dubonos, I. V. Grigorieva, and A. A. Firsov, "Electric Field Effect in Atomically Thin Carbon Films," *Science*, vol. 306, pp. 666–669, 2004. [Online]. Available: http://dx.doi.org/10.1126/science.1102896

[98] B. Z. Jang and A. Zhamu, "Processing of nanographene platelets (NGPs) and NGP nanocomposites: a review," *Journal of Materials Science*, vol. 43, no. 15, pp. 5092–5101, 2008. [Online]. Available: http://dx.doi.org/10.1007/s10853-008-2755-2

[99] J. J. Mack, L. M. Viculis, A. Ali, R. Luoh, G. Yang, H. T. Hahn, F. K. Ko, and R. B. Kaner, "Graphite nanoplatelet reinforcement of electrospun polyacrylonitrile nanofibers," *Advanced Materials*, vol. 17, no. 1, pp. 77–80, 2005. [Online]. Available: http://dx.doi.org/10.1002/adma.200400133

[100] R. Sattar, A. Kausar, and M. Siddiq, "Advances in thermoplastic polyurethane composites reinforced with carbon nanotubes and carbon nanofibers: A review," *Journal of Plastic Film and Sheeting*, vol. 31, no. 2, pp. 186–224, 2014. [Online]. Available: http://dx.doi.org/10.1177/8756087914535126

[101] "No TitleIndex of /img/samples." [Online]. Available: http://www.jameshedberg.com/img/samples/

[102] V. Dhand, K. Y. Rhee, H. J. Kim, and D. H. Jung, "A Comprehensive Review of Graphene Nanocomposites : Research Status and Trends," *Journal of Nanimaterials*, vol. 2013, 2013. [Online]. Available: http://dx.doi.org/10.1155/2013/763953

[103] S. D. Perera, A. D. Liyanage, N. Nijem, J. P. Ferraris, Y. J. Chabal, and K. J. Balkus, "Vanadium oxide nanowire-Graphene binder free nanocomposite paper electrodes for supercapacitors: A facile green approach," *Journal of Power Sources*, vol. 230, pp. 130–137, 2013. [Online]. Available: http://dx.doi.org/10.1016/j.jpowsour.2012.11.118

[104] J. You, J.-Y.-Q. Cao, S.-C. Chen, and Y.-Z. Wang, "Preparation of polymer nanocomposites with enhanced mechanical properties using hybrid of graphene and partially wrapped multi-wall carbon nanotube as nanofiller," *Chinese Chemical Letters*, 2016. [Online]. Available: http://dx.doi.org/doi:10.1016/j.cclet.2016.06.039

[105] T. Kavinkumar and S. Manivannan, "Synthesis, Characterization and Gas Sensing Properties of Graphene Oxide-Multiwalled Carbon Nanotube Composite," *Journal of Materials Science & Technology*, vol. 32, no. 7, pp. 626–632, 2016. [Online]. Available: http://dx.doi.org/10.1016/j.jmst.2016.03.017

[106] S. Stankovich, R. D. Piner, S. T. Nguyen, and R. S. Ruoff, "Synthesis and exfoliation of isocyanate-treated graphene oxide nanoplatelets," *Carbon*, vol. 44, no. 15, pp. 3342–3347, 2006. [Online]. Available: http://dx.doi.org/10.1016/j.carbon.2006.06.004

[107] S. Iijima, "Helical microtubules of graphitic carbon," *Nature*, vol. 354, pp. 56–58, 1991. [Online]. Available: http://dx.doi.org/10.1038/354056a0

[108] Q.-Q. Ni, C.-s. Zhang, Y. Fu, G. Dai, and T. Kimura, "Shape memory effect and mechanical properties of carbon nanotube/shape memory polymer nanocomposites," *Composite Structures*, vol. 81, no. 2, pp. 176–184, 2007. [Online]. Available: http://dx.doi.org/10.1016/j.compstruct.2006.08.017

[109] S. A. Madbouly and A. Lendlein, "Shape-Memory Polymer Composites," *Advances in Polymer Science*, vol. 226, pp. 41–95, 2010. [Online]. Available: http://dx.doi.org/10.1007/12_2009_28

[110] H. Carpenter, "Carbon Nanotubes May Restore Collapse Of Moore's Law: IBM." [Online]. Available: http://www.ozytive.com/2014/07/06/carbon-nanotubes-ibm/

[111] P. J. F. Harris, *Carbon nanotubes and related structures: New materials for the twenty-first century*. Cambridge University Press, 1999.

[112] J. N. Coleman, U. Khan, W. J. Blau, and Y. K. Gun'ko, "Small but strong: A review of the mechanical properties of carbon nanotube-polymer composites," *Carbon*, vol. 44, no. 9, pp. 1624–1652, 2006. [Online]. Available: http://dx.doi.org/10.1016/j.carbon.2006.02.038

[113] B. De Vivo, P. Lamberti, G. Spinelli, V. Tucci, L. Vertuccio, and V. Vittoria, "Simulation and experimental characterization of polymer/carbon nanotubes composites

for strain sensor applications," *Journal of Applied Physics*, vol. 116, no. 5, pp. 054 307–1 – 054 307–14, 2014. [Online]. Available: http://dx.doi.org/10.1063/1.4892098

[114] A. Alizadeh, A. Abdollahi, and H. Biukani, "Creep behavior and wear resistance of Al 5083 based hybrid composites reinforced with carbon nanotubes (CNTs) and boron carbide (B4C)," *Journal of Alloys and Compounds*, vol. 650, pp. 783–793, 2015. [Online]. Available: http://dx.doi.org/10.1016/j.jallcom.2015.07.214

[115] A. Yu, P. Ramesh, M. E. Itkis, E. Bekyarova, and R. C. Haddon, "Graphite Nanoplatelet - Epoxy Composite Thermal Interface Materials," *The Journal of Physical Chemistry C*, vol. 111, pp. 7565–7569, 2007. [Online]. Available: http://dx.doi.org/10.1021/jp071761s

[116] J.-W. Zha, F. Sun, S.-J. Wang, D. Wang, X. Lin, G. Chen, and Z.-M. Dang, "Improved mechanical and electrical properties in electrospun polyimide/multiwalled carbon nanotubes nanofibrous composites," *Journal of Applied Physics*, vol. 116, no. 13, pp. 134 104–1 – 134 104–5, 2014. [Online]. Available: http://dx.doi.org/10.1063/1.4897230

[117] T. K. Gupta, B. P. Singh, R. K. Tripathi, S. R. Dhakate, V. N. Singh, O. S. Panwar, and R. B. Mathur, "Superior nano-mechanical properties of reduced graphene oxide reinforced polyurethane composites," *RSC Advances*, vol. 5, no. 22, pp. 16 921–16 930, 2015. [Online]. Available: http://dx.doi.org/10.1039/C4RA14223C

[118] H. Xia and M. Song, "Preparation and characterisation of polyurethane grafted single-walled carbon nanotubes and derived polyurethane nanocomposites," *Journal of Materials Chemistry*, vol. 16, no. 19, pp. 1843–1851, 2006. [Online]. Available: http://dx.doi.org/10.1039/b601152g

[119] X. L. Xie, Y. W. Mai, and X. P. Zhou, "Dispersion and alignment of carbon nanotubes in polymer matrix: A review," *Materials Science and Engineering R*, vol. 49, no. 4, pp. 89–112, 2005. [Online]. Available: http://dx.doi.org/10.1016/j.mser.2005.04.002

[120] T. Kuilla, S. Bhadra, D. H. Yao, N. H. Kim, S. Bose, and J. H. Lee, "Recent advances in graphene based polymer composites," *Progress in Polymer Science*, vol. 35, no. 11, pp. 1350–1375, 2010. [Online]. Available: http://dx.doi.org/10.1016/j.progpolymsci.2010.07.005

[121] W. Gao and R. Huang, "Thermomechanics of monolayer graphene: Rippling, thermal expansion and elasticity," *Journal of the Mechanics and Physics of Solids*, vol. 66, no. 1, pp. 42–58, 2014. [Online]. Available: http://dx.doi.org/10.1016/j.jmps.2014.01.011

[122] N. Sorot and B. Gupta, "Effect of Temperature on Thermal Properties of Graphene," *Oriental Journal of Chemistry*, vol. 31, no. 3, pp. 1327–1330, 2015. [Online]. Available: http://dx.doi.org/10.1061/(ASCE)0899-1561(2003)15:2(101)

[123] A. M. Schmidt, "Electromagnetic activation of shape memory polymer networks containing magnetic nanoparticles," *Macromolecular Rapid Communications*, vol. 27, no. 14, pp. 1168–1172, 2006. [Online]. Available: http://dx.doi.org/10.1002/marc.200600225

[124] M. H. Jomaa, K. Masenelli-Varlot, L. Seveyrat, L. Lebrun, M. C. Dib Jawhar, E. Beyou, and J. Y. Cavaillé, "Investigation of elastic, electrical and electromechanical

properties of polyurethane/grafted carbon nanotubes nanocomposites," *Composites Science and Technology*, vol. 121, pp. 1–8, 2015. [Online]. Available: http://dx.doi.org/10.1016/j.compscitech.2015.10.019

[125] T. Chen, L. Pan, M. Lin, B. Wang, L. Liu, Y. Li, J. Qiu, and K. Zhu, "Dielectric, mechanical and electro-stimulus response properties studies of polyurethane dielectric elastomer modified by carbon nanotube-graphene nanosheet hybrid fillers," *Polymer Testing*, vol. 47, pp. 4–11, 2015. [Online]. Available: http://dx.doi.org/10.1016/j.polymertesting.2015.08.001

[126] D. Ljubic, M. Srinivasan, R. Szoszkiewicz, I. Javni, and Z. S. Petrović, "Surface modified graphene/single-phase polyurethane elastomers with improved thermo-mechanical and dielectric properties," *European Polymer Journal*, vol. 70, pp. 55–65, 2015. [Online]. Available: http://dx.doi.org/10.1016/j.eurpolymj.2015.07.008

[127] S. Gaidukovs, V. Kampars, J. Bitenieks, I. Bochkov, G. Gaidukova, and U. Cabulis, "Thermo-mechanical properties of polyurethane modified with graphite oxide and carbon nanotube particles," *Integrated Ferroelectrics*, vol. 173, no. 1, pp. 1–11, 2016. [Online]. Available: http://dx.doi.org/10.1080/10584587.2016.1182394

[128] A. Kausar and A. Ur Rahman, "Effect of graphene nanoplatelet addition on properties of thermo-responsive shape memory polyurethane-based nanocomposite," *Fullerenes, Nanotubes and Carbon Nanostructures*, vol. 24, no. 4, pp. 235–242, 2016. [Online]. Available: http://dx.doi.org/10.1080/1536383X.2016.1144592

[129] HUNSTSMAN, "ELASTOMERS - TPU Product Overview," 2008.

[130] K. Esumi, M. Ishigami, A. Nakajima, K. Sawada, and H. Honda, "Chemical treatment of carbon nanotubes," *Carbon*, vol. 34, no. 2, pp. 279–281, 1996. [Online]. Available: http://dx.doi.org/10.1016/0008-6223(96)83349-5

[131] British Standard, "BS EN ISO 527-2 : Plastics - Determination of tensile properties," 1996.

[132] R. F. Egerton, *Physical Principles of Electron Microscopy*. Springer, 2005.

[133] ASTM, "Standard Test Method for Enthalpies of Fusion and Crystallization of Polymers by Differential Scanning Calorimetry," 2013. [Online]. Available: http://dx.doi.org/10.1520/D3418-15

[134] G. W. H. Höhne, W. F. Hemminger, and H. Flammersheim, "DSC Curves and Further Evaluations," in *Differential Scanning Calorimetry*. Springer, 2003, ch. 5, pp. 115–146.

[135] Humboldt University of Berlin, "Investigation of Polymers with Differential Scanning Calorimetry," pp. 1–17.

[136] J. Xu, W. Shi, and W. Pang, "Synthesis and shape memory effects of Si-O-Si cross-linked hybrid polyurethanes," *Polymer*, vol. 47, no. 1, pp. 457–465, 2006. [Online]. Available: http://dx.doi.org/10.1016/j.polymer.2005.11.035

[137] E. Morîntale, A. Harabor, C. Constantinescu, and P. Rotaru, "Use of heat flows from DSC curve for calculation of specific heat of the solid materials," *Annals of the University of Craiova, Physics*, vol. 23, pp. 89–94, 2013.

[138] TAInstruments, "Thermal Conductivity and Thermal Diffusivity," pp. 1–20, 2014.

[139] British Standard, "EN ISO 527-1 : Plastics - General principles for the determination of tensile properties," 1996.

[140] M. Fang, K. G. Wang, H. B. Lu, Y. L. Yang, and S. Nutt, "Covalent polymer functionalization of graphene nanosheets and mechanical properties of composites," *Journal of Materials Chemistry*, vol. 19, no. 38, pp. 7098–7105, 2009. [Online]. Available: http://dx.doi.org/10.1039/B908220d

[141] P. Pötschke, A. R. Bhattacharyya, A. Janke, and H. Goering, "Melt mixing of polycarbonate/multi-wall carbon nanotube composites," *Composite Interfaces*, vol. 10, no. 4-5, pp. 389–404, 2003. [Online]. Available: http://dx.doi.org/10.1163/156855403771953650

[142] Z. Jin, K. P. Pramoda, G. Xu, and S. H. Goh, "Dynamic mechanical behavior of melt-processed multi-walled carbon nanotube/poly(methyl methacrylate) composites," *Chemical Physics Letters*, vol. 337, no. 1-3, pp. 43–47, 2001. [Online]. Available: http://dx.doi.org/10.1016/S0009-2614(01)00186-5

[143] B. J. Ash, D. F. Rogers, C. J. Wiegand, L. S. Schadler, R. W. Siegel, B. C. Benicewicz, and T. Apple, "Mechanical properties of Al2O3/polymethylmethacrylate nanocomposites," *Polymer Composites*, vol. 23, no. 6, pp. 1014–1025, 2002. [Online]. Available: http://dx.doi.org/10.1002/pc.10497

[144] Y. Liu, K. Gall, M. L. Dunn, and P. McCluskey, "Thermomechanics of shape memory polymer nanocomposites," *Mechanics of Materials*, vol. 36, no. 10, pp. 929–940, 2004. [Online]. Available: http://dx.doi.org/10.1016/j.mechmat.2003.08.012

[145] N. M. Barkoula, B. Alcock, N. O. Cabrera, and T. Peijs, "Preparation and Characterization of Nanocomposites Made From Chemoenzymatically Prepared Polyester Urethanes and Functionalized Multiwalled Carbon Nanotubes," *Polymer Composites*, vol. 16, no. 2, pp. 101–113, 2016. [Online]. Available: http://dx.doi.org/10.1002/pc.24133

[146] B. Weidenfeller and M. Anhalt, "Polyurethane-magnetite composite shape-memory polymer: Thermal properties," *Journal of Thermoplastic Composite Materials*, vol. 27, no. 7, pp. 895–908, 2012. [Online]. Available: http://dx.doi.org/10.1177/0892705712458446

[147] "NETZSCH." [Online]. Available: https://www.netzsch-thermal-analysis.com/en/landing-pages/definition-thermal-diffusivity/

[148] B. Safadi, R. Andrews, and E. A. Grulke, "Multiwalled carbon nanotube polymer composites: Synthesis and characterization of thin films," *Journal of Applied Polymer Science*, vol. 84, no. 14, pp. 2660–2669, 2002. [Online]. Available: http://dx.doi.org/10.1002/app.10436

[149] J. N. Coleman, M. Cadek, R. Blake, V. Nicolosi, K. P. Ryan, C. Belton, A. Fonseca, J. B. Nagy, Y. K. Gun'ko, and W. J. Blau, "High-performance nanotube-reinforced plastics: Understanding the mechanism of strength increase," *Advanced Functional Materials*, vol. 14, no. 8, pp. 791–798, 2004. [Online]. Available: http://dx.doi.org/10.1002/adfm.200305200

[150] Z. O. Gagolkina, N. V. Lemesh, E. V. Lobko, Y. V. Yakovlev, P. E. Strizhak, and V. V. Klepko, "Effect of Chemical Structure and Geometry of Carbon Nanotubes on Electrical and Mechanical Properties of Nanocomposites Based on Cross-Linked Polyurethane," *Theoretical and Experimental Chemistry*, vol. 52, no. 1, pp. 16–20, 2016. [Online]. Available: http://dx.doi.org/10.1007/s11237-016-9444-z

[151] P. Mallick, *Fiber- Reinforced Composites : Materials, Manufacturing and Design*, 3rd ed. CRC Press, 2007.

[152] D. Qian, E. C. Dickey, R. Andrews, and T. Rantell, "Load transfer and deformation mechanisms in carbon nanotube-polystyrene composites," *Applied Physics Letters*, vol. 76, no. 20, pp. 2868–2870, 2000. [Online]. Available: http://dx.doi.org/10.1063/1.126500

[153] W. D. Zhang, L. Shen, I. Y. Phang, and T. Liu, "Carbon nanotubes reinforced nylon-6 composite prepared by simple melt-compounding," *Macromolecules*, vol. 37, no. 2, pp. 256–259, 2004. [Online]. Available: http://dx.doi.org/10.1021/ma035594f

[154] M. Cadek, J. N. Coleman, V. Barron, K. Hedicke, and W. J. Blau, "Morphological and mechanical properties of carbon-nanotube-reinforced semicrystalline and amorphous polymer composites," *Applied Physics Letters*, vol. 81, no. 27, pp. 5123–5125, 2002. [Online]. Available: http://dx.doi.org/10.1063/1.1533118

[155] S. L. Ruan, P. Gao, X. G. Yang, and T. X. Yu, "Toughening high performance ultrahigh molecular weight polyethylene using multiwalled carbon nanotubes," *Polymer*, vol. 44, no. 19, pp. 5643–5654, 2003. [Online]. Available: http://dx.doi.org/10.1016/S0032-3861(03)00628-1

[156] A. Dufresne, M. Paillet, J. L. Putaux, R. Canet, F. Carmona, P. Delhaes, and S. Cui, "Processing and characterization of carbon nanotube/poly(styrene-co-butyl acrylate) nanocomposites," *Journal of Materials Science*, vol. 37, no. 18, pp. 3915–3923, 2002. [Online]. Available: http://dx.doi.org/10.1023/A:1019659624567

[157] F. Ren, G. Zhu, P. Ren, Y. Wang, and X. Cui, "In situ polymerization of graphene nanosheets and polyurethane with enhanced mechanical and thermal properties," *Journal of Materials Chemistry*, vol. 21, pp. 4222–4227, 2011. [Online]. Available: http://dx.doi.org/10.1039/C0JM03710A

[158] Q. D. Chen, L. M. Dai, M. Gao, S. M. Huang, and A. Mau, "Plasma activation of carbon nanotubes for chemical modification," *Journal of Physical Chemistry B*, vol. 105, no. 3, pp. 618–622, 2001. [Online]. Available: http://dx.doi.org/10.1021/jp003385g

[159] J. A. Kim, D. G. Seong, T. J. Kang, and J. R. Youn, "Effects of surface modification on rheological and mechanical properties of CNT/epoxy

composites," *Carbon*, vol. 44, no. 10, pp. 1898–1905, 2006. [Online]. Available: http://dx.doi.org/10.1016/j.carbon.2006.02.026

[160] M. Shaffer, X. Fan, and A. Windle, "Dispersion and packing of carbon nanotubes," *Carbon*, vol. 36, no. 11, pp. 1603–1612, 1998. [Online]. Available: http://dx.doi.org/10.1016/S0008-6223(98)00130-4

[161] J. Liu, A. Rinzler, H. Dai, J. Hafner, R. Bradley, P. Boul, A. Lu, T. Iverson, K. Shelimov, C. Huffman, F. Rodriguez-Macias, Y.-S. Shon, T. Lee, D. T. Colbert, and R. E. Smalley, "Fullerene Pipes," *Science*, vol. 280, no. 5367, pp. 1253–1256, 1998. [Online]. Available: http://dx.doi.org/10.1126/science.280.5367.1253

[162] C. Mu, L. Zhang, Y. Song, X. Chen, M. Liu, F. Wang, and X. Hu, "Modification of carbon nanotubes by a novel biomimetic approach towards the enhancement of the mechanical properties of polyurethane," *Polymer*, vol. 92, pp. 231–238, 2016. [Online]. Available: http://dx.doi.org/10.1016/j.polymer.2016.03.085

[163] R. Sattar, A. Kausar, and M. Siddiq, "Influence Of Conducting Polymer On Mechanical, Thermal And Shape Memory Properties Of Polyurethane/polythiophene Blends And Nanocomposite," *Advanced Materials Letters*, vol. 7, no. 4, pp. 282–288, 2016. [Online]. Available: http://dx.doi.org/10.5185/amlett.2016.6198

Appendices

Appendix A

Heat flow - Temperature curves

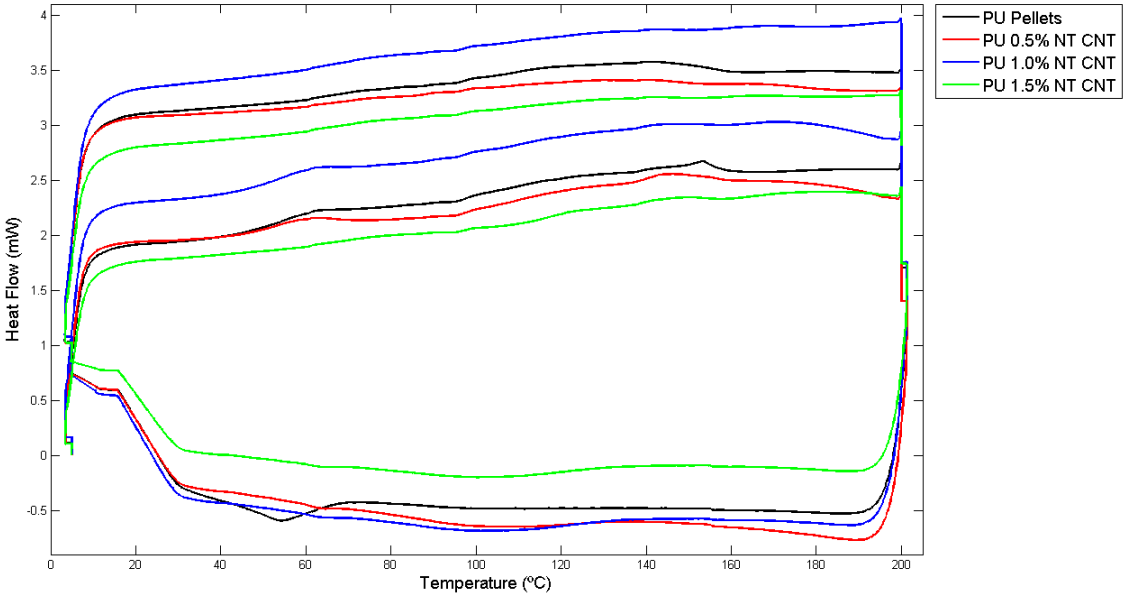

Figure A.1: Heat flow - Temperature curves for the NT CNTs/TPU nanocomposites.

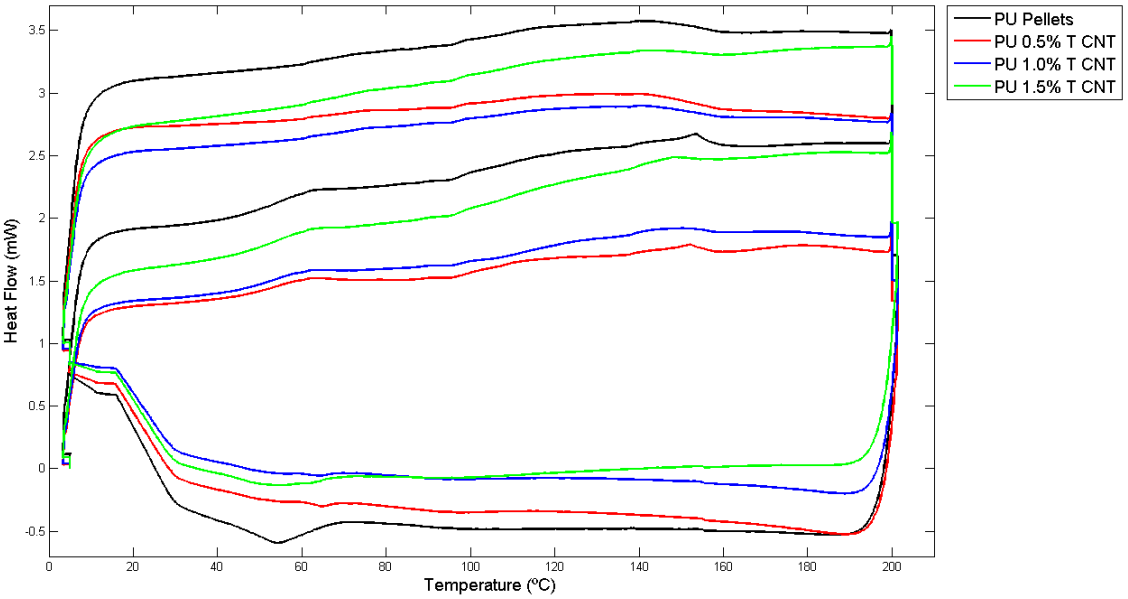

Figure A.2: Heat flow - Temperature curves for the T CNTs/TPU nanocomposites.

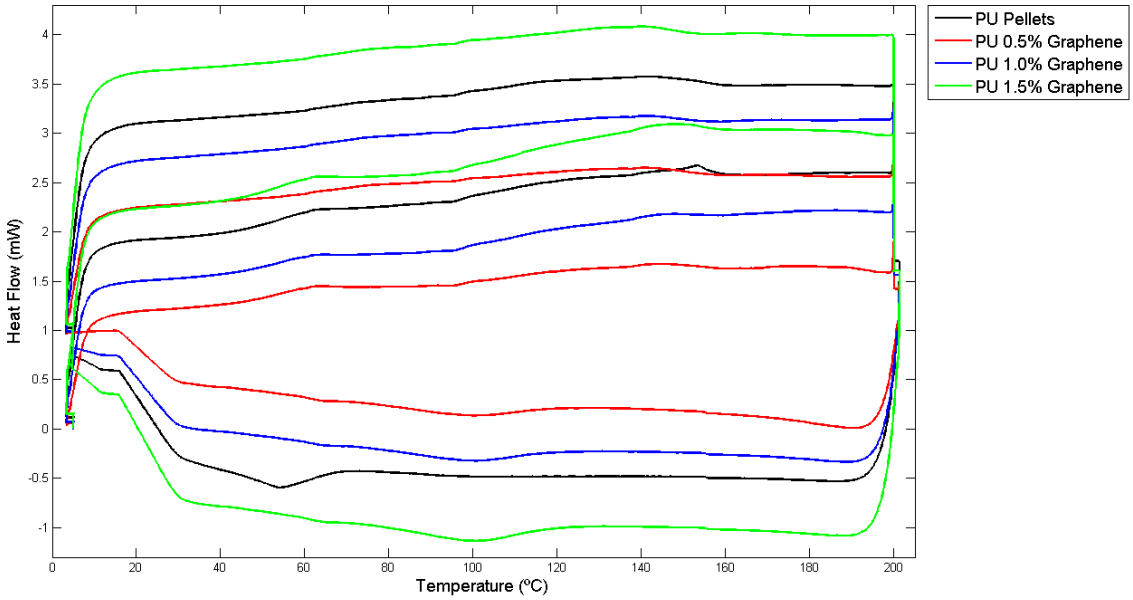

Figure A.3: Heat flow - Temperature curves for the graphene/TPU nanocomposites.

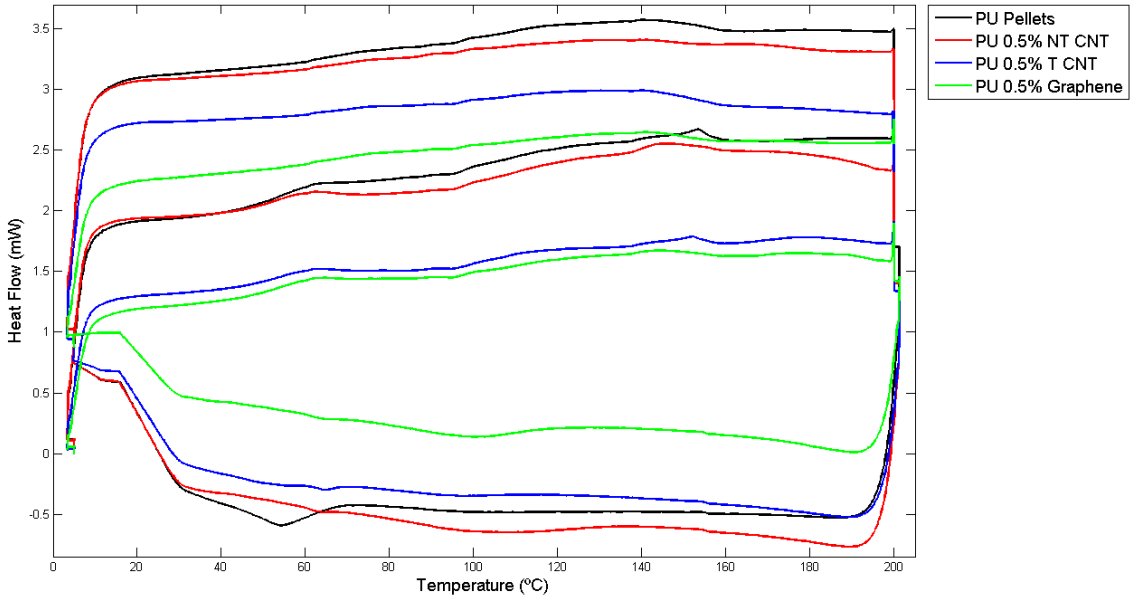

Figure A.4: Heat flow - Temperature curves for the nanocomposites containing 0.5 vol.% of filler (NT CNTs, T CNTs and graphene).

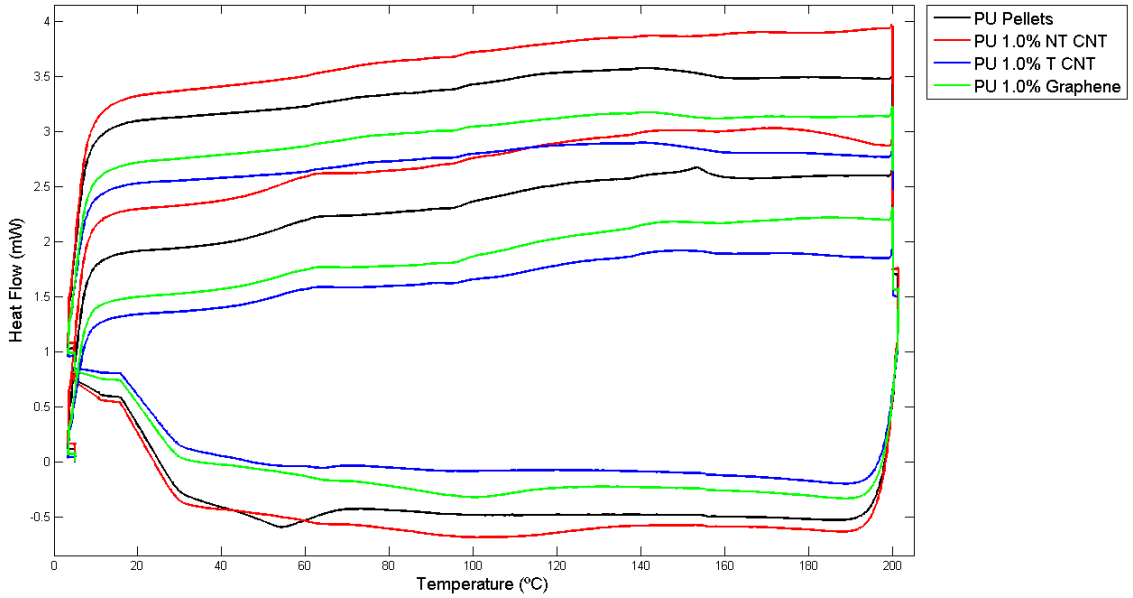

Figure A.5: Heat flow - Temperature curves for the nanocomposites containing 1.0 vol.% of filler (NT CNTs, T CNTs and graphene).

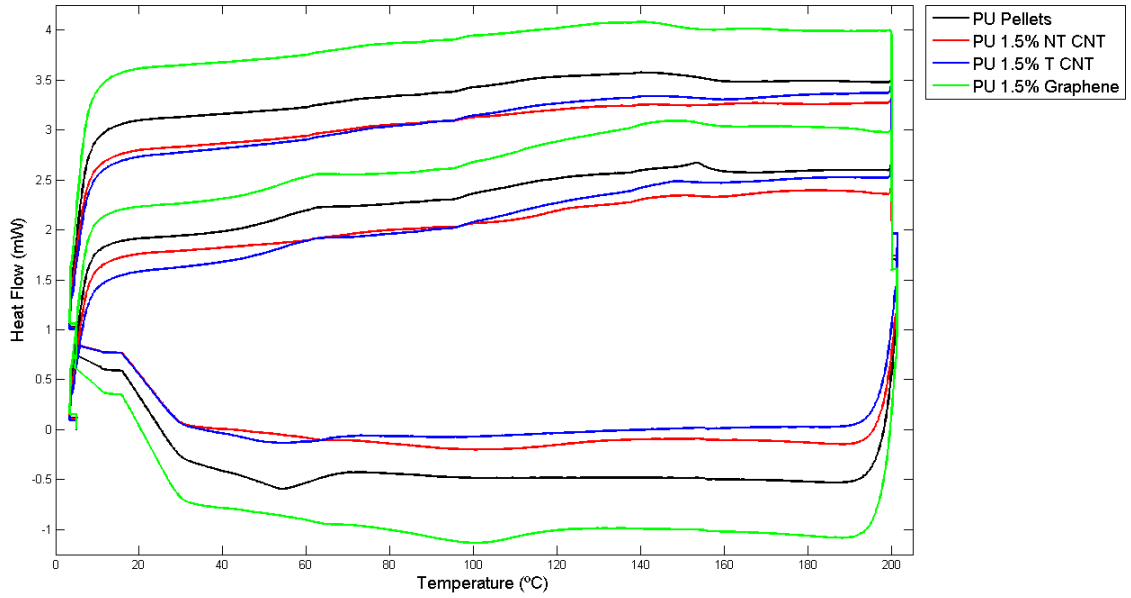

Figure A.6: Heat flow - Temperature curves for the nanocomposites containing 1.5 vol.% of filler (NT CNTs, T CNTs and graphene).

Appendix B

Stress - Strain average curves

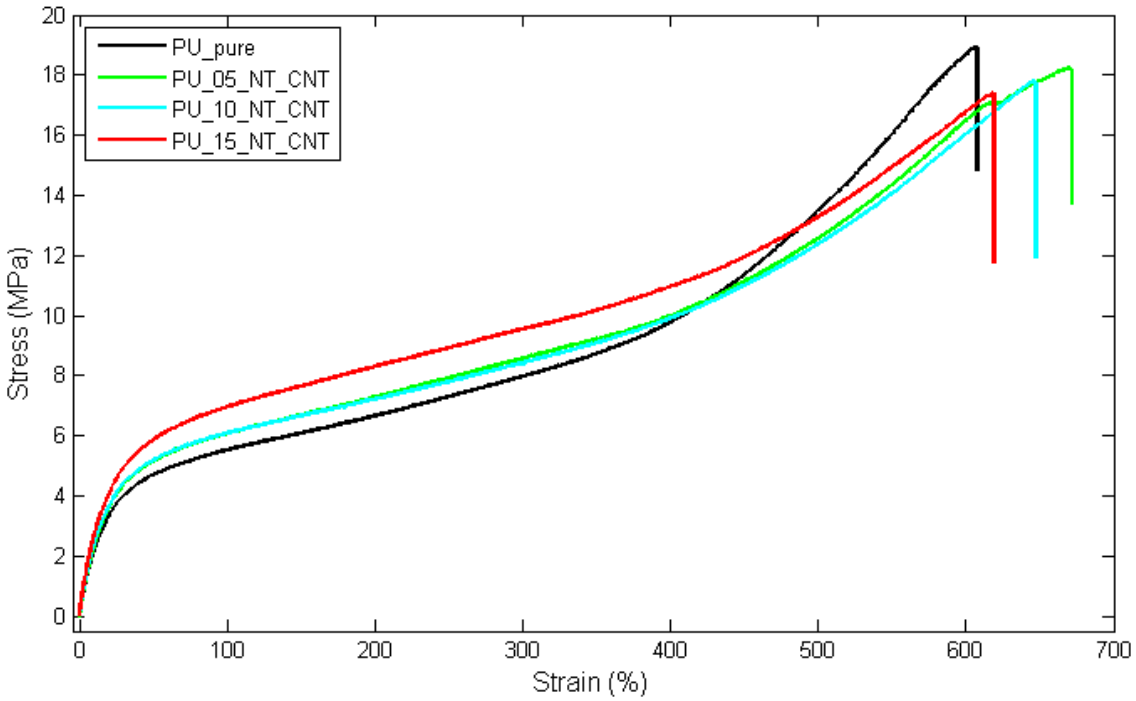

Figure B.1: Stress - Strain average curves for the NT CNTs/TPU nanocomposites.

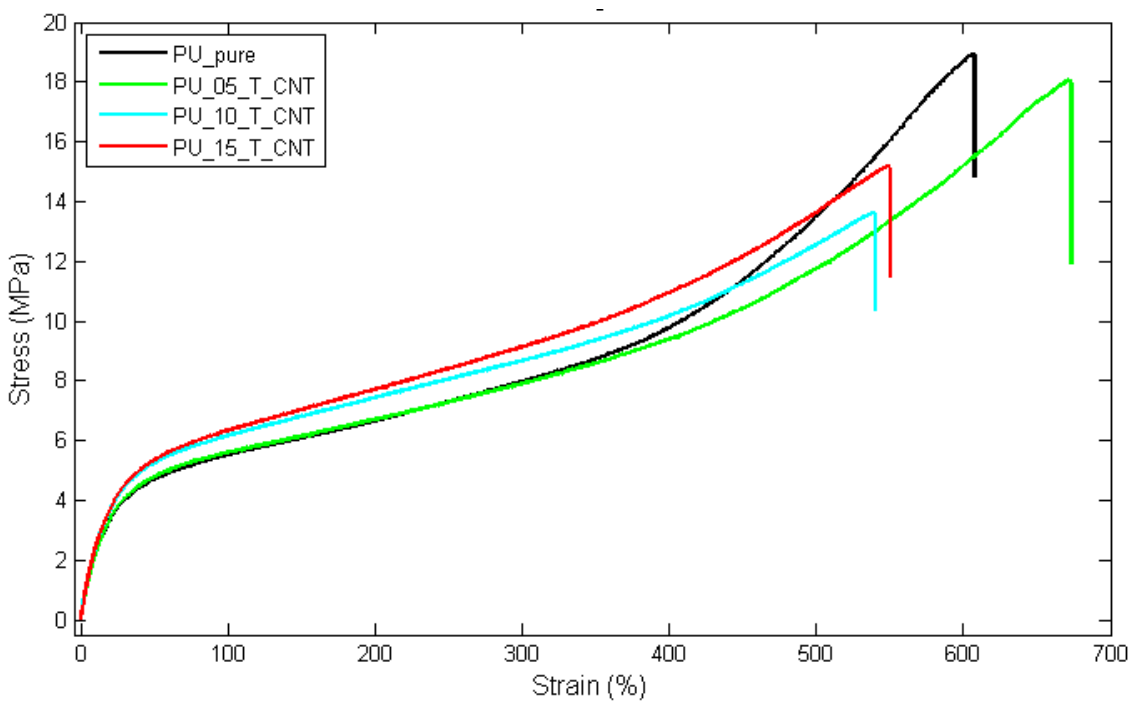

Figure B.2: Stress - Strain average curves for the T CNTs/TPU nanocomposites.

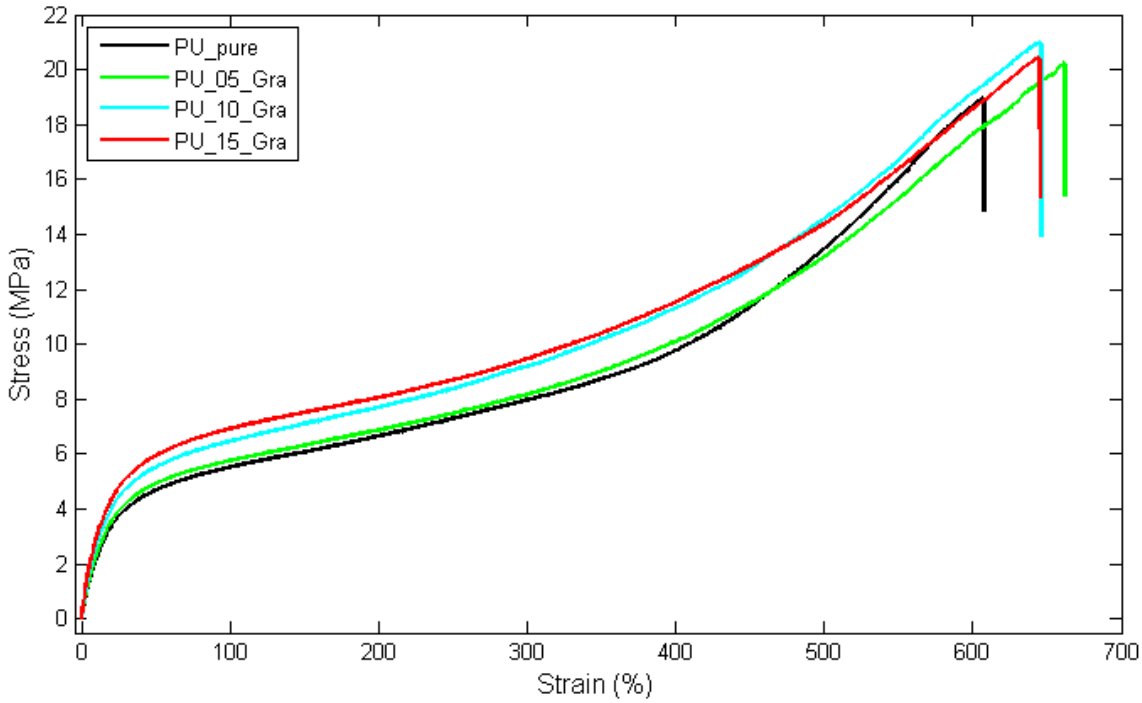

Figure B.3: Stress - Strain average curves for the graphene/TPU nanocomposites.

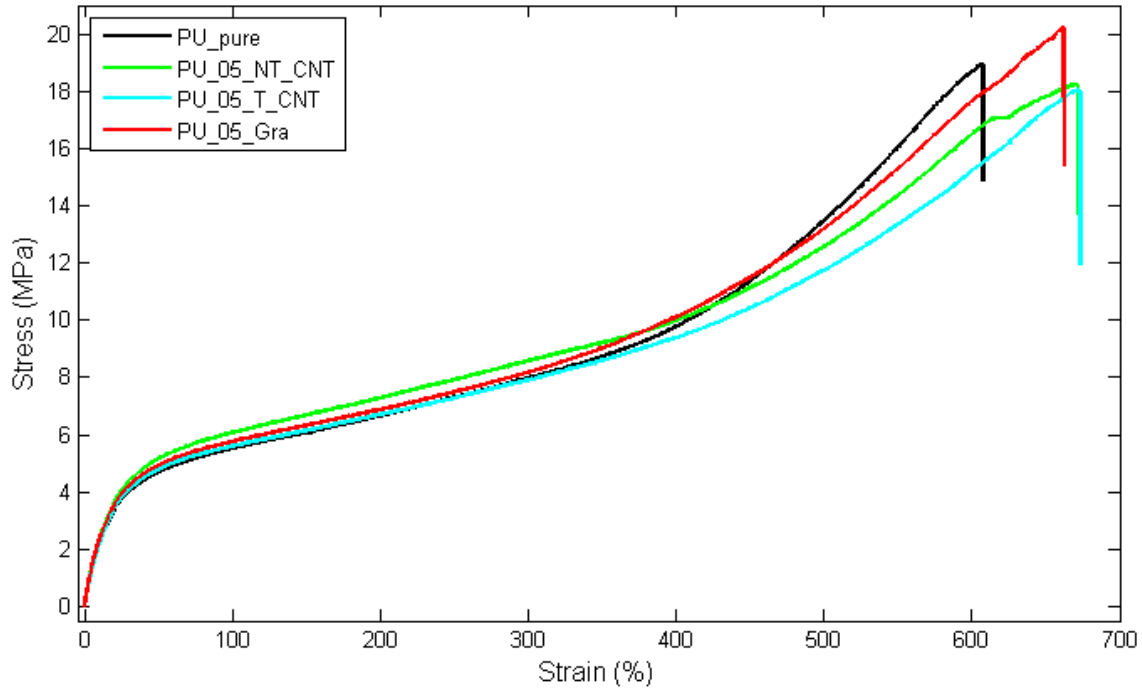

Figure B.4: Stress - Strain average curves for the nanocomposites containing 0.5 vol.% of filler (NT CNTs, T CNTs and graphene).

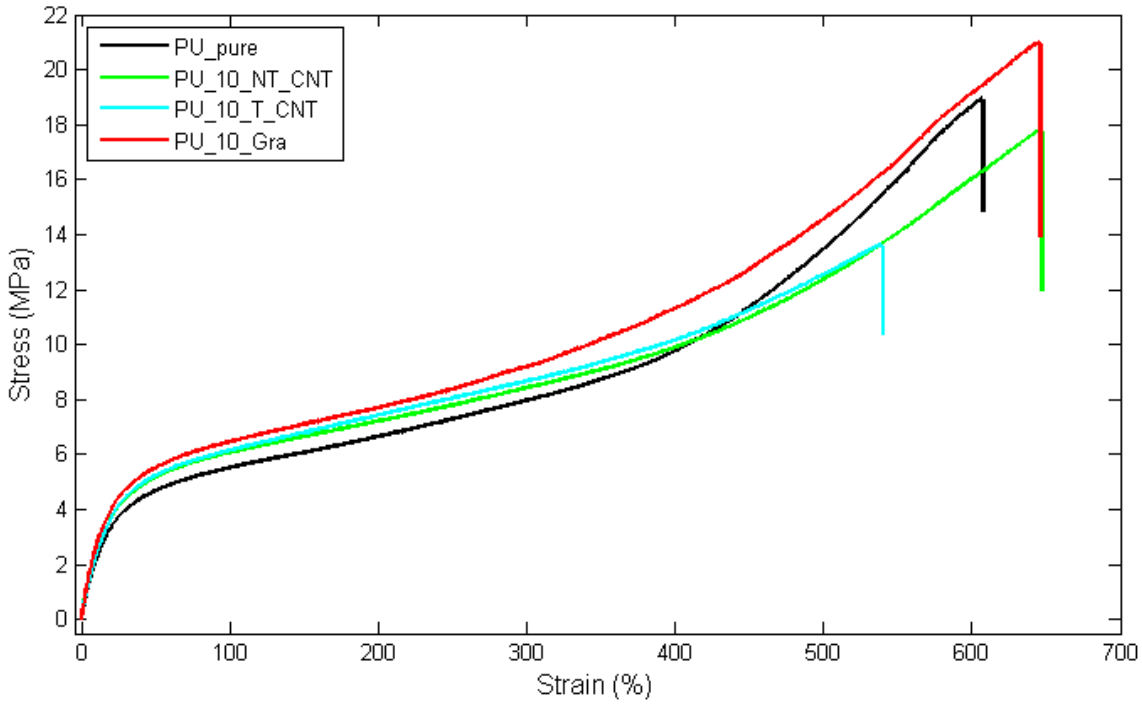

Figure B.5: Stress - Strain average curves for the nanocomposites containing 1.0 vol.% of filler (NT CNTs, T CNTs and graphene).

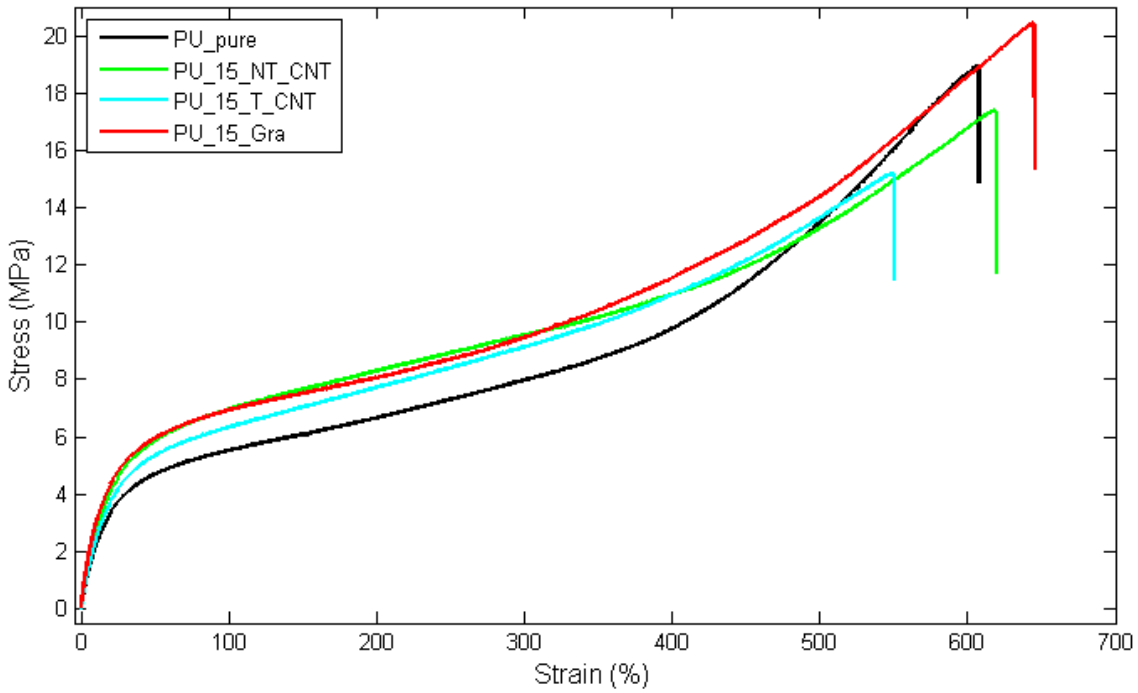

Figure B.6: Stress - Strain average curves for the nanocomposites containing 1.5 vol.% of filler (NT CNTs, T CNTs and graphene).